NASA Contractor Report 166525

UTRC Report R84-915774-24

Analytic Investigation of Helicopter Rotor Blade Appended Aeroelastic Devices

Richard L. Bielawa
United Technologies Research Center
East Hartford, CT 06108

Prepared for
Ames Research Center
under Contract NAS2-11008

National Aeronautics and
Space Administration

Ames Research Center
Moffett Field, California 94035

PREFACE

The results described herein were performed by United Technologies Research Center (UTRC) under contract NAS2-11008, "Analytic Investigation of Helicopter Rotor Blade Appended Aeroelastic Devices." This contract was through the Ames Research Center of NASA with Mr. Robert H. Stroub acting as contract monitor. The program manager for this study was Dr. Richard L. Bielawa. The study made extensive use of the G400PA aeroelastic analysis developed by UTRC for NASA Langley Research Center and the Structures Laboratory of the USRTL (AVRADCOM) under contract NAS1-16058.

TABLE OF CONTENTS

LIST OF FIGURES AND TABLES

LIST OF FIGURES AND TABLES
continued

LIST OF FIGURES AND TABLES
continued

TABLES

ANALYTIC INVESTIGATION OF HELICOPTER ROTOR BLADE APPENDED AEROELASTIC DEVICES

By Richard L. Bielawa
United Technologies Research Center

SUMMARY

Analytic evaluations of four different passive aeroelastic devices appended to helicopter rotor blades is presented. The devices consist of a passive tuned tab, a control coupled tab, an all-flying tip and a harmonic dilational airfoil tip; each device was conceived for improving either aerodynamic performance, or reducing vibratory control loads or hub shears. The evaluation was performed using a comprehensive rotor aeroelastic analysis (the G400PA code with appropriate modifications), together with data for a realistic helicopter rotor blade (the UH-60A Blackhawk) in high speed flight (90 m/s, 175 kts). The results of this study show that significant performance (L/D_e) gains can be achieved with the all-flying free tip. Results for the harmonic dilational airfoil tip show the potential for moderate improvements in L/D_e. Finally, the results for the passive tuned tab and the control coupled tab, as configured for this study, show these devices to be impractical.

Sections are included which describe the operation of each device, the required G400PA modifications, and the detailed results obtained for each device.

INTRODUCTION

Background

It has long been appreciated that so-called conventional helicopter rotors, both articulated and hingeless, are in of themselves less than optimal lifting elements for VTOL aircraft systems. Indeed, the basic elements of such conventional rotors offer few design options for improvements in dynamic/aeroelastic related performance parameters. State-of-the-art approaches to enhancing these parameters have typically consisted of recourse to some sort of ingenious gadgetry. One form of such gadgetry consists of incorporating innovative dynamic feature(s) into the blades themselves, such as aeroelastic conformality (Ref. 1), or into the integrated rotor system. Examples of the latter are the Advancing Blade

Concept (Ref.2) or the tilt-rotor concept (Ref. 3). A second form of gadgetry consists of the appending of a specialized aeromechanical device to an otherwise conventional (or itself aeroelastically enhanced) rotor blade. The present emergence of high performance, high strength materials, together with an improved ability to analyze and understand the physics involved have made the implementations of such devices more attractive as design solutions.

An example of a rotor blade appended mechanical device which can be readily assumed to be state-of-the-art is the blade pendular absorber (Ref. 4). The blade pendular absorber is characterized by being a purely dynamic device with no direct aerodynamic interactions and tuned to operate at n x rotor speed frequencies. As such, the pendular absorber is inherently only a passive vibration suppression device.

Other blade appended dynamic devices which do involve direct aerodynamic interaction have been conceived, but have not as yet been subjected either to in-depth analysis or experimental proof-of-concept. Reasons for this lack of technical underpinning would include the lack of applicability of state-of-the-art production oriented analysis codes, and the difficulties in designing and testing workable experimental hardware. A meaningful analytical study of such devices would require an appreciation of their germane characteristics and the implementation of these characteristics in a proven comprehensive aeroelastic analysis of the type presently used for state-of-the-art rotor systems.

The objective of the present study was, therefore, to determine the practicality, both absolute and relative, of four (4) different passive aeroelastic devices appended to helicopter rotor blades for improving rotor performance, control loads and/or vibration alleviation. It was believed that the four devices selected for this study could offer significant potential for achieving these improvements. It was hoped that the study might achieve a significant advance in helicopter aeroelastics technology through the express selection of only devices which are both passive and aeroelastically responsive.

The emphasis on passivity reflects the desire to achieve gains in performance, control loads reduction and vibration alleviation through the simplicity afforded by fundamental rotor blade aeroelastic responses in forward flight. There undoubtedly exist equally feasible and potentially attractive concepts for blade appended devices which utilize active control schemes to achieve these same improvements. However, active control implies complexity in the form of additional electronics and/or hydraulics which must ultimately result in increased cost and less attractive maintainability and reliability characteristics.

"Passive" appended devices would have potentially powerful advantages accruing from configuration simplicity. However, the actual operation of these devices is necessarily complex since intimate aeroelastic interaction between the blade proper is intentionally introduced. This complexity, coupled with the long-standing inadequacies of state-of-the-art rotor aeroelastics methodology, and the limits of materials and fabrication techniques have most likely been the major arguments against the incorporation or even serious consideration of these devices in helicopter blade designs heretofore. While the argument of limited material and fabrication resources is an important one, it is deemed beyond the scope of the present study. Nevertheless, it is the recent emergence of more efficient materials and construction techniques which has led, in part, to the challenging of this argument and a renewed interest in such devices. It is further believed that with the substantial gains made in rotor aeroelastics methodology within the last few years, the argument of analysis inadequacy is no longer valid.

Description of Selected Aeroelastic Devices

Four (4) aeroelastic devices were selected for analysis based upon their conformity to the characteristics discussed above. The devices are all passive in the sense that they are activated by the rotor operating in its normal flight envelope without requiring overt activation by the pilot, and that they do not use any other energy source except that arising from rotor rotation. The devices seek either to enhance performance, reduce control loads, and/or alleviate vibration.

1. Tuned Trailing Edge Tab

One scheme which could provide vibration alleviation is a Tuned (Trailing Edge) Tab concept. The objective of this tab is to create harmonic airloading of favorable amplitude and phase to vectorally cancel the inherent harmonic airloading which acts as a source of main rotor vibration.

A schematic of the passive tab concept is shown in Figure 1. Physically, the passive blade tab is appended near to the trailing edge of a standard rotor blade by some hinge configuration so that the tab can deflect freely about the hinge. The hinge could be mechanical in nature with bearings, etc., or it could be made of a composite material that has a large strain allowable such that the tab is actually "taped" to the blade by the composite hinge. The latitude in selecting the spring rate of the tab about the hinge would provide dynamic tuning capability; the spring rate could be provided either mechanically or by the elasticity of the material for a composite hinge.

The basis of the concept as outlined in Figure 1 is simple: When a rotor blade tab deflects it creates an incremental airload and pitching moment on the rotor blade as a result of the increased camber. The pitching moment also creates an additional airload on the rotor blade by elastic twisting to create an incremental angle-of-attack. The importance of this source of airloading is closely tied to the blade torsional stiffness and natural frequency. This source of incremental airloading is secondary to that obtained from the effective camber change for this concept. When the tab deflects harmonically, the airloads and pitching moment created by the tab deflection are also harmonic. Therefore, to derive benefit from the tab, the tab motion must be correctly phased to cancel the inherent harmonic airloading that excites the blade flatwise modes and produces vibration.

The driving forces on the tab are its own inertial loading as the blade flaps and pitches (both as a rigid body and flexibly) and the aerodynamics arising from blade and tab motion. By increasing the offset of the tab center of gravity from the hinge the inertial forcing can be increased. For a tab located at the blade tip, most of the vertical harmonic motion would come from the response of the flexible flatwise modes and nearly all of the torsion motion would be due to the response of the blade first torsion mode. Hence, there is a direct relationship between the motion that is inertially forcing the tab to deflect and the vibration that is a result of that same motion. Therefore, the success of this concept hinges on correctly sizing and placing the tab along the rotor blade span and choosing its mass and natural frequency so that the maximum vectoral cancellation of inherent harmonic airloading is achieved.

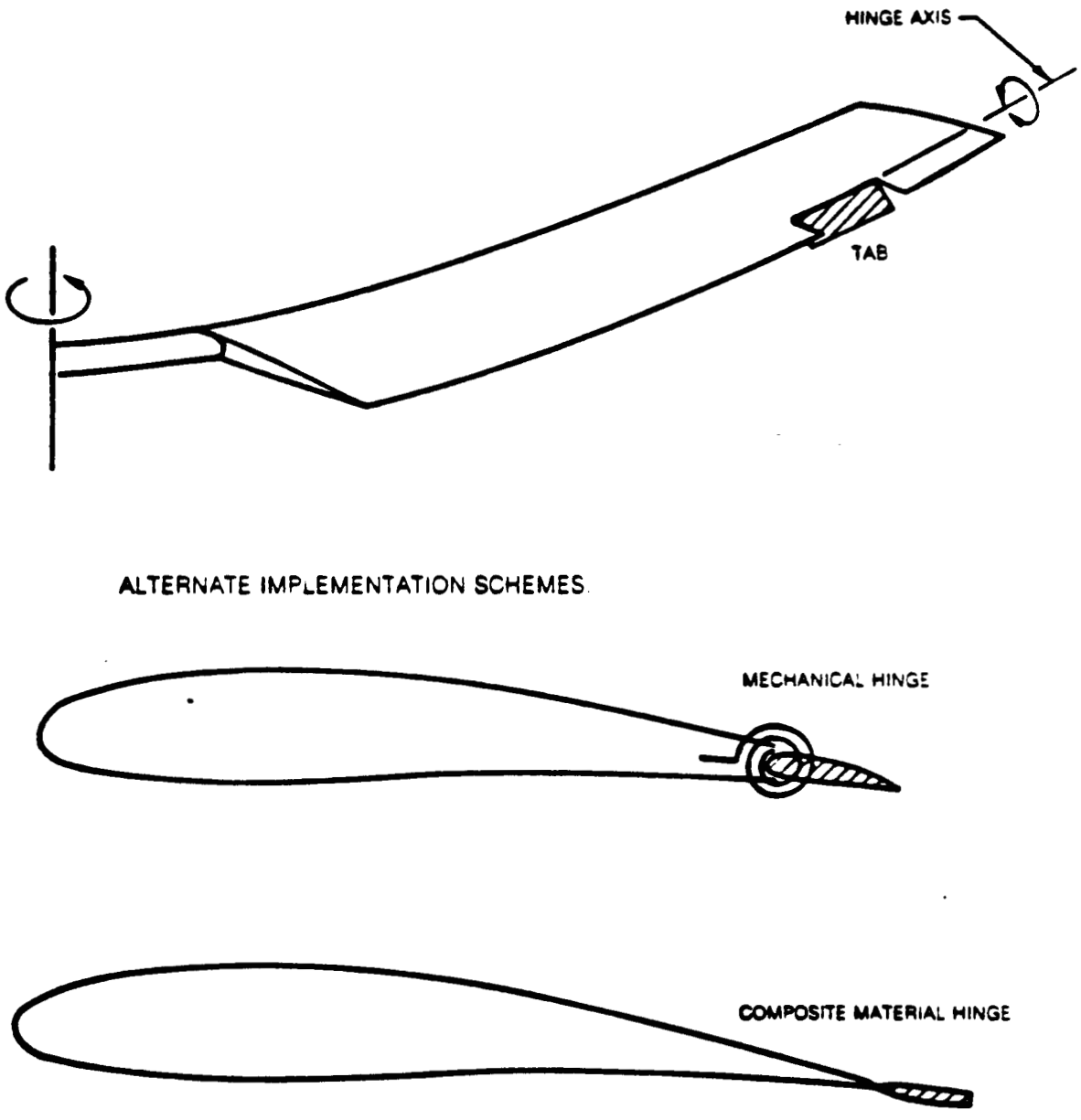

Figure 1. Pictorial of Tuned Trailing Edge Tab

2. Trailing Edge Tab Coupled to Blade Control Loads

The selection of airfoils for helicopter main rotor blades is limited to those airfoils which have low pitching moments because airfoils having high pitching moments cause excessive blade pitch control system vibratory loads and high blade torsional deflections in forward flight. The selection of airfoils has therefore been constrained to the use of symmetrical airfoils or at best, airfoils having 2 percent of camber. In addition to this fundamental constraint, helicopter maximum speeds are frequently limited by the rapid growth of vibratory control loads as blade stall is approached, particularly in maneuvering flight. If these constraints could be eliminated, airfoils with high camber could be employed and could be selected to operate at their optimum lift coefficients to delay stalling and consequently increase the maximum helicopter cruise speed for a given rotor blade loading. The achievement of higher blade loadings through the use of cambered airfoils would also permit operation of the rotor at reduced rotor noise. Reduction of rotor noise is emerging as a major requirement for civil helicopters, particularly those in the 20,000 pounds and larger size classes because of local and federal noise regulations.

The reduction of blade control system loads has the potential for providing several additional advantages. Because of high control system vibratory control loads many elements of the control system and airframe support structure are life-limited. A significant reduction of these loads would provide unlimited life for such components and would probably permit large weight reductions as well. Furthermore, the servo actuator size, weight and power requirements could be reduced. This is particularly significant where redundant control systems are required. Concommitantly, a large increase in control system reliability should be achievable.

A control force reduction device based on the use of a control load coupled tab system offers the potential for relaxing the constraints on the use of highly cambered airfoils and of providing more reliable and lighter control systems. The control load coupled tab rotor blade as conceived is described below with reference to Figure 2. This control force reduction device operates primarily by sensing the control load required to feather the rotor blade and, through a mechanical linkage, deflecting to counter the blade pitching moment in a direction to reduce the control load toward zero. As shown in Figure 2 the freely feathering blade is constrained in pitch angle by means of a control rod which is attached to the blade pitch horn at one end and to the rotating swashplate at the opposite end. The control rod contains a spring capsule which deflects in proportion to the control load by an amount which depends on the spring rate. By this means the control rod shortens when the spring is compressed and lengthens when the spring is extended.

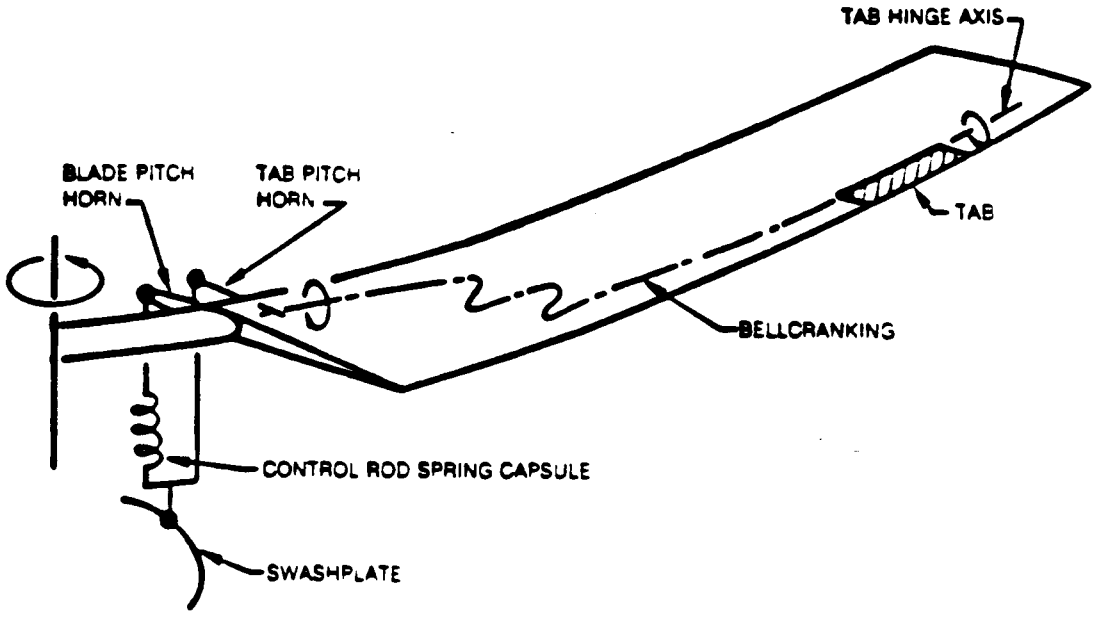

DEFLECTED TAB DEPICTION:

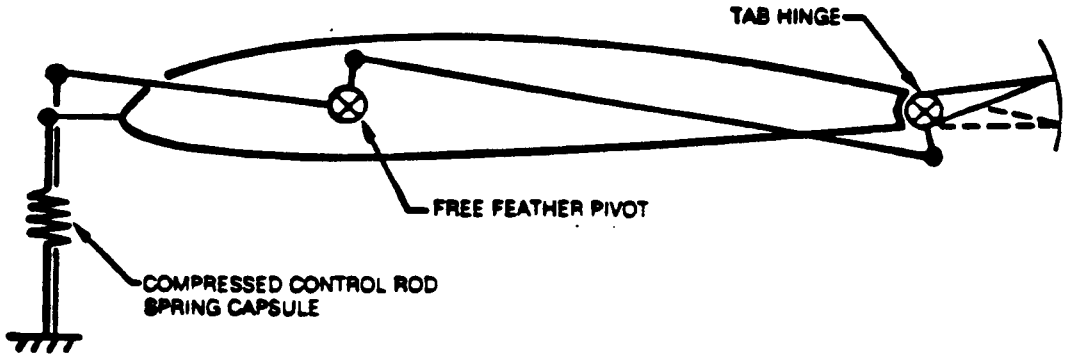

Figure 2. Pictorial of Trailing Edge Tab Coupled to Blade Control Loads

A second, but rigid, control rod is attached in parallel with the spring capsule and drives a tab torque tube. If the spring deflection is zero, the tab does not deflect. If the spring is compressed, the tab deflects to produce a pitching moment in a direction to relieve the load in the control rod. A particular advantage of this system is that the control load is driven toward zero regardless of the cause of the blade pitching moment.

3. All-Flying Torsion Tip

This concept, as analyzed herein, is a generalization of the Free-Tip Rotor concept originally studied in Reference 5, and is pictorially depicted in Figure 3. The over-all objective of this device is the improvement of rotor aerodynamic efficiency by the creation of a more uniform airload distribution around the azimuth of the tip region of the blade. This concept is primarily directed to the airloading of the blade tip region owing to the recognized potential for negative lifting loads in this blade region on the advancing side in forward flight.

The attainment of the over-all objective for this device is to be achieved by constraining the all-flying tip to generate positive lift through a controlled applied moment. As shown in Figure 3, an intentionally introduced offset between the hinge (pitch) axis and the aerodynamic center, Δchord, would enable the lift on the tip to be controlled by means of the applied moment to the tip:

$$\text{lift} \times \Delta\text{chord} = \text{controller applied moment.}$$

The controller applied moment is in turn determined by the placement of the aerodynamic and mass centers of the tip relative to the pitch axis of the tip, and the type of reaction moment provided by the tip moment.

In the original conception of the device, a constant torsional moment (preload) restraint is placed on the tip pitch axis and the tip, therefore, tends to fly so as to provide a nominally constant lift. As analyzed herein, the tip is additionally mounted with a finite torsion spring restraint to be sized relative to the effective aerodynamic spring. Although this departs somewhat from the constant moment restraint concept defined in Reference 5, it nevertheless represents a reasonable generalization of the original concept. The pertinent performance payoff parameter for the all-flying torsion tip is L/D_e.

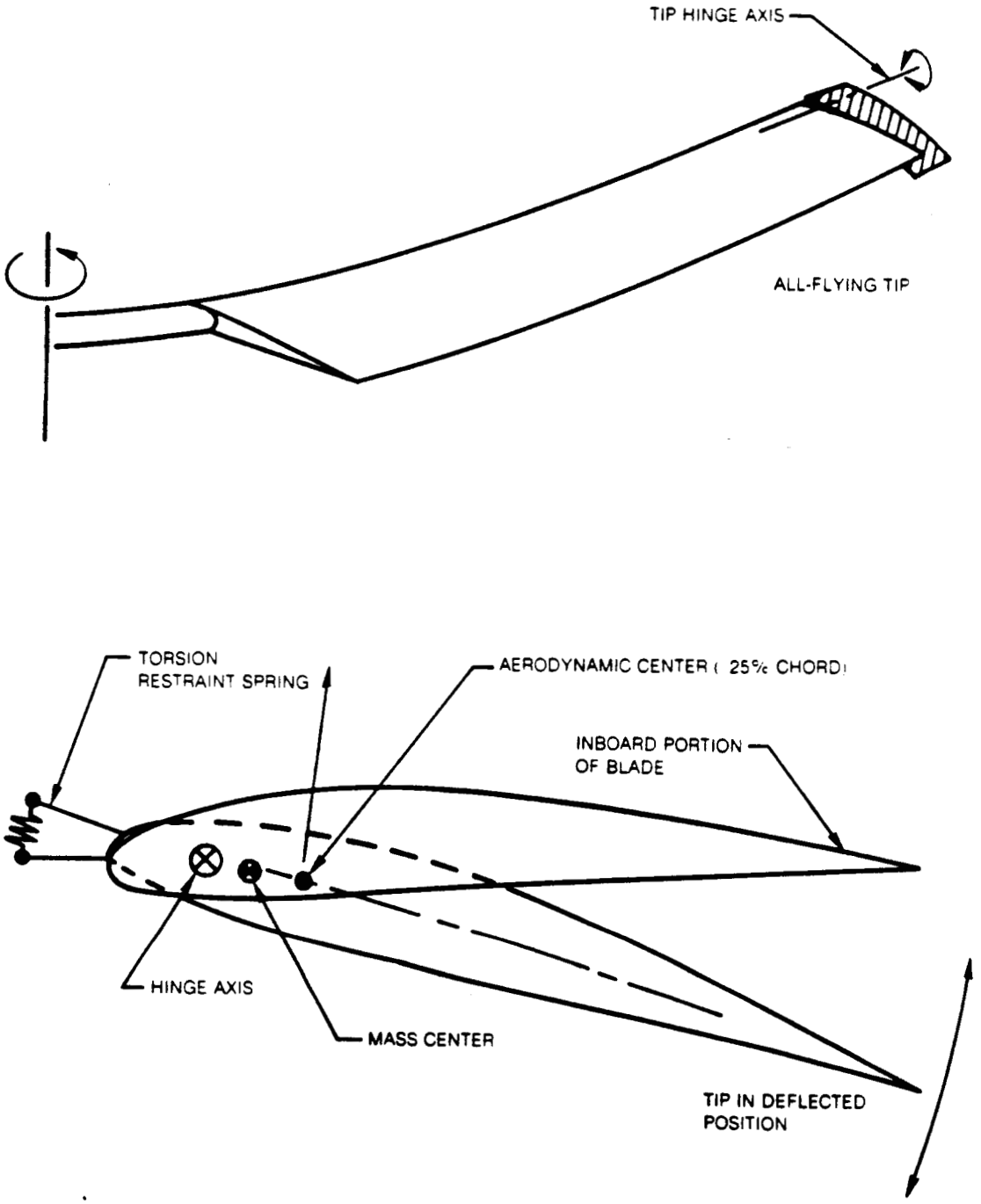

Figure 3. Pictorial of All-Flying Torsion Tip

4. Harmonically Deformable Airfoil Tip

As indicated in Figure 4, the outboard portion of a helicopter rotor blade in forward flight ideally requires two conflicting characteristics for optimal aerodynamic performance: thin sections are required on the advancing side to minimize transonic compressibility effects, and relatively thick, cambered sections are required on the retreating side to achieve high unstalled lift coefficients in low subsonic conditions. Furthermore, a compromise airfoil with camber would ideally be needed for hovering flight.

The harmonically deformable airfoil tip is a device which seeks to accommodate these conflicting requirements. It could consist of a tip portion of the blade whose airfoil section is so flexibly constructed and tuned as to harmonically deform in response to 1P dynamic pressure variations, As illustrated in Figure 5, the harmonic deformations of the device would be in the thicknesswise directions and would be tailored to produce both overall thickness and/or camber variations.

As conceived, and depicted in Figure 4, one implementation of the device could be accomplished using an airfoil section construction whose thicknesswise rigidity is controlled by the differential pressure within internal pressure cells attached to the inside of the flexible outer skin. Increased differential pressure within the cells would cause a thicknesswise contraction (and chordwise elongation) of the airfoil. Camber variations could be obtained by unsymmetric attachments to the inside surface of the flexible airfoil contour skin. Because of the inherently high fatigue stress environment of this device, and the need for high dynamic strains, such a construction scheme would benefit from composite material techniques.

Of greater importance than the construction techniques, however, are the required dynamic characteristics. Clearly, to produce significant harmonic variations in thickness at 1P, the device must be tuned to that frequency. The difficulty arises, however, in the proper phasing of the resonant response. The required response must be approximately 180 deg out-of-phase with the excitation rather than the 90 deg which normally occurs at resonance. That is, the airfoil must contract at the same instant that the 1P dynamic pressure is trying to dilate it.

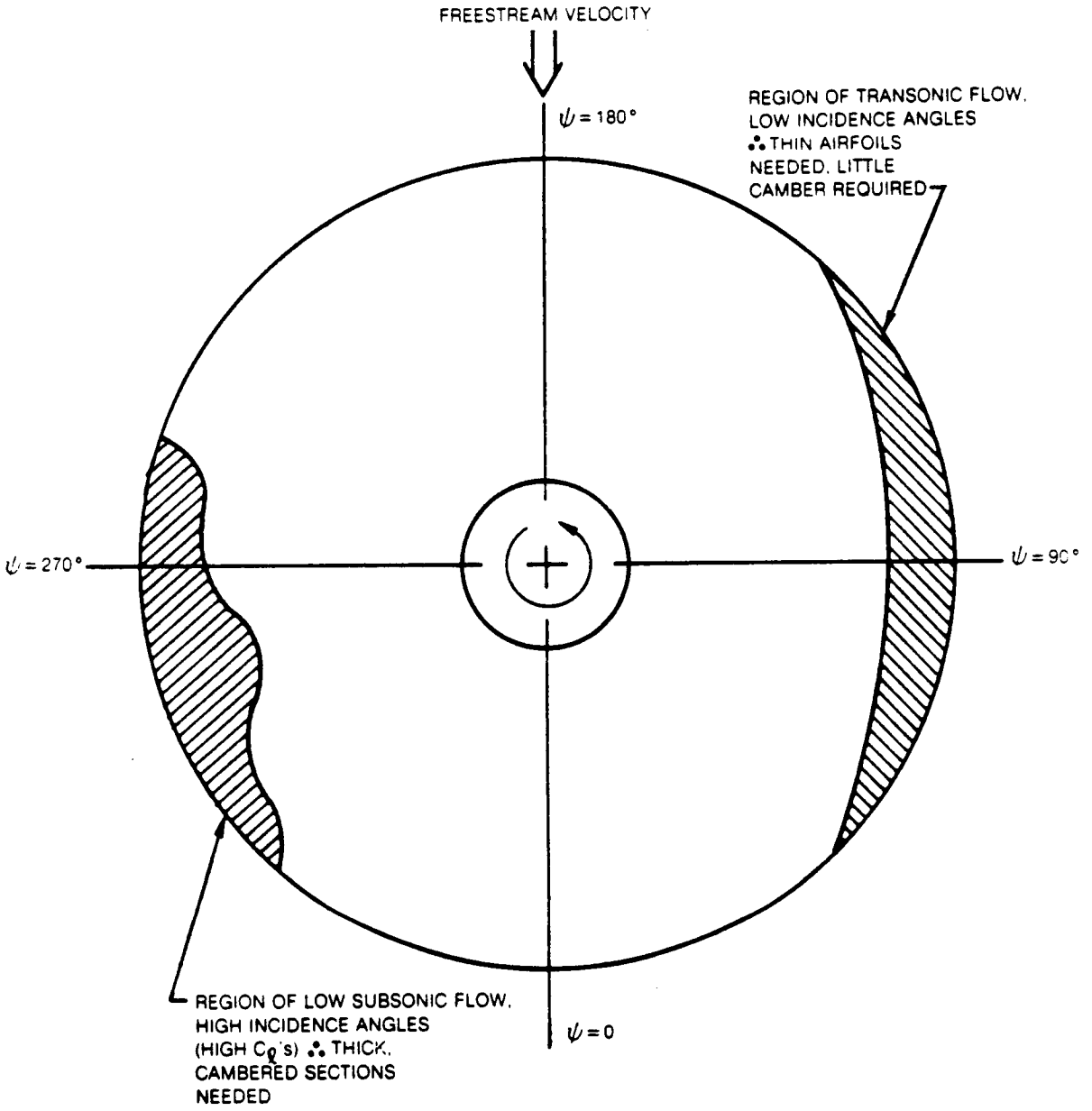

Figure 4. Pictorial of Helicopter Rotor Disk in Forward Flight Showing Conflicting Requirements for Blade Tip Sections

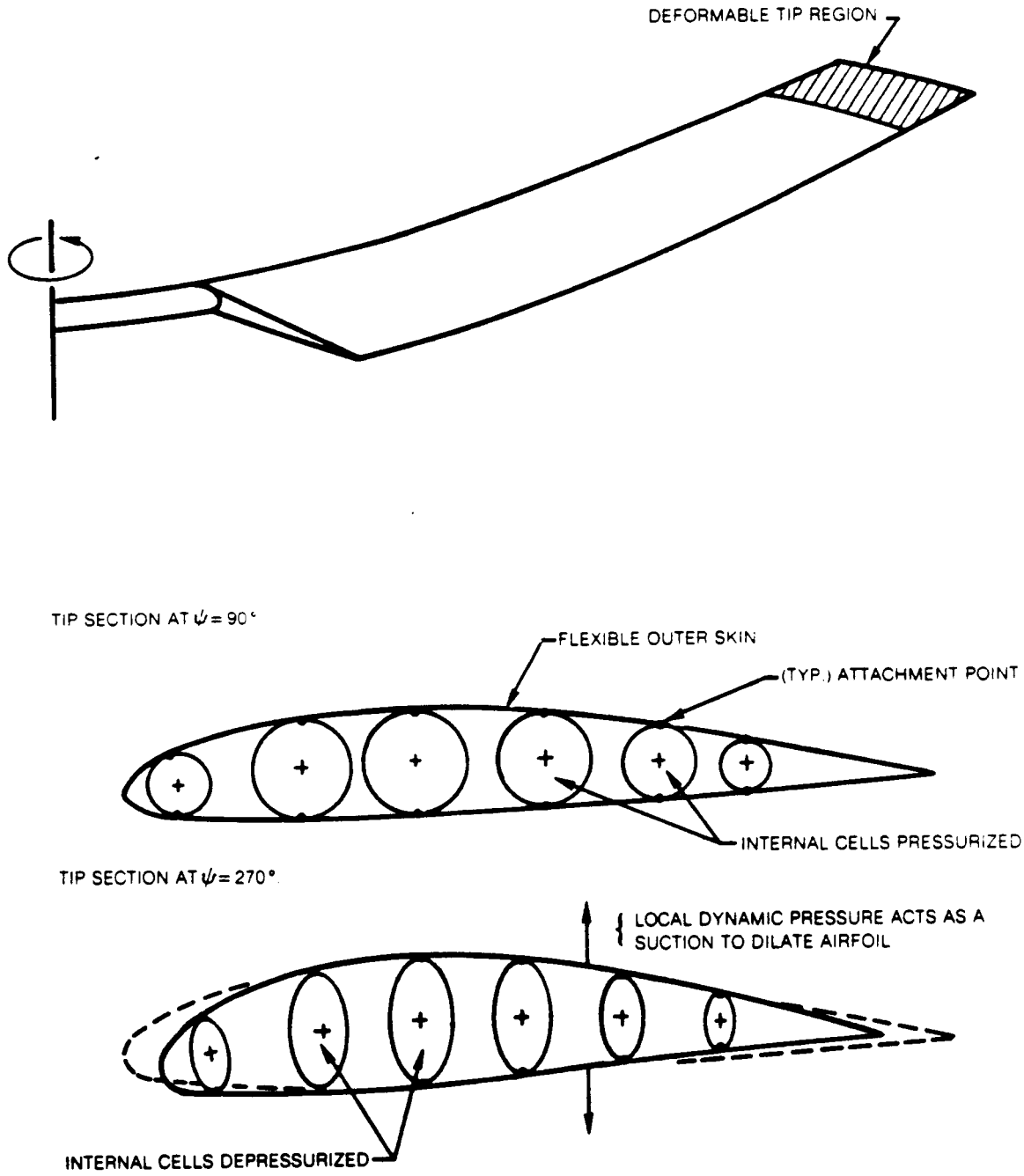

Figure 5. Pictorial of Harmonically Deformable Airfoil Tip

It is expected that appropriate gadgetry involving interblade coupling is required to achieve passive operation. Specific means for achieving this operation are discussed in the appropriate results subsection. As with the all-flying torsion tip, the pertinent performance payoff parameter for this device is the lift to (equivalent) drag ratio, L/D_e.

Analysis Requirements

Requirements for Present Study

As the descriptions of the selected appended aeroelastic devices offered in the above sub section demonstrate, these devices share identifiable characteristics which pertain intrinsically to the requirements for their successful analysis:

1. The devices each generally comprise a simple dynamic element (spring-mass-damper) with a single degree-of-freedom descriptor which couples with the aeroelastics of an otherwise conventional state-of-the-art rotor blade.

2. The direct dynamic influence of the aeroelastic devices on the hub harmonic loads is subordinate to their indirect influence via modifications to blade responses and resulting blade generated hub loads. Hence, whereas a fully-coupled, rotor-fuselage aeroelastic analysis would provide maximum rigor to the analysis, a more simple, conventional hub-fixed approach should yield adequate insights into the relative efficiencies of the devices.

3. Over some spanwise portions(s) of the blade, the incremental aerodynamic loading description must account for the motion of the aeroelastic device. Typically, this incremental loading modifies the basic aerodynamic excitations of the blade (incremental section coefficients) as well as generating airload excitations of the device itself. Furthermore, because the devices would generally be expected to produce abrupt deviations from the otherwise smooth blade geometries, abrupt and concentrated airloadings at these deviations would ensue.

4. The aerodynamic environment in which these devices (as well as the basic blade itself) operate is essentially unsteady. Multi-harmonic blade motions and potentially high reduced frequency transient phenomena impact on the operation of the three torsionally active devices and, hence, on their potential merit. This impact requires an attention to the attenuations and phase lags in both the stalled and unstalled aerodynamic loadings.

5. The operation of any blade appended device with respect to any one specific performance index cannot be isolated from the inherent aeroelastic stability of the device. Thus, the aeroelastic analysis must be sufficiently comprehensive as to be able to demonstrate any inherent instability condition caused by a selection of parameters which might otherwise demonstrate superior performance in specific selected payoff parameter.

G400PA Rotor Aeroelastic Analysis

The analysis selected as the tool for analyzing the four appended devices is the "PA" version of the United Technologies Corporation G400 Rotor Aeroelastic Analysis. As first reported in Reference 6, this basic analysis has evolved into a family of multi-purpose programs directed to the analysis of all major rotor types and complexities with application to helicopters, wind turbines and propellers.

Generally the G400 analyses are formulated on a beam bending-torsion basis and include a rigorous modeling of large, nonlinear and time-varying structural twist. The differential equations of blade bending (flatwise and edgewise) and torsion incorporate the salient features of Reference 7 and are solved using a Galerkin procedure wherein normal "uncoupled" vibration mode shapes and their spanwise derivatives along with the spanwise derivative of the blade (nonlinear) twist are combined to approximate "coupled" blade deflections. The aerodynamic description includes the use of predetermined static airfoil data, constant or variable (multiply harmonic and spanwise variable) inflow and unsteady airload effects (both unstalled and stalled). An important capability of the G400 analysis to the present study is the implementation of a rigorous method for including detailed inertial and aerodynamic loadings and internal structural (elastic) characteristics with unlimited attention to nonlinearities. An important contribution to this implementation and to the ability to calculate dynamic loads arising from concentrated load sources such as pendulum absorbers and the herein considered appended devices is the force-integration method for calculating blade stresses and hub loads (Reference 8).

The "PA" version of G400, as reported in Reference 9, was selected for the present study because it provided the best basis for meeting the above itemized requirements. In particular, by virtue of the explicit modeling of pendulum absorbers, this version already incorporated the structuring required to accommodate the differential equations for a single degree-of-freedom dynamic system attached to the rotor blade. Beyond this existing capability, however, explicit modifications were required and are described in a subsequent section.

LIST OF SYMBOLS

[A]	Spanwise aerodynamic diffusion matrix for six outermost blade segments. ND.
a_{x_5}, a_{y_5}, a_{z_5}	Components of inertial acceleration in the "5" coordinate system. m/s^2.
b	Number of blades
C	Theodorsen function
C_L/c, C_{PF}/c	Rotor aerodynamic lift and propulsive force coefficients over solidity, respectively.
C_T	Damper rate of explicit restraint of torsionally active device, Nms/rad.
c	Blade section chord, m.
c_T	Chord of appended device, m
D_e	Rotor equivalent drag (see Eq. 19), N.
e	x_2 coordinate of coincident flat-lag hinge or hingeless blade offset point m.
f	Equivalent flat plate area for defining aerodynamic drag, N.
G_T	Coupling gain for tab motion per root deflection, ND.
HP	Rotor horsepower.
K_T, K_{β_T}	Spring rate of explicit restraint of torsionally active device, (alternate forms), Nm/rad.
K_{θ_R}	Blade root torsion spring to account for control system flexibility, Nm/rad
K_1, K_2	Gain constants used for passive dynamic implementation of the harmonic dilational airfoil tip.
k_{y_T}, k_{z_T}	Mass radii of gyration of tab (or tip) mass center inertia about axes parallel and normal to tab chordline, respectively, m.

LIST OF SYMBOLS
continued

$k_{y_{10}}$, $k_{z_{10}}$	Mass radii of gyration of blade section about axes through and perpendicular to the spanwise (x_5) axis and in the chordwise and thicknesswise directions, respectively, m.
L	Rotor lift, N.
ℓ_T	Distance from tab device hinge aft to tab mass center, m.
M	Mach number
M_{app_T}	Constant applied moment about hinge for torsionally active device, Nm.
M_{resid}	Residual elastic moment about hinge resisting aerodynamic and inertia loads, Nm.
M_T	Mass of the torsionally active device, kg.
$M_{x_{6_T}}$	Moment about hinge axis of the torsionally active device.
m_o	Reference blade mass distribution, taken to be that of the 5th blade segment, kg/m.
$\bar{m}$	Blade mass distribution, (ND)
n	Blade segment index
P	Per rotor revolution
PF	Rotor propulsive force, N.
P_{x_5}, P_{y_5}, P_{z_5}	Section shear load distributions in directions of axes in the 5- coordinate system, (ND)
P_1, P_2, P_3	Static airfoil pressures defining the operation of the harmonic dilational airfoil tip, Pa.

LIST OF SYMBOLS
continued

Q	Quasi-static airfoil downwash velocity function for airfoils with tabs, m/s.
Q_E	Effective airfoil downwash velocity function for airfoils with tabs, m/s.
Q_W	Airfoil downwash velocity function for airfoils with tabs, corrected using unsteady decay parameter algorithm, m/s.
q_{θ_j}	Blade j'th torsion modal response variable.
R	Rotor radius, m.
ΔR_T	Spanwise extent of appended device, m.
$\bar{r}$	Blade spanwise coordinate, measured from offset, e, in x_5 direction, (ND)
$\bar{r}_{eff}$	Effective (area center) radius of the planform of the harmonic dilational tip, ND with respect to R.
Δr_n, Δx_n	n'th blade spanwise segment (arc) length, (ND)
S_T	Friction (Coulomb) damping moment about hinge for torsionally active device, Nm.
S_{x_1}, S_{y_1}, S_{z_1}	Components of Blade Root Shears in (nonrotating) longitudinal, lateral and vertical directions, respectively, N.
s	Aerodynamic time
V_T	Trimmed rotor flight speed, m/s and (kts)

LIST OF SYMBOLS
continued

$\left\{ \Delta X_5 \right\}$	Vector of components of incremental displacement of a point in the "5" coordinate system, m.
x_{cen}	Nondimensional blade spanwise station measured from center of rotation.
x_5, y_5, z_5	Components of the 5-coordinate system, defined to be rotating with the hub, but at the blade coned and lagged position, (ND)
$y_{10_{CG}}$	Chordwise distance of blade section mass center forward from the elastic axis, (ND).
Z_i	Perturbational thickness ratio response for the i'th blade.
α	Section angle-of-attack, deg and rad
α_e	Effective aerodynamic section angle-of-attack, including effects of unsteady decay parameter, deg.
α_Q	Quasi-static angle-of-attack, rad.
α_W	Aerodynamic section unsteady decay parameter, rad.
β	Prantl-Glauert transformation factor, ($= \sqrt{1 - M^2}$)
β_T	Torsion deflection of torsionally active device, positive TE up, rad.
β_{T_o}	Steady component of torsion related device deflection, rad.
β_{T_1}	Component of tab torsion motion due to ganging with root torsion motion, rad.
γ_{θ_j}	Deflection mode shape for the j'th torsion normal mode, (ND)

LIST OF SYMBOLS
continued

θ	Total local blade pitch angle, radians.
μ	Rotor advance ratio, (= flight speed/ΩR)
σ	Rotor solidity (= bc/πR).
τ/c	Airfoil thickness ratio.
$(\tau/c)_{1_c}$, $(\tau/c)_{1_s}$	First harmonic cosine and sine components of perturbational thickness ratio.
ϕ_c	Generalized Wagner function, with compressibility corrections.
ψ	Blade azimuthal (angular) position, rad and (deg)
Ω	Rotor rotational frequency, or speed (rpm)
$\bar{\omega}_{w_i}$, $\bar{\omega}_{v_k}$, $\bar{\omega}_{\epsilon_j}$	(Nondimensional) uncoupled natural frequencies of i'th flatwise bending mode, k'th edgewise bending mode and j'th torsion mode,

Subscripts

$( )_a$	Arising from aerodynamic loading
$( )_T$	Relating to the appended device (tip or tab)

Superscripts

$( )^{(D)}$	Pertaining to dynamic inertia loads
$( )^{(E)}$	Pertaining to elastic restraints
$( )'$	Differentiation with respect to (r/R)
$(\tilde{\ })$	Perturbational quantity
$(\bar{\ })$	Nondimensionalization by combinations of m_o, R and/or Ω
$(\overset{*}{\ })$	Differentiation with respect to (Ωt)

MATHEMATICAL DEVELOPMENT

For purposes of this study, the required modifications of the G400PA analysis fall into two main categories: those needed for the three torsionally active devices (tuned tab, control coupled tab, and the all-flying tip), and those for the dilational section tip. The first part of this section describes the additional formulations required to convert the existing G400PA formulations for a purely mechanical conventional blade appended, pendular absorber to those for an aerodynamically active pendular mass whose hinge is now oriented parallel to the blade pitch axis. These formulations are more or less common to all three torsionally active devices. Where noted, some are appropriately pertinent to only one or two of these devices. The last part of this section deals with design considerations relevant relevant to the dilational section tip and with those G400PA modifications necessary for its analysis within the scope of the present study.

Torsionally Active Devices

Four basic formulations and subsequent modifications of the G400PA were required:

- Development of the inertia loadings for a pendular mass with an axially mounted hinge.
- Inclusion of elastic and/or coupling constraints of the device about the hinge.
- Extension of classic (frequency domain) unsteady airloads formulations to a time-history solution format.
- Development of a method for accounting for spanwise aerodynamic cross-talk effects. These arise from the abrupt loadings changes at the boundaries of the devices.

Supplementary Assumptions

To achieve a successful modeling of the torsionally active devices the following list of assumptions were made (in addition to those stated in Reference 9):

1. The device is a rigid body attached to the blade proper at two points as defined by the spanwise centers of two selected blade segments, as typically used for blade segmentation. The hinge line defined by these two points is nominally parallel to the blade (reference) pitch axis.

2. The torsional device is uniform in properties in the spanwise direction.

3. For purposes of defining the incremental inertia loads on the blade proper due to device motion, the device is approximated by two incremental mass distributions at each of the two attachment segments, each defined by half the device mass.

4. The device is mechanically restrained to the blade by a parallel combination of spring, damper, friction, constant valued and control coupled moments (see Figure 6).

5. The normal (uncoupled) mode input preparation calculations for the blade proper are to be performed with a blade mass distribution appropriate to the blade (as designed to include the device) but with the actual moveable device mass removed. This moveable device mass must then be explicitely added in the G400PA equation description.

6. The aerodynamic descriptions for both the device and blade proper should include unsteady effects. Because stall flutter represents a "higher-order" dynamic phenomenon beyond the scope of the present study, the appropriate unsteady effects are those two-dimensional formulations based on unstalled potential flow. The classic theory of Theodorsen and Garrick (Reference 10) is an appropriate basis.

7. Aerodynamic spanwise crosstalk effects are limited to those circulatory airloads accruing only from the incremental lift loads due to device deflection. These crosstalk effects are approximated by a constant (cross-talk) matrix premultiplying the (two-dimensional) strip theory incremental spanwise airload distribution.

Inertia Load Distributions for Pendular Mass

The derivation of the dynamic loads acting on the torsionally active device follows from a straightforward application of appropriate coordinate transformations and differentiations of a position vector. Using Equation (35) of Reference 6 as a starting point and referring to Figure 6, one can write the

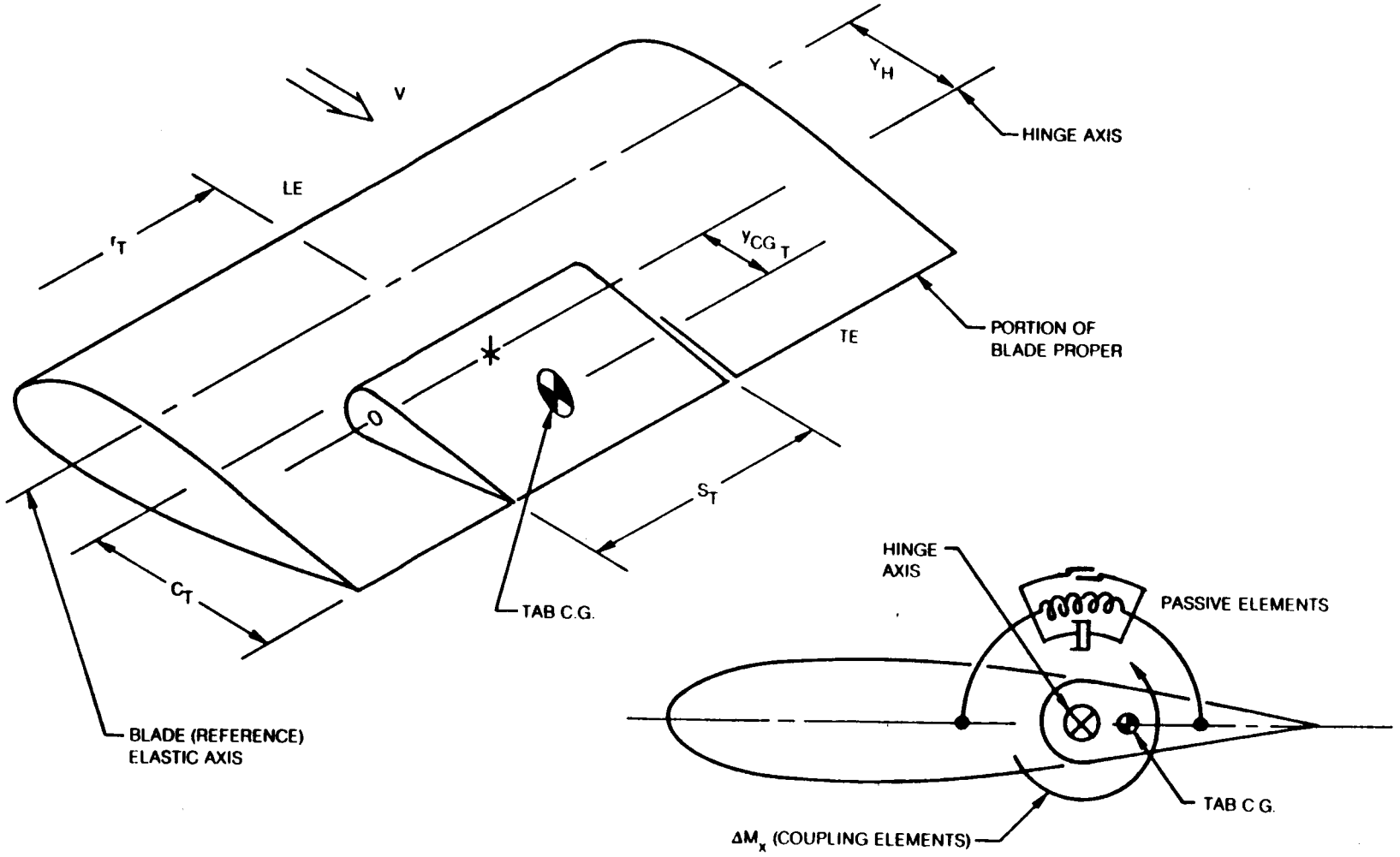

Figure 6. Geometrical and Mechanical Modeling of the Torsionally Active Devices

incremental (nondimensional) position vector for a mass element on the torsional device as:

$$\left\{\Delta x_5\right\} = (\ell_T - y)\begin{Bmatrix} -z_5' \sin\beta_T \\ -\cos\Theta\cos\beta_T - \sin\Theta\sin\beta_T \\ -\sin\Theta\cos\beta_T + \cos\Theta\sin\beta_T \end{Bmatrix} + z\begin{Bmatrix} -z_5' \cos\beta_T \\ \cos\Theta\sin\beta_T - \sin\Theta\cos\beta_T \\ \sin\Theta\sin\beta_T + \cos\Theta\cos\beta_T \end{Bmatrix} \quad (1)$$

Θ and β are, respectively, the total pitch angle of the blade section and the (T.E. up) deflection of the torsion device about the hinge. From Equation (1) can be derived the components of incremental inertial acceleration, $\left[\Delta a_{x_5}, \Delta a_{y_5}, \Delta a_{z_5}\right]$, which arise solely from the pendular motion of the torsionally active device. Combination of these incremental acceleration components with those components arising from motion of the blade itself defines the total inertia loads acting on the point mass of the torsional device.

The inertia moment acting on the torsional device about the hinge is obtained by integrating the differential inertia moments over the device corss section area:

$$M_{x_{6_T}}^{(D)} = -\Delta R_T \int_A \Big\{ a_{y_5}\left[(\ell_T - y)\sin(\beta_T - \Theta) + z\cos(\beta_T - \Theta)\right] + (a_{z_5} - z_5' a_{x_5})\left[(\ell_T - y)\cos(\beta_T - \Theta) - z\sin(\beta_T - \Theta)\right]\Big\} dm \quad (2)$$

Upon expansion of the inertia acceleration components (a_{x_5}, a_{y_5}, and a_{z_5}) in a Taylor Series in the chordwise and thicknesswise position vector components, y and z, respectively, Equation (2) can be written in terms of conventional mass descriptors:

$$M_{x_{6_T}}^{(D)} = -M_T\Big\{\ell_T\left[a_{y_5}\sin(\beta_T - \Theta) + (a_{z_5} - z_5' a_{x_5})\cos(\beta_T - \Theta)\right] + k_{y_T}^2\left[\frac{\partial a_{y_5}}{\partial z}\cos(\beta_T - \Theta) - \frac{\partial}{\partial z}(a_{z_5} - z_5' a_{x_5})\sin(\beta_T - \Theta)\right] + k_{z_T}^2\left[-\frac{\partial a_{y_5}}{\partial y}\sin(\beta_T - \Theta) - \frac{\partial}{\partial y}(a_{z_5} - z_5' a_{x_5})\cos(\beta_T - \Theta)\right]\Big\}_{y=z=0} \quad (3)$$

Equation (3) is then used as the basis for defining the dynamic equation for the torsional device.

The modifications to the blade modal dynamic equations utilize supplementary assumption 3 given above. At each of the two blade spanwise segments wherein the device is attached, the inertia load distribution is modified to include three effects:

- o The incremental load due to torsion device motion about the hinge using tab mass and the incremental inertial acceleration components.
- o The combined masses of the blade proper and the device together with the inertia accelerations of the blade proper.
- o The effective change in combined section center-of-gravity location (both chordwise and thicknesswise) caused by tab deflection.

Elasto-mechanical Torsion Restraints

As shown in Figure 6, four types of elasto-mechanical constraints are used to attach the torsional device to the blade. The three passive elements, (spring, damper, and friction) are common to all three torsionally active devices:

$$\left(M_{x_6}^{(E)}\right)_1 = -K_T\beta_T - C_T\dot{\beta}_T - S_T\,\mathrm{sgn}(\dot{\beta}_T) \tag{4}$$

For the all-flying tip, an additional constant moment constraint, M_{app_T}, is added. This constant applied moment could be implemented through the use of internal gadgetry which might utilize the centrifugal force field, or by combining the torsion spring rate, K_T, together with a built-in tip deflection. The combined passive restraint is then given by:

$$M_{x_6}^{(E)} = -K_T\beta_T - C_T\dot{\beta}_T - S_T\,\mathrm{sgn}(\dot{\beta}_T) + M_0 \tag{5}$$

As can be seen in Figure 2, the motion of the tab is actually comprised of two parts: a gross motion part, β_{T_1}, directly geared by appropriate bellcranking to the elastic torsion deflection of the blade at the root, and a perturbational part, $\tilde{\beta}_T$, governed by the passive impedances (stiffness and damping) of the bellcranking itself. The gross motion part of the tab deflection is, therefore, defined using blade torsion mode shapes which are

calculated using root torsion springs. Such mode shapes have nonzero root values, $\gamma_{\theta_j}(0)$, which can be geared ghrough a gain parameter, G_T, to define the gross motion. Thus, the total control coupled tab motion is defined by:

$$\beta_T = \beta_{T_1} + \tilde{\beta}_T \tag{6}$$

where

$$\beta_{T_1} = G_T \sum_{j}^{NTM} \gamma_{\theta_j}(0)\, q_{\theta_j} \tag{7}$$

Time Domain Unsteady Airloads

Each of the three torsionally active devices entails a significant degree of coupling between the blade flatwise bending modes and the torsional response of the device itself. Consequently, the potential exists for aeroelastic instability with these devices. Such instabilities, moreover, could occur at response frequencies sufficiently high to warrant the inclusions of the lags and attenuations due to unsteady aerodynamic effects. This is especially true for the passive tuned tab which is to operate at blade passage frequencies. The presence of a trailing edge tab with two of the torsion devices, as a distinct aerodynamic element, further defines an aerodynamic modeling over and above the usual quasi-static strip theory typically used for the nonappended blade. Finally, the inclusion of these unsteady airloading and trailing edge tab features is required in a time-domain format. All the G400PA response calculations are performed by (time) integrating the nonlinear dynamic equations and the aerodynamics must therefore be defined by appropriate differential equations.

Unsteady Decay Parameter

The approach followed herein draws upon the use of the unsteady decay parameter, α_W, described in detail in Ref. 11 and defined as follows:

$$\alpha_w = \alpha_0 \cdot \frac{1}{2} + \int_0^s \alpha_0 \beta \frac{\partial \phi_c}{\partial s}(s-\sigma, M)\, d\sigma \tag{8}$$

This parameter is an equivalent embodiment of the Wagner function (and its Fourier transform counterpart, the Theodorsen function - see Ref. 12). This α_W parameter when taken together with the quasi-static angle-of-attack defines an equivalent angle-of-attack:

$$\alpha_E = \alpha_0 - \alpha_w \tag{9}$$

which when used quasi-statically produces airloads which closely approximate the unsteady loadings resulting from indicial responses (Wagner problem) as well as sinusoidal ones (Theodorsen problem).

Trailing Edge Tab Effects

In the Ref. 10 formulation for the unsteady aerodynamic loading for a two-dimensional airfoil with tab, the effects of circulatory unsteady effects are seen to be contained in the single product CQ. This product consists of the familiar Theodorsen function, C, and a function Q which is analogous to a product of the quasi-static angle-of-attack (without tab), α_Q, and the freestream velocity, V. This analogy suggests the heuristic approach selected herein for combining the unsteady decay parameter approach described above with the formulations of Theodorsen and Garrick (Ref. 10).

Specifically, but for the CQ terms in the equations for lift, moment and tab moment given by Theodorsen and Garrick, all other terms are already defined in the time domain. The CQ term is redefined into the time domain by means of an equivalent Q:

$$Q_E = Q - Q_w \tag{10}$$

where

$$Q_w = Q \cdot \frac{1}{2} + \int_0^s Q\beta \frac{\partial \phi_c}{\partial s}(s-\sigma, M)\, d\sigma \tag{11}$$

Just as α_E is used quasi-statically to include unsteady effects, so too is the Q_E parameter used as a substitution for the CQ frequency-domain defined product.

Spanwise Crosstalk Effects

As demonstrated by References 13 and 14, the sole use of strip theory cannot adequately describe the airloading in the vicinity of either boundary of the tab. In such instances the incremental loadings predicted over the span of the tab are realistically diffused over the adjacent portions of the blade (or wing). This has the result that the actual effectivity of the tab is somewhat reduced from what would be calculated using strip theory.

The rigorous accounting of the three-dimensional characteristics of a deflected tab on a helicopter rotor blade in forward flight does not yet exist and some form of "first order" approximation is required. The approach used herein is based on a "spanwise diffusion" matrix, which when post-multiplied by the two-dimensional loading distribution vector gives an approximation to the three-dimensional loading. As per supplementary assumption 7 given above, this spanwise diffusion matrix, A, is applied only to the incremental loading caused by device deflection:

$$\left\{\Delta p_{z_{5_a}}\right\}_{3D} = \left[\ A\ \right]\left\{\Delta p_{z_{5_a}}\right\}_{2D} \tag{12}$$

The actual spanwise diffusion matrix used for the calculations to be discussed in the next section was calculated using NASA supplied test data for a Blackhawk helicopter rotor blade for the six (6) outboard segments selected:

$$[\ A\ ] = \begin{bmatrix} .510 & .094 & .0285 & .0239 & .0096 & .0012 \\ .100 & .500 & .160 & .080 & .028 & .0014 \\ .095 & .187 & .493 & .148 & .056 & .0016 \\ .050 & .146 & .180 & .370 & .080 & .002 \\ .050 & .0563 & .107 & .170 & .243 & .00413 \\ .120 & .150 & .205 & .395 & .600 & .100 \end{bmatrix}$$

where

$\{\ \Delta p_{z_{5_a}}\ \}$ = Incremental airload distribution due to flap (tab) deflection for segments 10 through 15. Note that the selected spanwise segmentation is as follows:

$$[\Delta x]_{10\text{-}15} = [0.5,\ 0.5,\ .05,\ .05,\ .04,\ .01\ ]$$

Harmonically Dilational Airfoil Tip

In contrast to the three torsionally active devices the operation of the harmonically dilational airfoil tip does not involve potential encounters with any known unstable aeroelastic phenomena. Thus, any aeroelastic or rather aeromechanical instabilities of this device would be governed by the type of excitation scheme used and would not necessarily be inherent in the concept itself. Thus, the focusing of the analysis on the dynamics of any one type of excitation scheme would appear to be inappropriate to the intent of the present study (i.e., to assess the aerodynamic performance payoff of the device). For this reason no incorporation of the dynamics of a potentially practical excitation scheme was made in the G400PA program. Instead, the response of the dilational tip was modeled directly wherein the amplitude and phases were input for parametric variation. For completeness, however, a potential scheme for excitation was conceived as part of this study. In the subsections to follow the actual program modifications incorporated are first discussed. Then, the potential scheme for passive excitation is described.

Variable Airfoil Thickness Ratio

The original G400PA storage and utilization of static airfoil data consisted of multi-variable tables of C_ℓ, C_d, and $C_{m_{c/4}}$ aerodynamic coefficients. Interpolation table look-up was based on selected radial station (airfoil type variation), Mach number, and angle-of-attack. For analysis of the harmonically dilational airfoil tip, the table look-up organization and interpolation with regard to radial station variation, r_n, was replaced by thickness ratio variation, τ/c:

$$C_q(M,\alpha,r_n) \rightarrow C_q(M,\alpha,\tau/C)$$

where q refers to either aerodynamic type (ℓ, d, $m_{c/4}$). Further, the total thickness ratio was assumed to consist of a steady value, $(\tau/c)_o$ which is dependent on span, and a perturbational part which varies dynamically in accordance with the operation of the device. Assuming the total thickness ratio to be limited by minimum and maximum values, the total thickness ratio is expressible as:

$$\tau/C_{use} = \begin{cases} (\tau/C_{max} ; (\tau/C) \geq (\tau/C)_{max} \\ (\tau/C \quad ; (\tau/C)_{min} < (\tau/C) < (\tau/C)_{max} \\ (\tau/C)_{min} ; (\tau/C) < (\tau/C)_{min} \end{cases} \tag{13}$$

where

$$(\tau/c) = (\tau/c)_0 + \Delta(\tau/c) \tag{14a}$$

$$= (\tau/c(r_n)) + \Delta(\tau/c(r_n,\psi)) \tag{14b}$$

The implementation of Eq. (14b) requires the definition and input of a spanwise distribution array, $(\tau/c)_{o_n}$, for the description of the baseline rotor blade, and a definition of a harmonic representation for the perturbation part:

$$\Delta(\tau/c) = \Delta(\tau/c)_{1_c}\cos\psi + \Delta(\tau/c)_{1_s}\sin\psi \tag{15}$$

The coefficients, $\Delta(\tau/c)_{1c}$ and $\Delta(\tau/c)_{1s}$, are thus the cyclic components of harmonic airfoil dilation. Together with the spanwise extent of the dilational tip, these cyclic components form the principal parameters to be varied in this study.

Preliminary Conception for Implementation

Physical Description

As schematically depicted in Fig. 7, a preliminary concept for implementation of the device would use an airfoil construction whose thicknesswise rigidity is controlled by three pressures: p_1, p_2, and p_3. The pressure p_1 is the static pressure outside the flexible outer skin and is chordwise location dependent. The pressure inside the internal pressure cells is denoted as p_2 and that inside the airfoil, but outside the internal pressure cells is denoted as p_3. Increased differential pressures within and outside the pressure cells ($\Delta p = p_2 - p_3$) would cause a thicknesswise contraction (and chordwise elongation) of the airfoil.

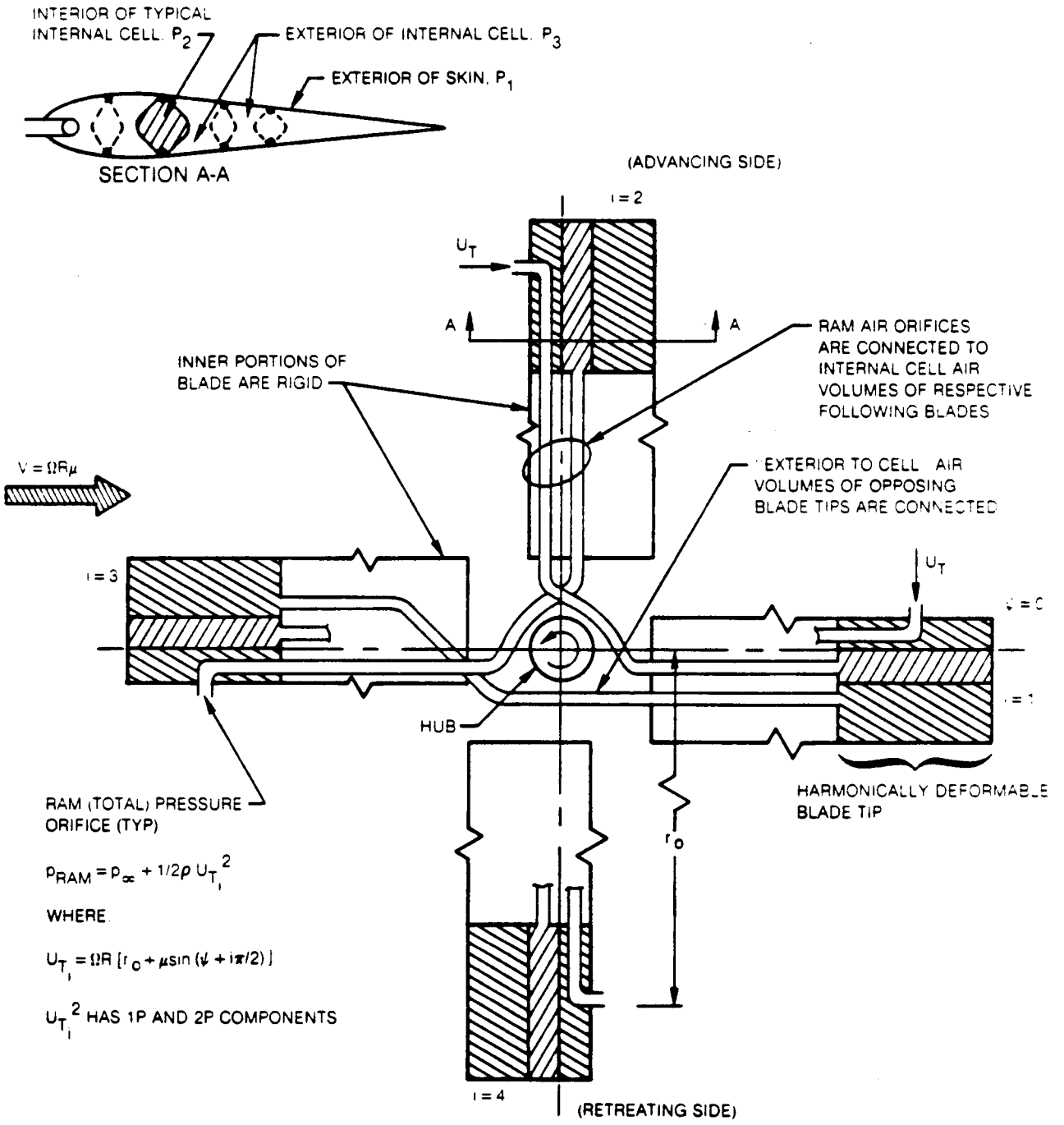

Figure 7. Schematic of Excitation Scheme for Harmonically Deformable Airfoil Tip

Because of the inherently high fatigue stress environment of this device and the need for high dynamic strains, a construction scheme utilizing composite materials might be employed. Furthermore, because the device must maintain a reasonably smooth airfoil contour within the dilational range, the outer airfoil skin would have to be structurally reinforced between the internal cell to skin attachment points.

Of equal importance to these construction considerations, however, are the required static and dynamic characteristics. Statically, the airfoil must maintain its "compromise" thickness ratio, roughly halfway between the fully dilated and contracted positions (as defined in hovering flight), in all flight conditions. That is, it must not become dilated due to the basic steady component of dynamic pressure. Dynamically, the airfoil must oscillate with significant harmonic variations in thickness at a once per rev (1P) frequency, and, hence, must be tuned to resonate at that frequency. A requirement in implementing such a device successfully arises, however, in the proper phasing of the resonant response. The required response must be approximately 180 degrees out-of-phase with the excitation from the outer static pressure, p_1, rather than the 90 degrees which would normally occur from this excitation.

An implementation of this device which potentially satisfies these requirements is based on a four-bladed rotor configuration as shown in Fig. 7. This implementation consists of the following elements: (1) total or "ram" pressure orifices located on each blade at or near the stagnation point on the leading edge, as far outboard along the blade as is practical; (2) connections of these ram pressure orifices to the internal cells of their respective following blades; and (3) interconnections of the p_3 internal pressures between opposite blades.

This implementation satisfies the phasing requirement in that the contractional excitation, 1P variation in p_2-p_3, is applied 90 deg in phase ahead of when the contraction is to occur. Furthermore, the use of ram pressure for the internal cell pressure, p_2, acts to stabilize the airfoil statically in hover. The interconnection of the p_3 pressure of the opposing blades serves the function of giving the internal ($p=p_3$) air, in effect, a harmonic accumulator so that the airfoil can undergo a 1P volume change with negligible impedance. In effect this implementation insures that the $\Delta p(=p_2-p_3)$ pressure differential is proportional to the dynamic pressure ($=\frac{1}{2}\rho V^2$) at the preceding blade.

Mathematical Modeling

A simplified mathematical modeling of the perturbational thickness ratio, ($Z=\Delta(\tau/c)$) assumes that for the ith blade, Z_i is governed by a basically second

order linear differential equation with excitation sources from static and blade advanced ram pressures:

$$\ddot{Z}_i + 2\zeta\omega_z \dot{Z}_i + \omega_z^2 Z_i = (F_i)_{static} - (F_i)_{dynam.} \tag{16}$$

where the excitation components are given by:

$$(F_i)_{static} = K_1 \frac{\rho}{2} (\Omega R)^2 \cdot 2\mu \bar{r}_{eff} \left[\sin(\psi + \frac{i\pi}{2}) - \sin(\psi + \frac{(i+2)\pi}{2}) \right] (\frac{\tau}{c}) \tag{17}$$

$$(F_i)_{dynam.} = K_2 \frac{\rho}{2} (\Omega R)^2 \left[r_0 + \mu \sin(\psi + \frac{(i+1)\pi}{2}) \right]^2 \tag{18}$$

Note that the dynamic excitation of the ith blade given in Eq. (17) uses the orifice ram pressure from the (i+1)th blade. Note also that the static pressure excitation is proportional to the total thickness ratio, (τ/c). Thus, the section dilational pressure is itself proportional, in part, to the perturbational dilation, Z_i.

The above mathematical modeling represents a first cut at defining the physics of the device. The various constants used in Eqs. (16) through (18) can presently only be roughly estimated. These equations could have been implemented in the G400PA analysis and, with appropriate estimations of the constants, solved as part of the aeromechanics of the dilational tip. This approach, however, was deemed outside the principal scope of this study and was, therefore, deferred to a more intensive design study and evaluation of this device.

RESULTS

Baseline Rotor Configuration

For the purpose of providing a numerical vehicle for evaluating the four aeroelastic appended devices, the Blackhawk UH-60A rotor blade was selected. This particular selection was made based on the timely availability of the data, and on the fact that this rotor represents a relevant, state-of-the-art, conventional (articulated) blade design. The appropriate basic blade geometry and dynamic data for this blade are summarized in Tables I and II. Table I presents the basic gross design parameters which size and dynamically define the baseline rotor blade. As this table implies, three flatwise (uncoupled) modes, one edgewise mode and one torsion mode, were used to approximate the elasto-mechanics of the blade. Table II presents the detailed distribution of pertinent geometric and mechanical (reference) blade properties used in the calculations. In subsequent calculations for each of the devices under consideration, various of these entries were appropriately altered to accommodate the physical constraints required by that device.

Trimmed Flight Conditions

Selection of Cases

Each of the four appended devices was conceived for attaining improvements in some type of performance index, either dynamic or aerodynamic, generally at the high speed end of the flight envelope. Accordingly, two basic trimmed flight conditions, which accentuate the high speed aspect, were selected for evaluating the potential gains achievable with the selected devices. Table III below summarizes the trim conditions selected for the UH-60A rotor. Note that the trims are defined for conditions at 1219 m (4000 ft) altitude and 95 deg temperature:

TABLE I

BASELINE (UH-60A) ROTOR BLADE PHYSICAL PARAMETERS

Design Parameters	Full Scale Values
Tip Speed, ΩR, m/s (f/s)	221.0 (725)
Rotor Speed, Ω, rpm	258.0
No. of Blades, b	4
Radius, R, m (ft)	8.179 (26.833)
Chord, c, m (ft)	0.527 (1.73)
Solidity, σ	0.0821
Blade Root Offset, e	0.0466R
Pitch-Flap Coupling, θ_β	-0.0170
Pitch-Lag Coupling, θ_δ	-0.030
Lag Damper Rate, Nms/rad (lb_f-ft-s/rad)	3401.7 (2509)
Effective Blade Twist, θ_1, deg	-12.8
Parameters Calculated or Estimated	
Uncoupled Mode Natural Frequencies	
1st Flatwise, ω_{w_1}, Hz	12.08 (2.809P)
2nd Flatwise, ω_{w_2}, Hz	21.14 (4.915P)
3rd Flatwise, ω_{w_3}, Hz	33.09 (7.696P)
1st Edgewise, ω_{v_1}, Hz	19.80 (4.604P)
1st Torsion, $\omega_{\theta 1}$, Hz	18.14 (4.218P)
Elastic Structural Critical Damping Ratio	
1st Edgewise Mode	0.02
Other	
Reference Mass Distribution, m_o, kg/m (lb-sec^2/ft^2)	10.642 (0.22226)
Root Torsion Motion, 1st Torsion Mode, $\gamma_{\theta_1}(0)$	0.4104

TABLE II

DISTRIBUTIONS OF GEOMETRIC AND MECHANICAL

PROPERTIES FOR BASELINE ROTOR BLADE

n	Δx	x_{cen}	$\bar{c}$	t/c	$\bar{m}$	$\bar{y}_{10cg}$	$\bar{k}_{z_{10}}$
1	.1434	.1183	.01863	.0945	3.0249	-.0001	.00570
2	.1100	.2450	.06447	.0945	.9496	-.0033	.01320
3	.1000	.3500	.06447	.0945	.9638	-.0033	.01340
4	.1000	.4500	.06447	.0945	.9683	-.0033	.01350
5	.0500	.5250	.06447	.0955	1.0000	-.0019	.01360
6	.0500	.5750	.06447	.0955	.9779	-.0016	.01370
7	.0500	.6250	.06447	.0955	.9903	-.0016	.01365
8	.0500	.6750	.06447	.0955	1.0520	.0014	.01350
9	.0500	.7250	.06447	.0955	1.2324	.0015	.01440
10	.0500	.7750	.06447	.0955	1.2331	.0015	.01466
11	.0500	.8250	.06447	.0955	1.2270	.0013	.01470
12	.0500	.8750	.06447	.0950	1.4755	.0030	.01388
13	.0500	.9250	.06447	.0945	1.6298	-.0010	.01410
14	.0400	.9700	.06447	.0945	1.2923	-.0010	.01340
15	.0100	.9950	.06447	.0945	0.3784	-.0010	.01390

TABLE III

SELECTED BASIC TRIM CONDITIONS FOR THE

UD-60A BLACKHAWK ROTOR

Case No.	V_T m/s(kts)	f $m^2(ft^2)$	Prop Force $N(lb_f)$	Lift $N(lb_f)$	C_L/σ
1	74.6(145)	2.54(27.4)	5275(1186)	77404(17401)	0.09314
2	90.0(175)	1.84(19.8)	5553(1248)	77404(17401)	0.09314

Rolling and pitcking moments are each to be trimmed to zero with a tolerance of 4067 Nm (3000 lb_f ft).

These basic trim cases were further expanded depending on the type of optional aerodynamic refinement included in the calculation. For each flight speed, three subcases were defined as A, B, or C in accordance with the aerodynamic description, respectively, being (A) quasi-static airloads, no variable inflow, (B) unstalled unsteady airloads, no variable inflow, and (C) unstalled unsteady airloads, with (quasi) variable inflow. These three subcases were alternately used for gaging the appropriate performance indices of the devices according to the accuracy refinements, respectively, required by each. The quasi-static (A) subcases were used for the harmonically deformable tip. The unsteady airloads (B) subcases were generally used for the three torsionally active devices and the (C) subcases were used for isolated calculations for the all-flying torsion tip. For the (C) subcases, the variable inflow calculations were performed using the UTRC Prescribed Wake Rotor Inflow Analysis (RIA) described in Ref. 15.

The variable inflow data input to G400PA were first calculated in the RIA with a trimming procedure using the Table III values. By this procedure, variable inflow data consistent with the trimmed conditions were obtained for use in G400PA. It should be stressed that this procedure represents an ad hoc method for including variable inflow in the aeroelastic code. The usual, more rigorous method for including variable inflow typically requires a few iterations between the rotor inflow analysis and the aeroelastic code until convergence (consistency) is reached. This procedure, however, is quite CPU time intensive even without the further onus of having to trim the two analyses. Consequently, because of the limited resources available to this study the herein ad hoc method was instead used, in hopes of obtaining at least a "first-cut" indication of the effects of variable inflow. To distinguish the results obtained herein from those which would be obtained using the more rigorous procedure they are referred to as "quasi" variable inflow results. It should be further stressed that this ad hoc method for including variable inflow would produce results which are approximately correct in G400PA only at the respective trimmed flight conditions.

Calculated Results

The results of the six trim calculations are summarized in Table IV and Figures 8 through 11. Table IV presents the actual hub forces and moment achieved (to be compared with respective values from Table III). Generally, the hub moments could be obtained to within the selected tolerances only for

the lower 145 kt flight condition. Obtaining convergent trims at the higher 175 kt flight speed conditions was a consistently difficult procedure throughout this study. The difficulty experienced in achieving systematic convergence is believed to be related to the increased extent of stall experienced on the retreating blade side at this flight speed, which thereby renders the trim process highly nonlinear. Of particular usefulness in this table are the baseline values of lift per equivalent drag, L/D_e, of median and ½PTP root torsion moment, $M_{x_5}(0)$, and of the 4P amplitudes of the components of hub shears, S_{x_1}, S_{y_1}, and S_{z_1}. Note that the lift per equivalent drag, L/D_e, accounts for required rotor power and is defined as:

$$L/D_e = \frac{L}{325.647\,HP/V_T - PF} \tag{19}$$

Table IV clearly shows the strong impact of variable inflow on L/D_e, median root torsion moment, and 4P vertical hub load calculations. Figures 8 and 9 show the ½PTP flatwise and edgewise bending moments, respectively, for the six trim conditions defined in Table IV. Since the ½PTP values include contributions from all harmonics, Figures 10 and 11 present only the 4P amplitudes of flatwise and edgewise bending moments, respectively, as an alternate basis for interpreting and evaluating the performance of the appended devices. In the subsections to follow the results will be nondimensionalized, where possible, by the appropriate baseline values given in either Table IV or Figure 8 through 11.

TABLE IV

SUMMARY OF G400PA TRIM CALCULATIONS ACHIEVED

FOR UH-60A BLACKHAWK ROTOR

	Trim Case					
	1A	1B	1C	2A	2B	2C
V_T, m/s (kts)		74.6 (145)			90.0 (175)	
Advance Ratio, μ		0.338			0.407	
Unsteady Airloads	N	Y	Y	N	Y	Y
Quasi-Variable Inflow	N	N	Y	N	N	N
Hub Moment, Nm, (lb_f-ft)	2252 (1661)	764 (563)	348 (257)	4603 (3394)	5300 (3909)	3626 (2674)
C_L/σ	0.0885	0.0944	0.0915	0.0961	0.0950	0.0881
C_{PF}/σ	0.00661	0.00633	0.00643	0.00764	0.00679	0.00653
L/D_e	7.184	7.417	9.919	6.684	6.572	5.405
$M_{x_5}(0)$, Nm (lb_f-in)	-580.0 (-5133)	-542.1 (-4798)	-417.1 (-3692)	-661.8 (-5857)	-655.0 (-5797)	-492.7 (-4361)
$\frac{1}{2}PTP(M_{x_5}(0))$, Nm, ($lb_f$-in)	694.4 (6146)	656.8 (5813)	668.0 (5912)	984.3 (8712)	903.4 (7996)	809.0 (7160)
$S_{x_1}^{(4)}$, N (lb_f)	1157 (260)	1312 (295)	783 (176)	2082 (468)	1948 (438)	1517 (341)
$S_{y_1}^{(4)}$, N (lb_f)	520 (117)	930 (209)	547 (123)	1366 (307)	1472 (331)	1192 (268)
$S_{z_1}^{(4)}$, N (lb_f)	351 (78.9)	377 (84.8)	816 (183.4)	314 (70.7)	234 (52.8)	940 (211.21)
Device Applicability						
Passive Tuned Tab		X			X	
Control Coupled Tab		X			X	
All-Flying Tip		X	X		X	X
Harmonic Dilational Airfoil	X			X		

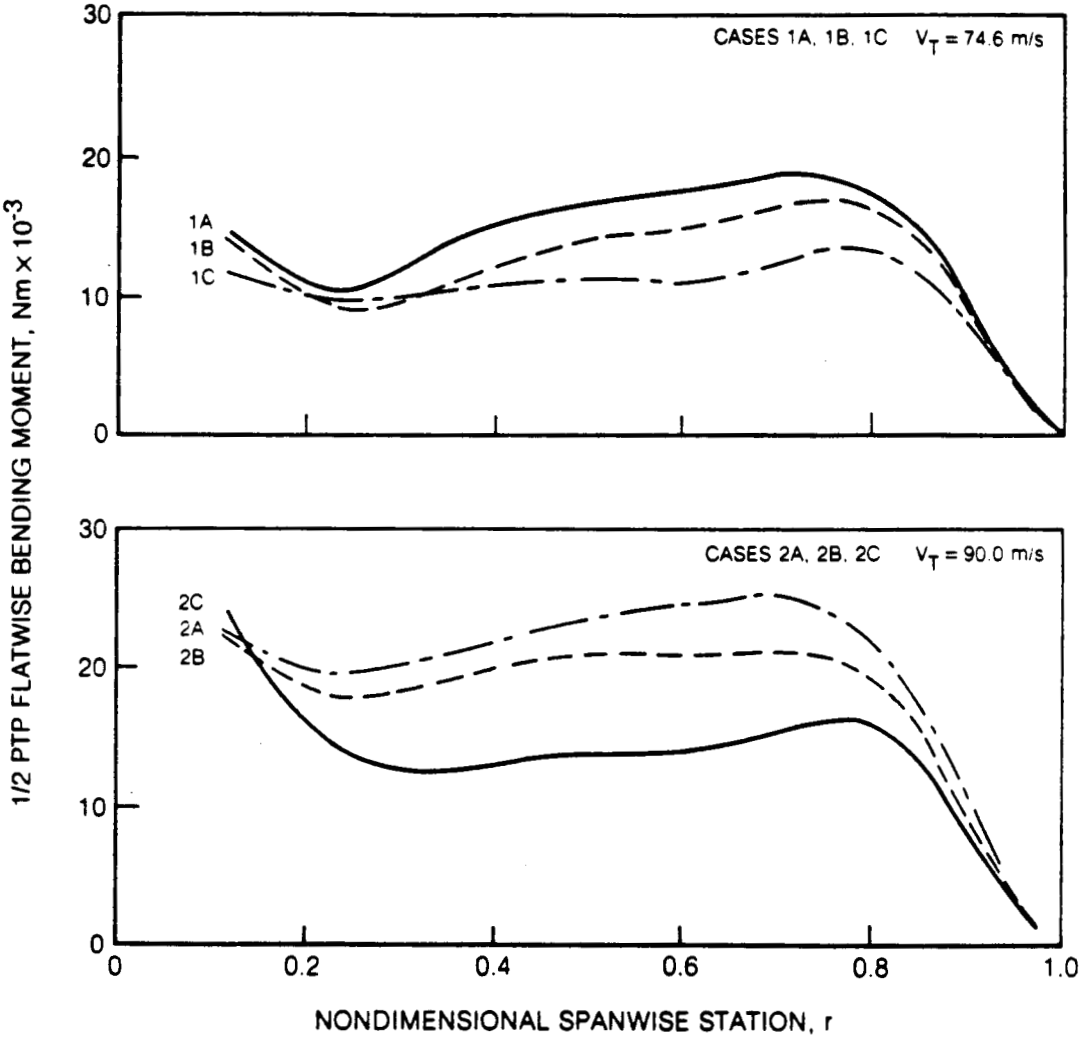

Figure 8. Spanwise Variation of 1/2PTP Flatwise Bending Moment for Trimmed Baseline Cases

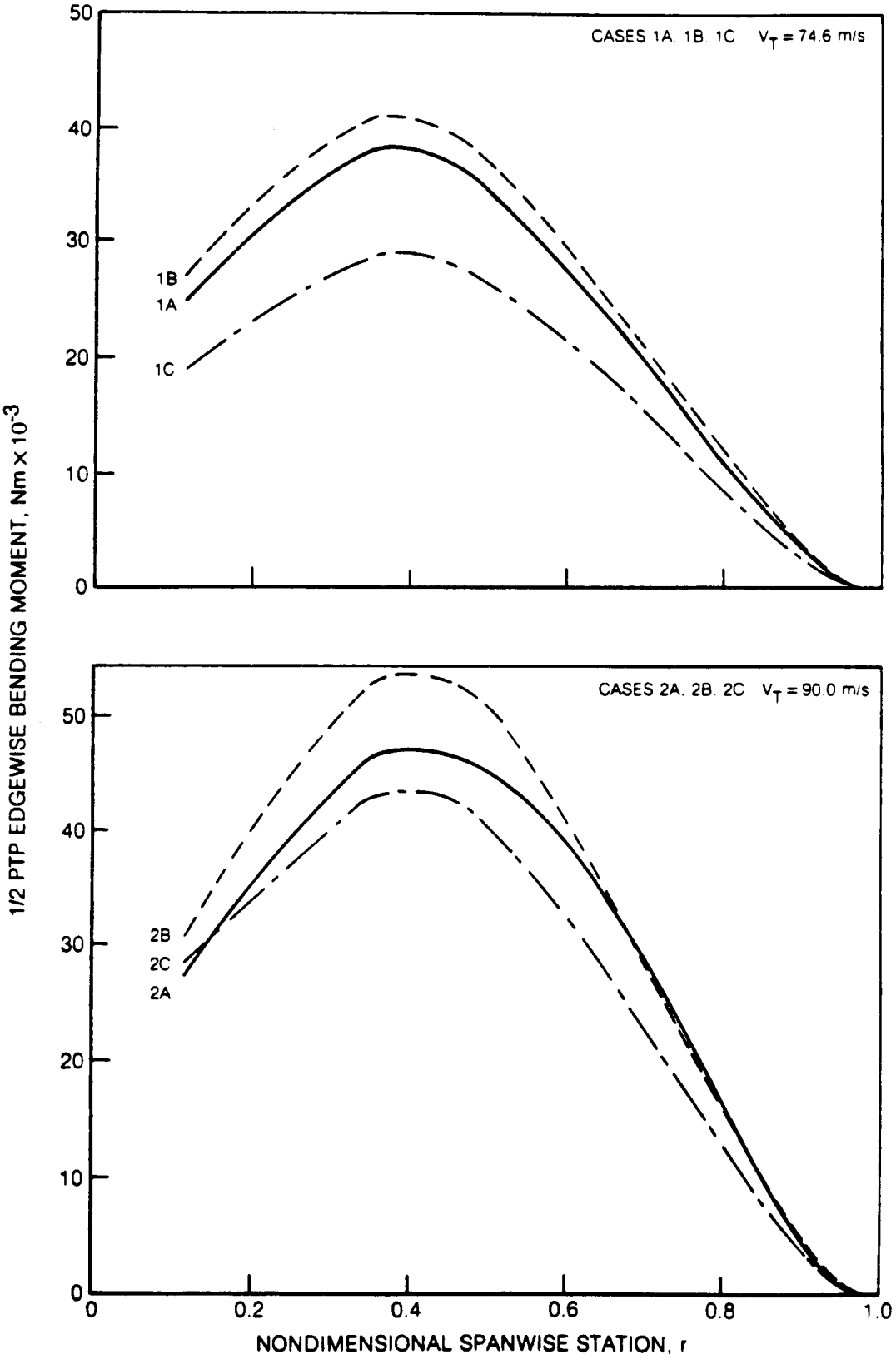

Figure 9. Spanwise Variation of 1/2PTP Edgewise Bending Moment for Trimmed Baseline Cases

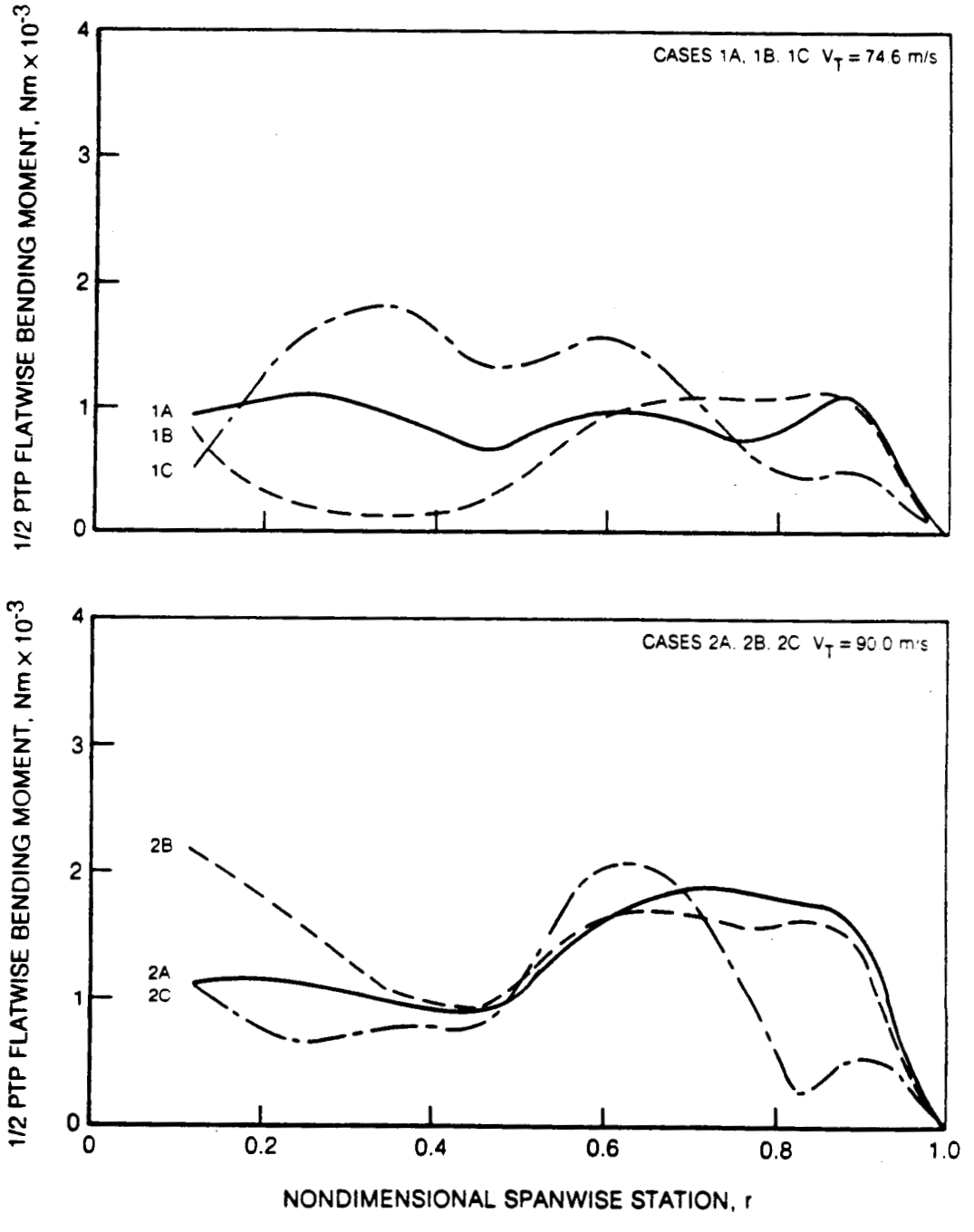

Figure 10. Spanwise Variation of 4P Flatwise Bending Moment for Trimmed Baseline Cases

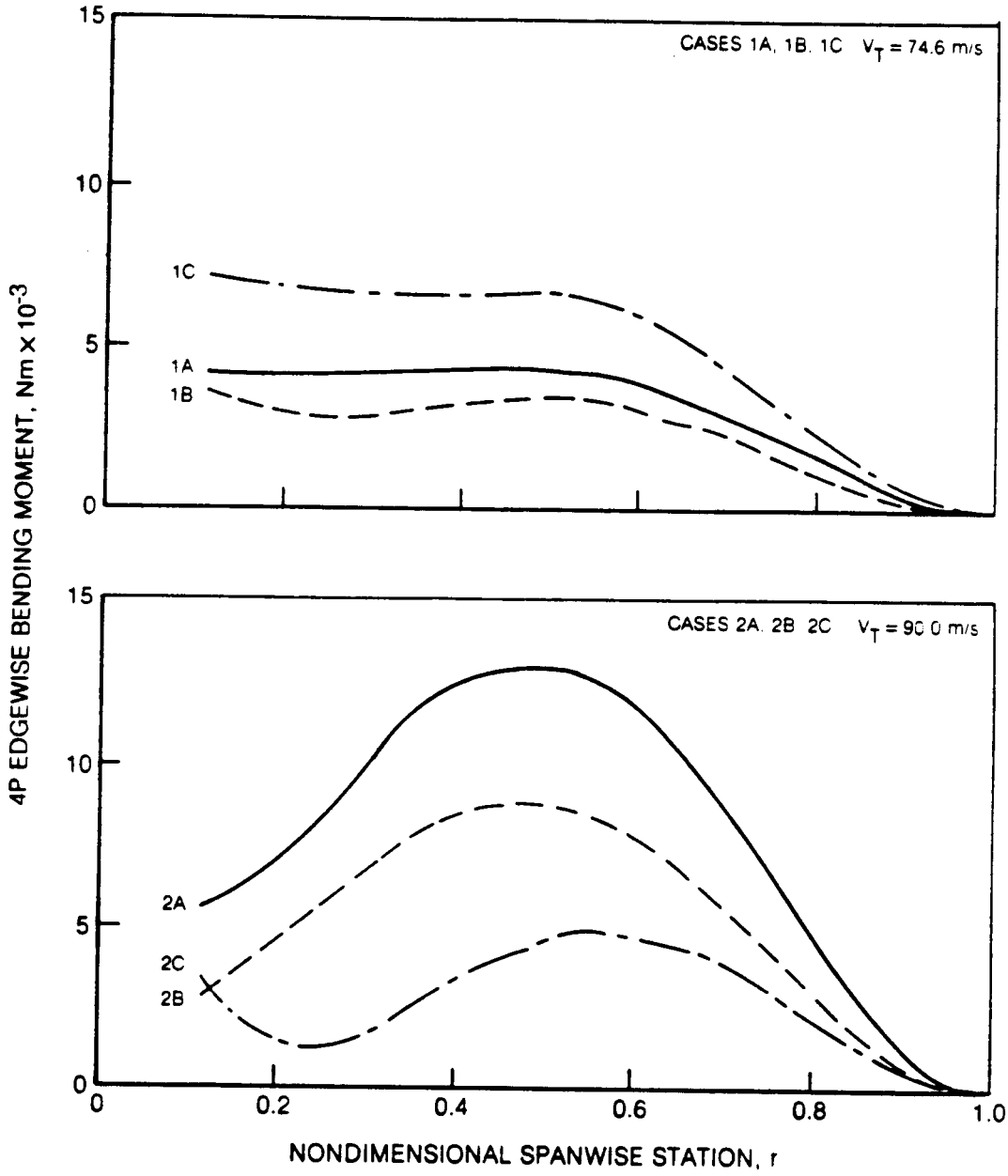

Figure 11. Spanwise Variation of 4P Edgewise Bending Moment for Trimmed Baseline Cases

Passive Tuned Tab

Background

The preliminary development of this device was performed using a separate simplified aeroelastic analysis which was only loosely coupled with the G400PA analysis (see Reference 16). As described in this report, the basis of the passive tuned tab was simply conceptualized as shown in Figure 12. Generally, this conceptualization assumes that the effect of the tab motion on the blade proper is limited to the incremental airloads derived from the tab motion. As shown in the figure, one incremental normal airload results from an effective camber induced shift of the lift coefficient for a fixed section angle-of-attack. The camber change also creates a shift in the blade pitching moment coefficient which in turn creates an additional airload by twisting the blade to create a change in the section angle-of-attack itself. When the tab responds harmonically, the resulting incremental airloads can add to or subtract from the inherent (blade alone) airloading depending on the amplitude and phase of tab motion.

The excitation of the tab was assumed to be limited to that induced inertially by the blade as it flaps (both as a rigid body and flexibly) and pitches. The role of the G400PA analysis in this simplified tab analysis was to provide the basic blade aeroelastic responses used to excite the tab. The final harmonic hub shears can then be calculated using the incremental tab loads (both inertial and aerodynamic) together with those predicted by the G400PA analysis.

Preliminary Analytic Results

An example of the vertical hub shear loads as predicted by this simplified analysis for the Blackhawk rotor is presented in Figure 13 (taken from Reference 16). It is the favorable findings reported in this reference that identified the potential for this device. As reported in this reference, the interpretation of the Figure 13 results are as follows:

"To study the effectiveness of the passive tuned tab, a baseline tab configuration was selected and variations in tab design parameters from the baseline configuration was selected and variations in tab design parameters from the baseline configuration were investigated...

Placement of the tab along the blade span is critical for tab effectiveness. This is shown in Figure (13). The predicted vibratory root vertical shears are shown as a function of tab spanwide location for a tab with length equivalent to 10 percent of the blade radius. Results are shown for two tab tunings: 5/rev and 10/rev. The tab location for maximum effectiveness is between 50 and 70

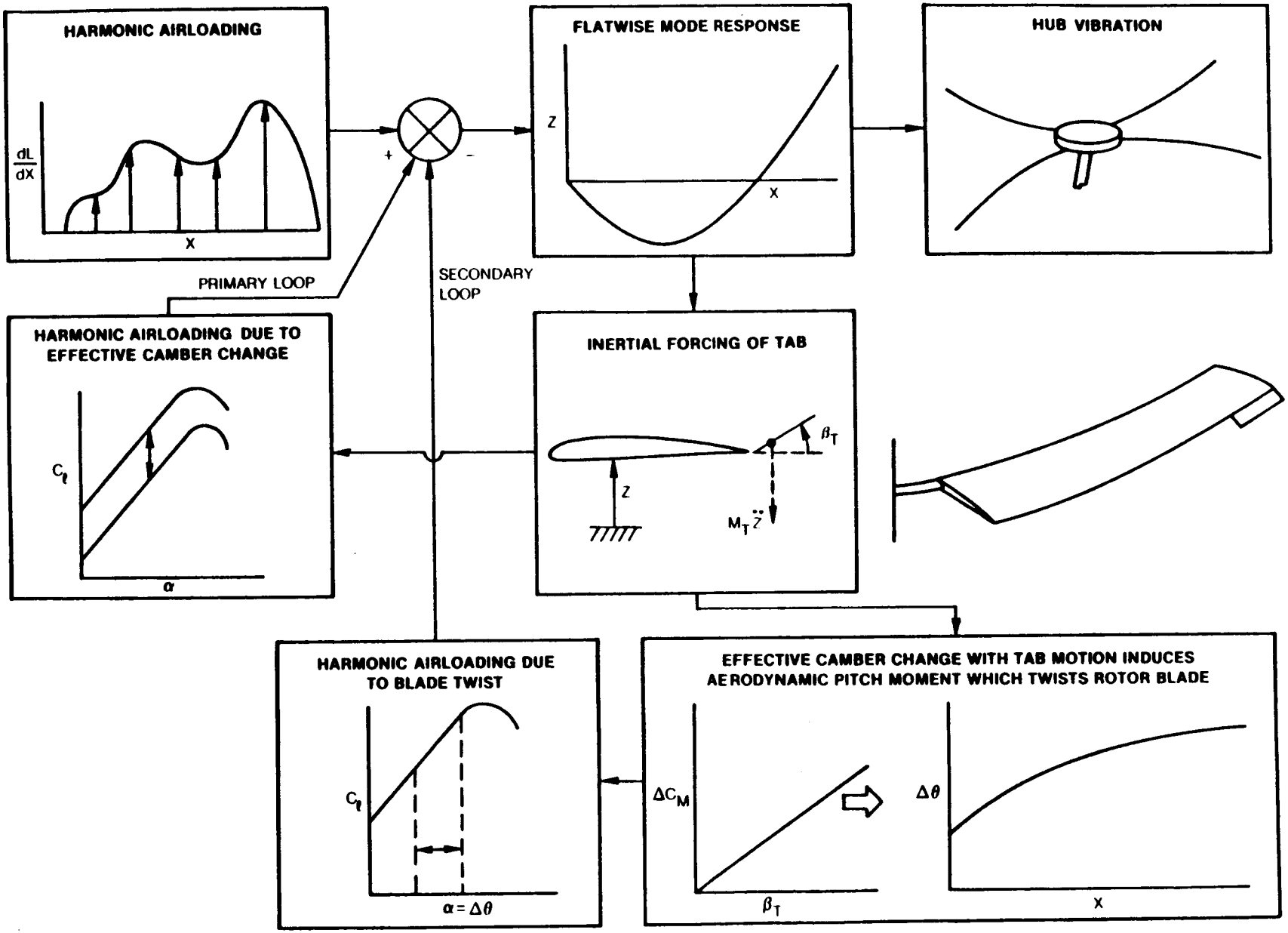

Figure 12. Simplified Conceptualization of the Passive Tuned Tab

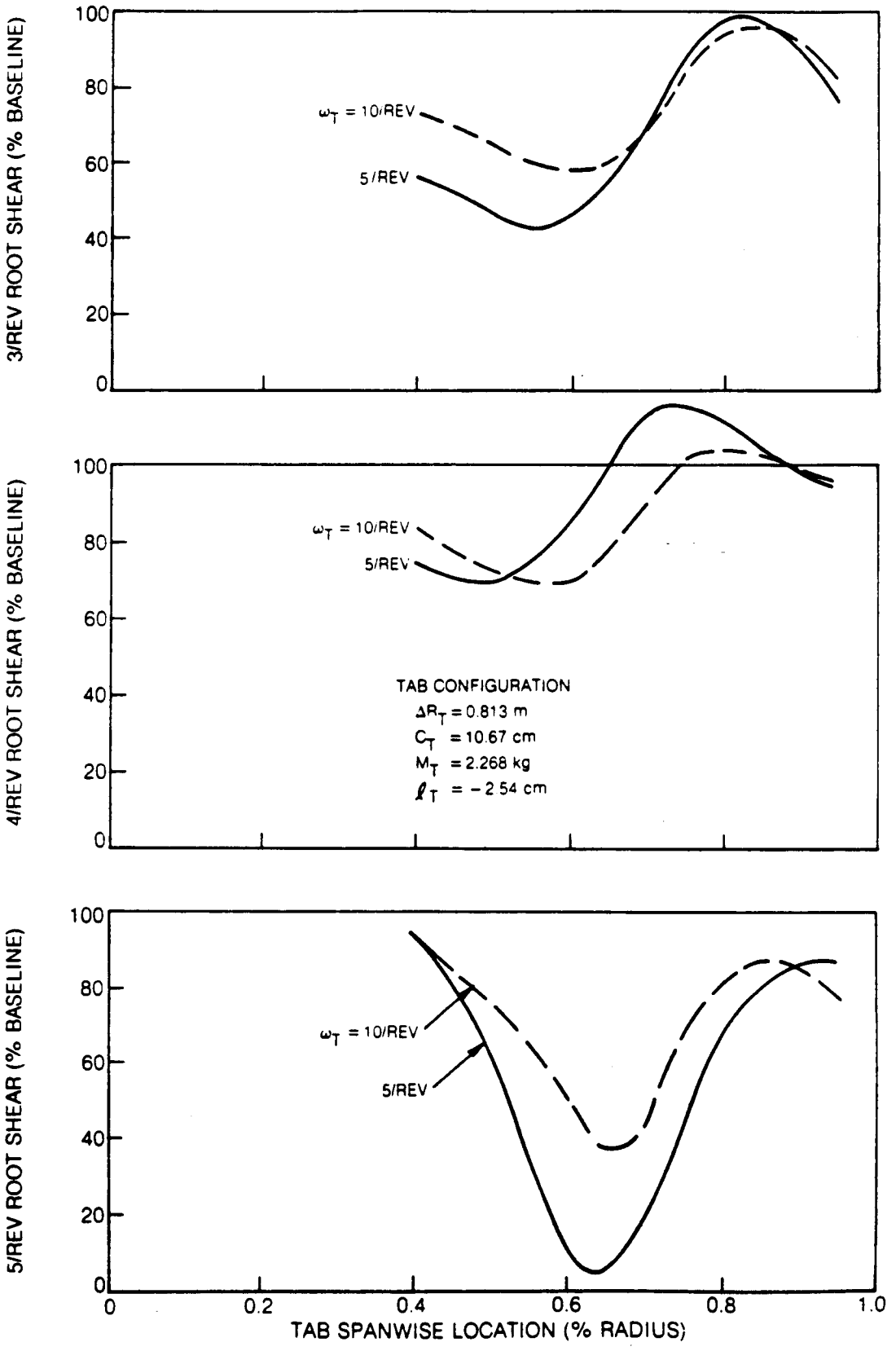

Figure 13. Results of Simplified Analysis — Effect of Passive Tab Spanwise Location on Root Vertical Shears, $\mu = 0.4$, $C_T/\sigma = 0.09$

percent blade radius. This result is attributed directly to the influence of the flatwise mode shapes on the excitation of the tab. Both first and second flatwise modes have antinodes in this region, and since the tab is inertially excited by the blade flatwise motion, more excitation occurs at flatwise antinodes than at flatwise nodes. The node points for these same two flatwise modes are between 75 and 90 percent and Figure 13 shows that this is the region of lowest tab effectiveness. In fact, amplification of the 4/rev root vertical shears also occurs in this region. The blade tip is also an antinode for the blade flatwise modes but Figure 13 shows that effectiveness for a tab located at the blade tip is not as good as for a tab near midspan. The reason for this apparent anomaly is related to the influence of the rigid body flatwise mode on tab excitation. Even though the rigid body flatwise mode contributes little to the root vertical shear, its motion is appreciable at 3, 4, and 5/rev. In fact, the rigid body flatwise mode has more motion at 3, 4, and 5/rev than the second flatwise mode (ω=5.1 rev). The influence of the rigid body mode on the tab excitation is therefore detrimental because the tab responds to null the vertical shear caused by the vertical motion. From this it is clear that, based on the rigid body flatwise mode shape, an inboard tab location is better than an outboard tab location in order to reduce the tab response to the rigid body mode. For example, at mid span the rigid body flatwise mode shape has only half the deflection at the blade tip, so the influence of the rigid body flatwise mode on the tab response is also cut in half.

Figure 13 also shows the effect of tab tuning on the vibratory root vertical shears. Overall, the 5 per rev tuning provides better vibration alleviation than the 10 per rev tuning. This is because tab angular motion increases with a decrease in tab natural frequency, and increased tab motion provides increased control authority. For a tab located at 60 percent radius with a 5/rev tuning, the percent reductions in vibratory shears are 54, 15, and 88 percent for 3, 4 and 5/rev, respectively. However, the tab angular motions associated with this level of root shear reduction may violate design constraints."

Limitations of Simplified Analysis

As articulated in an above subsection, the simplified analysis omits two forms of blade-to-tab coupling: the aerodynamic excitation of the tab due to blade motion, and the inertia excitation of the blade proper due to that motion. The latter type of coupling in large measure defines the elasto-mechanical "pendular absorber" dynamics which the tab imposes on the blade because of its mass. A potentially weak element of the simplified analysis is the ad hoc combining of some calculations of the (nonlinear) G400PA calculations with those of the (linear) simplified tab equations. A major limitation of the forced response simplified analysis is that it only obtains

response solution at integral order harmonics of rotor speed. As such, the flutter eigenvalue solution is eliminated. Thus, this simplified analysis cannot identify aeroelastically unstable configurations.

Parameter Selection For G400PA Calculations

Based on the results of the Reference 16 simplified calculations, an initial design tab configuration was selected and variations were made in four of the primary parameters.

Initial Design Configuration

The initial design configuration was defined by the following parameter selection:

- o nominal span, ΔR_T 0.15R
- o mass, M_T . . . . . 1.612 kg
- o (aft) hinge location, y_{10_H} . . . . . 0.290 m
- o tab chord, c_T . . . . . 0.105 m
- o coincident tab L.E. and hinge
- o (aft) tab c.g. location from hinge . . . . . -0.026 m (-.25 c_T)
- o chordwise radius of gyration (about c.g.) . . . . . 0.030 m
- o viscous damper rate . . . . . 0.122 Nms/rad
- o torsion spring rate . . . . . 653.5 Nm/rad

This combination of parameters gives an uncoupled, undamped natural frequency of 13.105P.

Parametric Variations

The parametric variations used are as follows:

- o (2) spanwise c.g. locations . . . . . (0.575R, 0.913R)
- o (2) masses (and proportional spring rates to maintain uncoupled frequency) . . . . . (3.225 kg, 0.806 kg)
- o (3) uncoupled frequencies (maintaining constant mass) . . . . . (3.91P, 7.62P, 11.37P)
- o (3) chordwise c.g. locations . . . . . (-.125 c_T, 0, +.125 c_T)

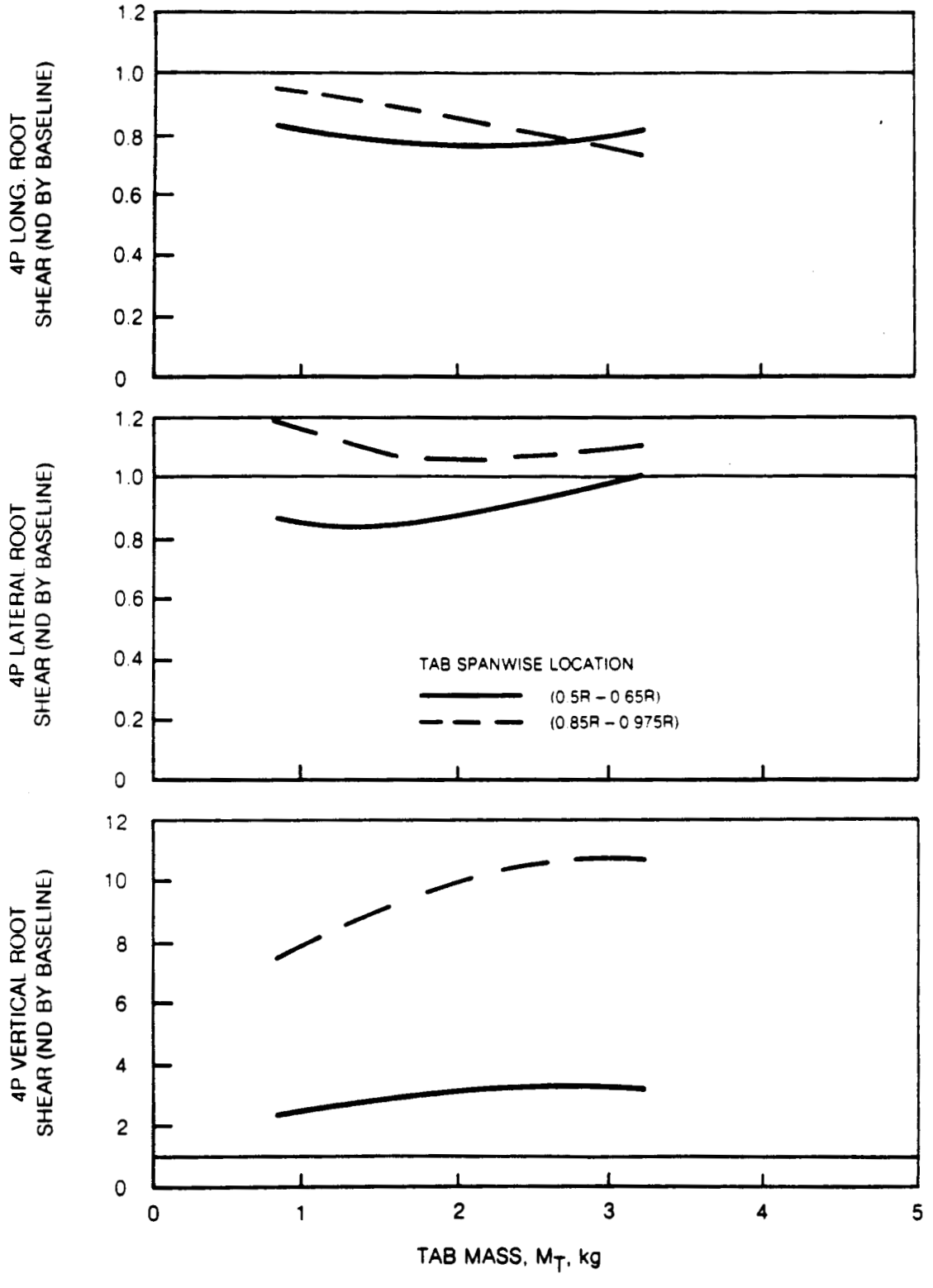

Figure 14. Variations in Components of 4P Hub Shear with Passive Tuned Tab Mass, 90 m/s Flight Speed ($\mu = 0.4$)

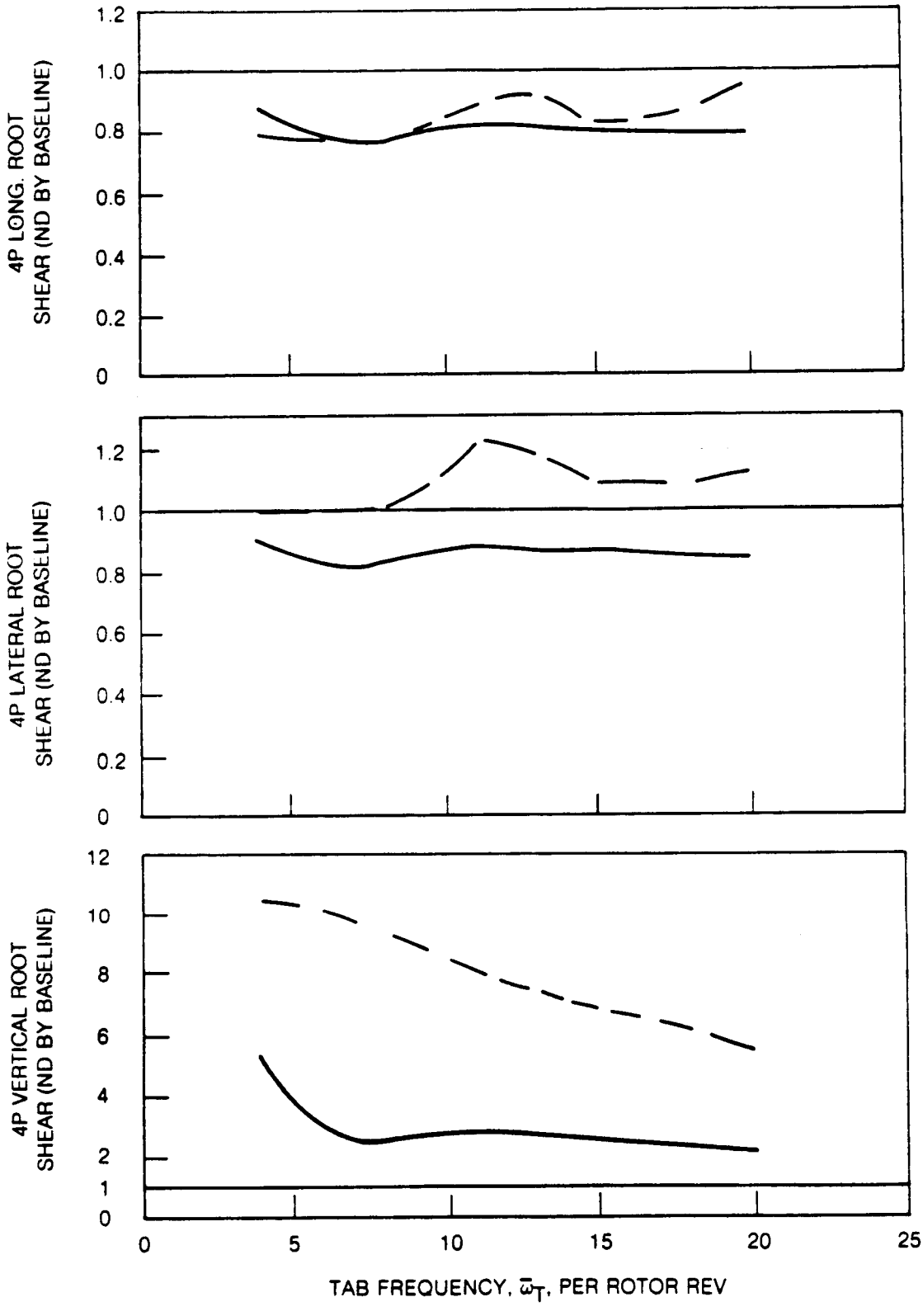

Figure 15. Variations in Components of 4P Hub Shear with Passive Tuned Tab Uncoupled Tab Frequency, 90 m/s Flight Speed ($\mu = 0.407$)

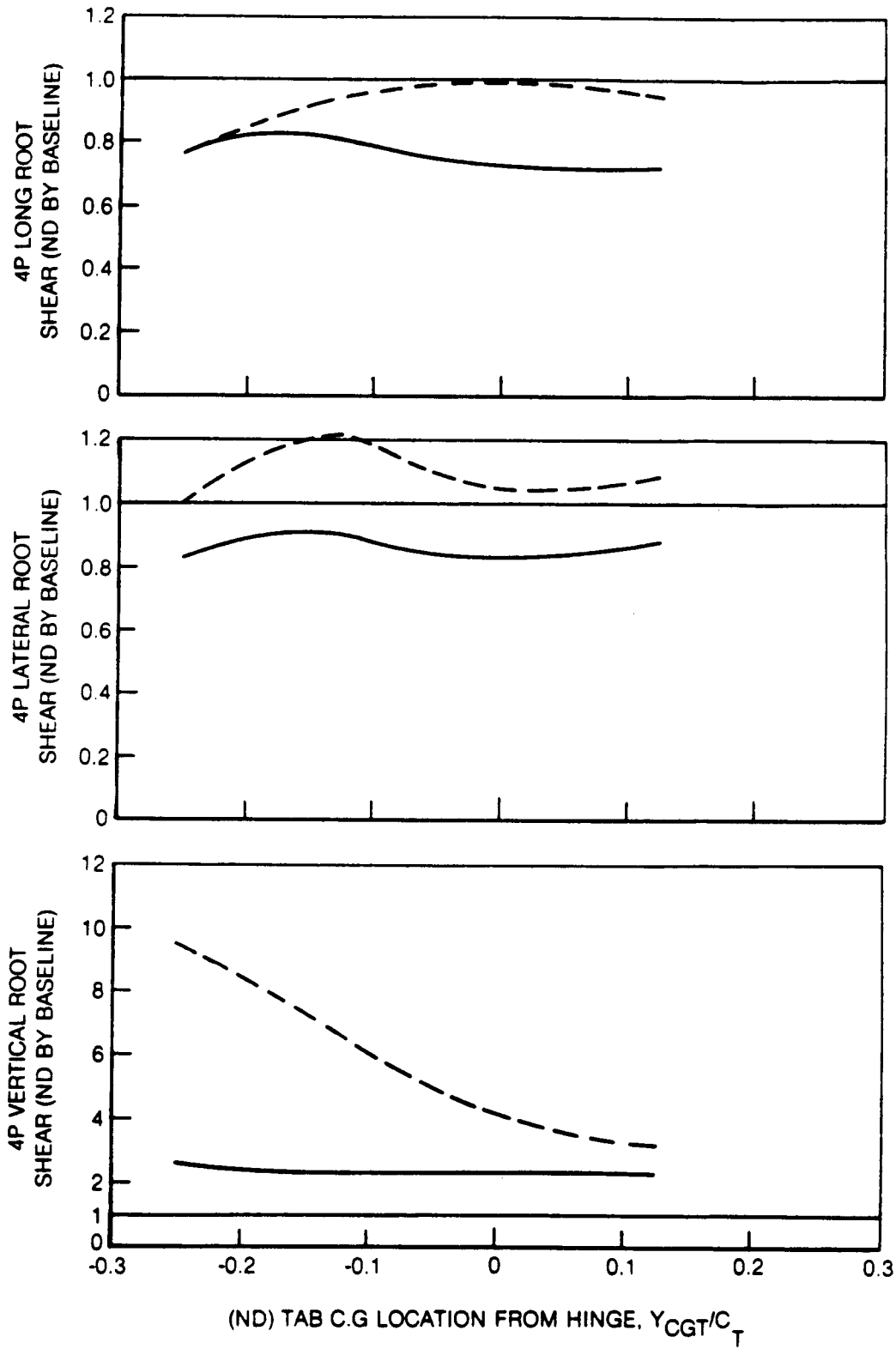

Figure 16. Variations in Components of 4P Hub Shear with Passive Tuned Tab Mass Center Location, 90 m/s Flight Speed ($\mu = 0.4$)

Generally, the results are consistently poor. While some modest gains (reductions in vibratory shear) are noted for the longitudinal and lateral component predictions, the major increases in the vertical component would clearly be unacceptable. Note that because of the extent of these counter-productive results, other lesser parameters which could have been varied, such as tab chord and flight speed, were not. Since the major parameter variations did not result in a design enhancing prediction, the resources of this study were directed to more productive purposes.

The reason for the highly counter-productive results actually obtained, in view of the optimistic results from the simplified analysis, is not fully understood, however. One possible explanation is that the tab, at these parameter values, is operating as a badly mistuned pendular absorber. Another reason is that the proper, more fully coupled analysis of this device (as afforded by the G400PA analysis) requires a more detailed accounting of all the various balancing forces and moments than the simplified analysis is capable of. These questions, however, are beyond the scope of the present study.

Control Coupled Tab

Initial Parameter Selection for G400PA Calculations

Because of the high degree of mechanical similarity between the control coupled tab (CCT) and the passive tuned tab (PTT), the nominal design configuration selected for the CCT was the same used for the PTT. The tab was located at the outboard position (r_{CG_T}=0.913R) and the minimum mass (.806 kg), zero c.g. offset configuration was used throughout. Of the remaining principal parameters impacting on the CCT, the blade root torsion stiffness, K_{θ_R}, (as defined by control system stiffness), and the control coupling gain, G_T were selected for major parameter variation. Specifically, variations in K_{θ_R} were selected to yield uncoupled blade torsion frequencies, $\bar{\omega}_{\theta_j}$, of 2.25P, 3.19P and 4.73P (compared with 4.22P for the baseline configuration). The selected variations in coupling gain, G_T, were determined by matching in nondimensional units the dimensional gain variations used in Reference 16 (0, -.00885, and -.01770 deg/Nm).

In contrast to the intent of the passive tuned tab, the "tab alone" dynamics of the CCT about its hinge are not germaine to its operation and, hence, should be isolated from the dynamics due to coupling. Accordingly,

the spring restraint of the tab to the coupling attachment was set to a suitably high value to insure that the uncoupled tab frequency, $\overline{\omega}_{\theta_T}$, would be in excess of 20P. The actual value achieved was 26.7P. Since the control loads would be expected to be a function of the trim conditions, it was concluded that all calculations for the CCT would necessitate the use of the trim procedure.

G400PA Calculation Results

Using the parameter selection strategy defined above, initial calculations were made with combinations of root torsion stiffness and the resulting values of coupling gain. In every instance, it was found that trim calculations could not be achieved due to gross losses of rotor lift. In an attempt to shed light on this phenomenon, non-trim calculations were made for simple perturbations of the coupling gain, $G_T = \pm 0.5$ (deg/deg) with the nominal root torsion stiffness. These trends are presented in the form of partial derivatives of various pertinent performance parameters with respect to coupling gain, G_T.

TABLE V

PARTIAL DERIVATIVES OF PERFORMANCE PARAMETERS

WITH RESPECT TO COUPLING GAIN FOR CONTROL

COUPLED TAB, $\mu = 0.338$

Parameter	∂(Parameter) $/\partial G_T$	
	Dimensional Value	% Baseline
$C_T/$	.00943	10.4
L/D_e	0.403	5.6
$\frac{1}{2}$PTP $M_{x_5}(0)$, Nm	- 8.71	-1.2
$S_{x_1}^{(4)}$, N	-231.3	-7.2
$S_{y_1}^{(4)}$, N	- 57.8	-4.4
$S_{z_1}^{(4)}$, N	- 1.4	-0.2

Observations and Interpretations

The principal result to be gleaned from Table V is that, for the tab geometry used, the device is functioning almost exclusively as a generator of additional rotor lift rather than as a reliever of vibrational push-rod loads. Surprisingly, the potential for changes in vibrational push-rod load level per coupling gain is not only quite low in magnitude (relative to the lift change potential), but is of the opposite sign from what would normally be expected based on the findings of Reference 16.

Two explanations have been identified for the disagreement of the present findings with those of Reference 16:

1. The configuration used herein has twice the tab chord/airfoil chord ratio as that used in Reference 16 (20% vs. 10%). The twofold increase in this ratio should have a comparable increase in Δc_{ℓ}, but the accompanying increase in $\Delta c_{m_{c/4}}$ should be relatively less because of the shortening of moment arm. Indeed, for flat plate theory in the limit of unit chord ratio, the increment in moment coefficient approaches zero.

2. The calculation for incremental moment due to tab deflection used herein was made using the analytic formulation of Theodorsen and Garrick (Reference 10), whereas that used in Reference 16 was made using experimental values as given in Reference 17. Except for the fact that this experimental data was limited to a chord ratio of not more than 0.10, the experimental data source would have been a better alternative than the analytic one used. Within the context of the unsteady airloads methodology adapted herein, however, the inclusion of such experimental static data would result in an ad hoc formulation requiring some engineering judgment.

One observation which can be made of the CCT is that aeromechanically it bears a strong resemblance to the Kaman servo-tab rotor system. In that rotor concept a tab is used to produce blade torsional moments for the purpose of rotor cyclic control. Although the intent is somewhat different from that of the CCT, the aerodynamic principle invoked is the same: torsion moment control using a trailing edge tab. In the Kaman system, which after several years of development can be assumed to be reasonably optimized, the tab is of small chord ratio and located an exaggeratedly aft distance so as to be removed from the blade proper entirely. This configuration would clearly maximize the incremental aerodynamic moment generation while minimizing the incremental lift generation.

Thus, for purposes of the CCT, the selected tab configuration is far from optimal and a complete evaluation of this concept would require an optimization study of the design parameters. This additional optimization study, was beyond the resources of the present study.

All-Flying Torsion Trip

Preliminary Analysis

Initial G400PA calculations were made for the all-flying torsion tip using quasi-static airloads and a straight-forward implementation of a nominal selection of tip dynamic parameters. Included in input parameters for the basic blade (without tip) was a 95% reduction in mass distribution over the tip span regions where the tip was to be located. This subtracted mass was then included in the tip mass description. With these selected dynamic parameters, the calculations uncovered a number of problem areas. As shown in Figure 3, the concept necessarily entails offsets of the tip aerodynamic center from both the hinge axis and the mass center. Nominally, the mass center would be located coincident with the hinge axis.

Aeroelastic Stability

Preliminary calculations were made using the nominal configuration with the aerodynamic center maintained at the quarter chord point. This results in a significant forward mass center consistent with a placement of the tab hinge axis 12% of the chord in front of the blade pitch (elastic) axis. In this configuration, severe oscillations were calculated which were subsequently ascertained to be flutter involving the second flatwise bending and first torsion modes. A temporary fix for this condition was to displace the tip aft so that the hinge line (and mass center) were coincident with the elastic axis. This configuration was found to be stable and convergent responses were thereby achieved.

Subsequent attempts to return to the original configuration, with the forward tip mass center, were eventually successfully made. The stabilization of this original configuration was achieved by adjusting the mass centers of blade segment numbers 2, 7 and 11 to null the inertial coupling of the second flatwise bending and torsion modes. It is of interest to note that the aeromechanical stability analysis of Chopra (Reference 18), while predicting some low frequency instabilities associated with rigid flapping and lead-lag motions, does not predict or anticipate this essentially classic bending-torsion flutter. Probable reasons for the discrepancy in findings of the present work with those

of Reference 18 are that the present analysis included the aeroelastic equations for elastic modes, a tip hinge axis displaced from the elastic axis, and used realistic amounts of damping, both structural and that from the lead-lag damper, in the calculations. The analysis of Reference 18, however, used a simplified modeling without elasticity directed to the flap-lag-torsion instability problem, and considered no stiffness restraint to the free torsion sections.

Impact of Rotor Trim

A second difficulty experienced in the preliminary calculations was that the expected increase in L/D_e did not materialize with the device activated even with sufficient (constant) applied moment about the tip axis to maintain positive lift on the advancing side. In these calculations, no attempt was made to retrim the rotor and the control settings and inflow values appropriate to the trimmed unappended blade were used directly. In this condition, the constant applied moment was found to be aggravating the stall condition on the retreating blade side of the rotor disk, thereby increasing the equivalent drag D_e. It was subsequently found that the potential for increased L/D_e could be obtained, however, only when the rotor was retrimmed.

Characteristics of the Torsional Restraint

Additional preliminary calculations were performed to establish trends with regard to the interplay between the offset applied (zero deflection) torsion moment and the torsion spring rate. The results of these calculations are shown in Figures 17 thru 19. Figure 17 presents the basic trends achieved with separate variations in offset moment and spring rate. The four calculation points in this figure (denoted by the square symbols) define the range of mean tip deflection angles achieved together with the resulting average equilibrium (inertial and aerodynamic) loading moments, M_{EQUIL} . The equilibrium loading moment is a direct measure of the steady lift sustained on the blade sections comprising the tip. The principal finding presented by this figure is the relative insensitivity of the performance indicator (L/D_e) to offset moment, M_O, and the strong sensitivity to spring rate, K_{β_T}. A related secondary result shown in the figure is the small variation in equilibrium loading with offset moment. The offset moment is seen to affect principally only the value of the mean tip deflection angle, β_{T_O}.

Figure 18 presents the results achieved by linearly ganging the offset moment and spring rate so that all combinations would tend to equilibrate at a selected tip deflection angle and equilibrium loading moment. The values so selected for Figure 18 are, respectively, -1.07 degrees and 381 Nm. With

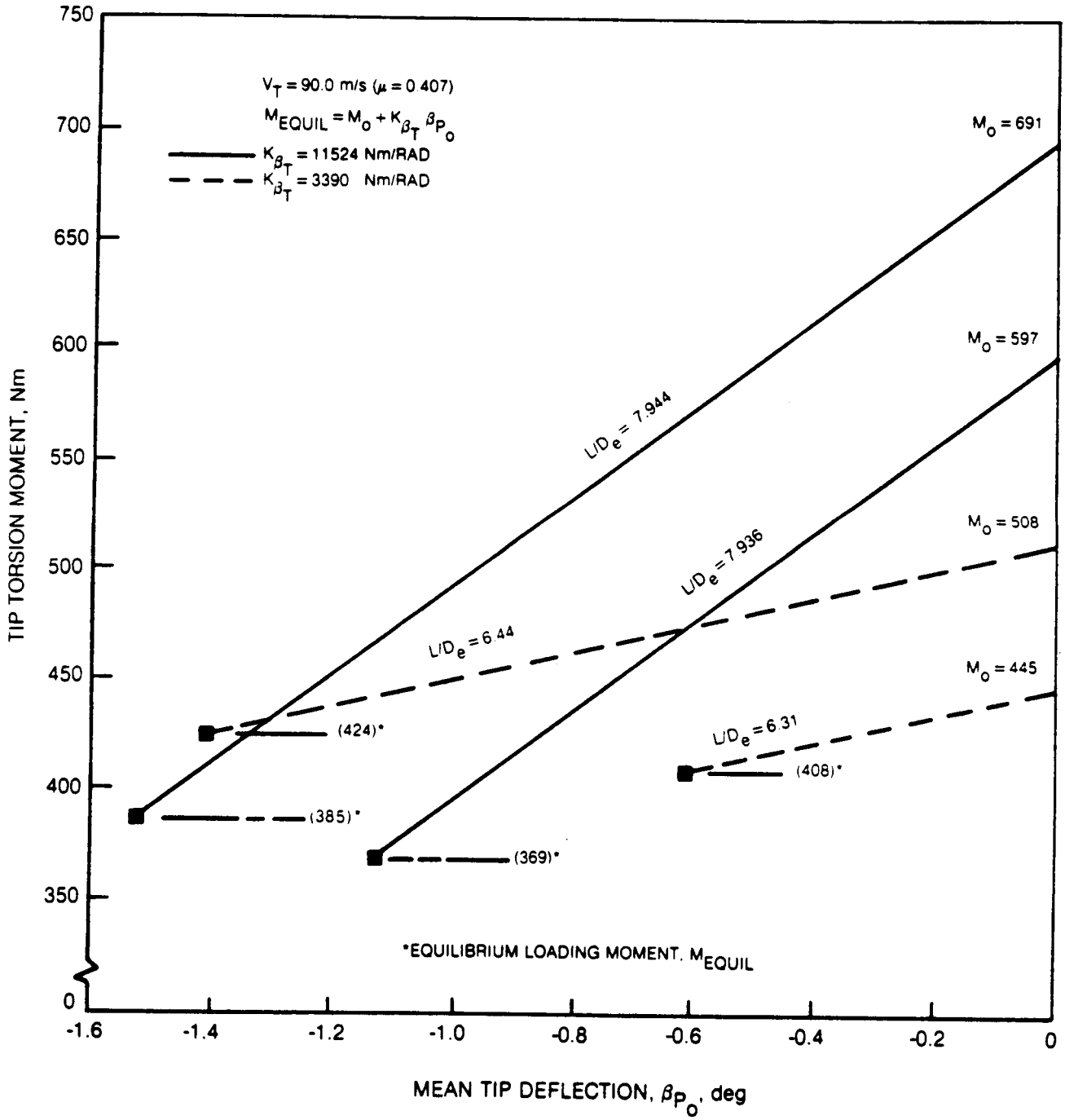

Figure 17. Effects of Offset Moment and Spring Rate on Operation of All-Flying Tip-Preliminary Analysis

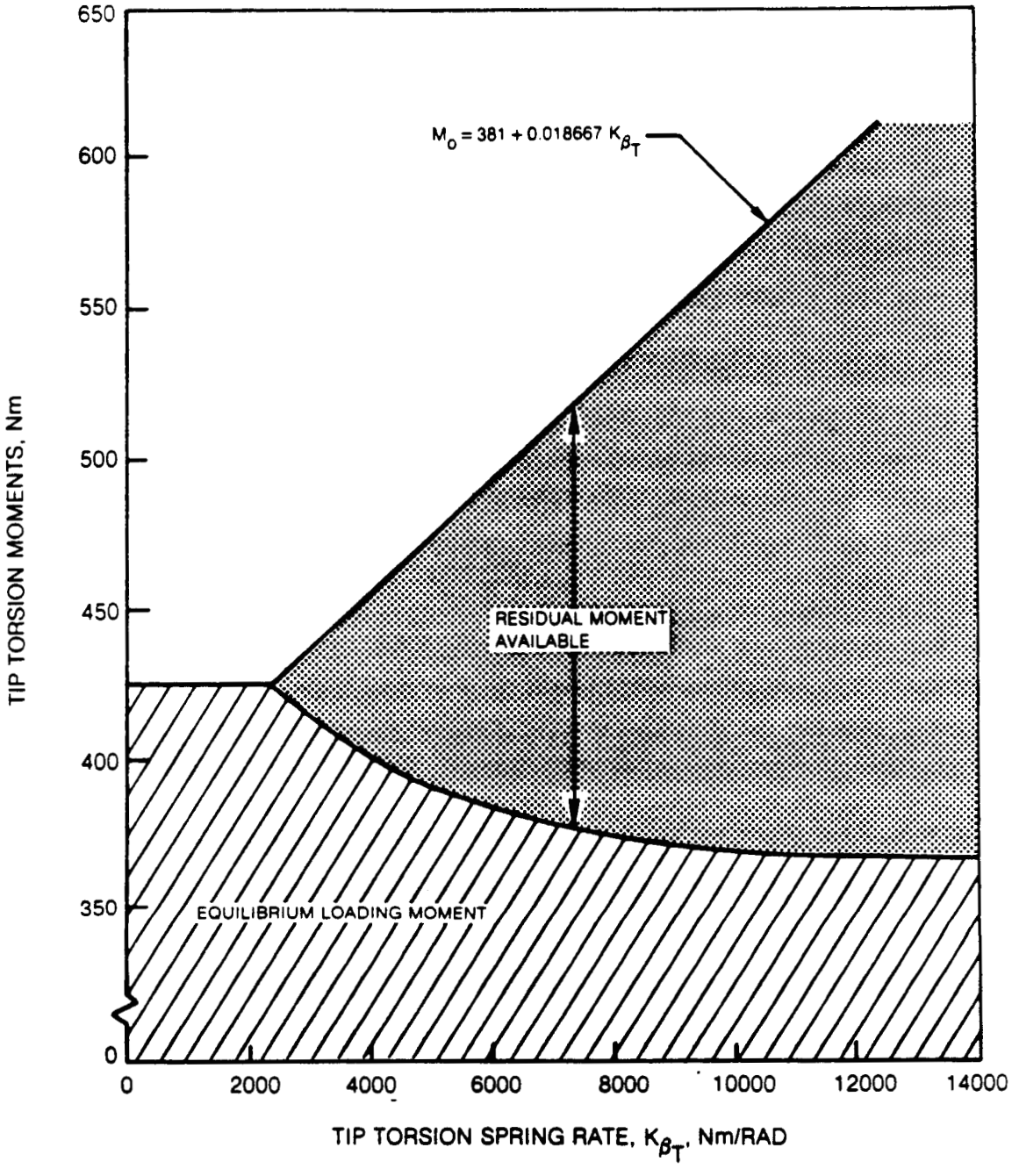

Figure 18. Effect of Linearly Combined Offset Moment and Spring Rate on Equilibrium Loading Moment for All-Flying Tip-Preliminary Analysis

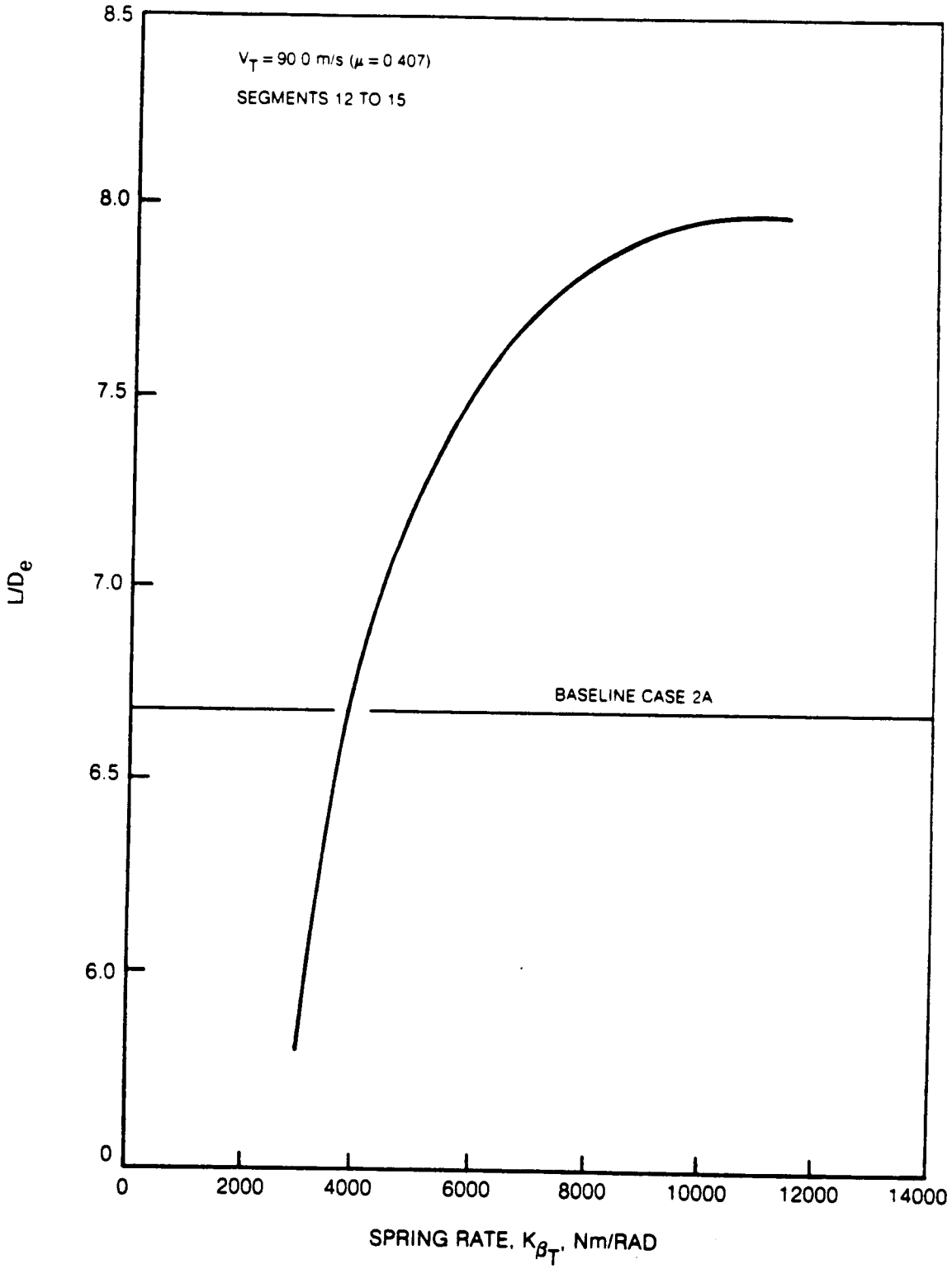

Figure 19. Variation of L/D_e with Spring Rate for All-FLying Tip-Preliminary Analysis

variations in the spring rate (and, commensurately, in offset moment) the actual resulting equilibrium loading moment is seen to vary inversely and intersect the offset moment at a spring rate of approximately 2373 Nm/radian (applied moment of 426 Nm). This result suggests that, for this linear combination, spring rates below this value would result in mean tip deflection angles, β_{T_o}, which were positive (LE nose down) and, hence, counterproductive. In all other calculations involving different linear combinations of applied moment and spring rate, a minimum spring rate was generally defined by the intersection of the two curves.

The effectiveness of these principles to obtain a more nearly optimized L/D_e is shown in Figure 19; a 20 percent improvement is indicated. These results include the concurrent use of variations in offset moment, and are based on the relative insensitivity of L/D_e to offset moment.

Aerodynamic Refinements

Based on the favorable results obtained using only quasi-static airloads and uniform inflow shown in Figure 19, a more in-depth analysis of the all-flying tip appeared justified. The successful operation of and, hence, payoff for the device appear to be closely dependent on three factors: (1) the extent to which the lift, L, is influenced by the inflow conditions on the advancing blade side, (2) the extent to which the equivalent drag, D_e, is influenced by inflow conditions on the retreating blade side, and (3) the extent to which the dynamic operation of the device is influenced by the lags and attenuations of the unsteady character of the airloads.

Reference 1 shows that the substantial downloads typically predicted on the advancing side using simple uniform inflow become significantly diminished with the use of variable inflow. As that reference demonstrates, the L/D_e calculated can depend in large measure on the optional use of variable inflow or uniform inflow. For use with the G400PA, however, the rigorous usage of variable inflow in a combined trim iteration program interactional mode is extremely computer CPU time intensive. Such a complete usage of variable inflow as beyond the scope of the present study and only a cursory assessment of the impact of variable inflow was therefore attempted. The inclusion of unsteady aerodynamics, on the other hand, was easily accomplished and was used in all the final calculations.

Parameter Selection for G400PA Calculations

For all the final calculations the unsteady airloads option was invoked and the tip hinge axis and mass center were maintained at a chordwise location .13c behind the leading edge (.12c in front of the blade pitch axis). The mass

of each of the tip sections was chosen to be approximately 95% of the corresponding unappended blade section mass. The parameter variations used in the final calculations are as follows:

- o torsion spring rate: (0→14000 Nm/rad)
- o moment constraint relation between offset moment and spring rate:

$$(M_O = 381 + .0187\ K_{\beta_T},$$
$$= 267 + .0187\ K_{\beta_T})$$

- o spanwise extent: * (0.10R, 0.15R)
- o flight airspeed: (74.6, 90.0 m/s)

In addition, for the best configuration obtained from the parameter variations, the approximate effects of variable inflow were investigated for the two flight speeds.

G400PA Calculation Results

The calculated results for the all-flying tip consist predominantly of a single performance index: lift to equivalent drag ratio (see Equation 19). For isolated conditions, results are also presented for 1/2PTP blade bending and torsion moment distributions. Generally, the calculation procedure defined in the above Preliminary Analysis Subsection is adhered to. The results are presented in Figures 20 thru 32.

Effects at Unsteady Airloads

Figure 20 compares the predicted L/D_e variations with restraint stiffness as made with and without the effects of unsteady airloads for the high speed (μ= 0.407) flight condition and the 15% radius tip span configuration. The comparison appears to be reasonably close with no significant changes in character. The favorable gains obtained with a quasi-static airloads formulation discussed above are maintained and even improved upon with the inclusion of unsteady airloads. On a percent improvement over baseline basis, the impact of unsteady airloads appears to be advantageous.

---

* Note that the corresponding tip masses are: (11.32 kg, 13.07 kg)

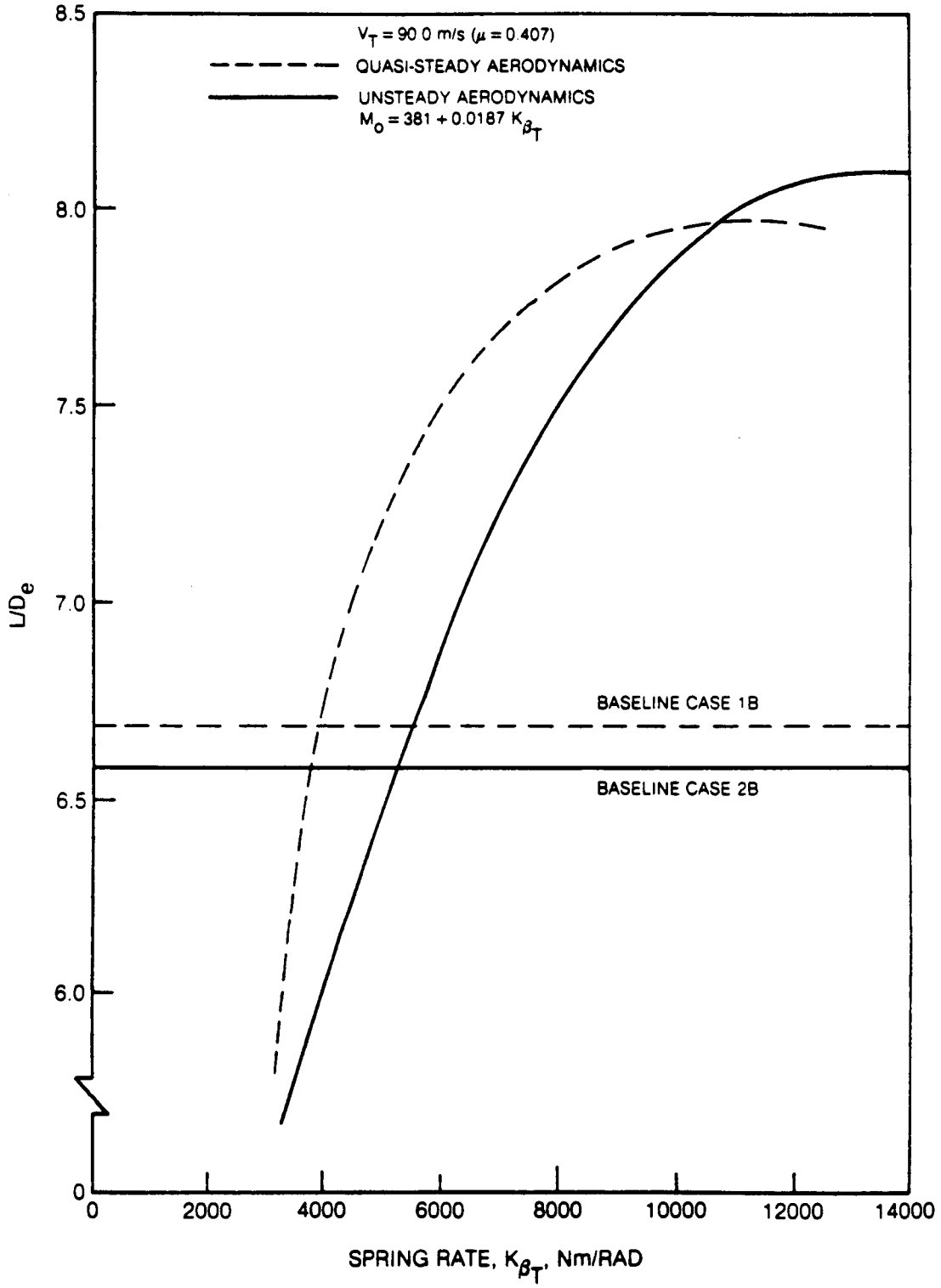

Figure 20. Comparison of L/D_e Characteristics of All-Flying Tip Using Quasi-Static vs. Unsteady Airloads Formulations, 90.0 m/s Flight Speed (μ = 0.407), 0.15 Tip Span

83-6-103-17

Reduced Spanwise Extent

Performance characteristics for the reduced span (.10R) are presented in Figures 21 and 22. The primary comparison made in these figures is with regard to the variation in the offset moment schedule with spring rate. The reduced value of offset moment at zero spring rate, 267 Nm, corresponds to that for the 15% span ratioed by the areas weighted by r^2. The principal effect of the reduced offset moment is seen to occur at the low spring rate conditions, wherein the greatest differences in equilibrium moment and steady tip deflections would occur. As Figure 22 shows, however, the maximum L/D_e values are obtained at spring rates wherein the equilibrium moments are very nearly equal. The results shown in Figure 22 confirm the expectation that the lower (area scaled) applied moment would produce a more nearly optimal performance index than would the moment appropriate to the 15% span configuration. Figures 21 and 22 also show the optimum L/D_e values to occur at similar values of equilibrium moment.

Reduced Flight Speed

Figure 23 contrasts the equilibrium moments obtained for each of the two spanwise configurations (10% and 15% span) at the two flight speeds. Generally for either spanwise extent the trends are similar, in that the higher equilibrium moment occurs at the higher flight speed. As would be expected, the 15% span configuration would operate at a commensurately higher equilibrium moment. Figure 24 presents a summary of the best calculations for the two spanwise extent configurations each at the two flight speeds.

Tip Dynamic Response Characteristics

Figures 25 thru 28 present time-history responses of the tip sections for various offset moment/spring rate schedules, tip spans and flight speeds. Figures 25 and 26 each compare the responses resulting from various spring rates (and concomitant offset moments) at the same high speed flight conditions (μ= .407) but for the 15% and 10% tip spans, respectively. Both these figures show the substantial oscillatory characteristics of the tip at the lower spring rates and the subsequent stabilization induced by the higher spring rates. The figures also graphically show the negative peaks which occur at the ψ= 90 advancing blade position, reflecting the required operation of the tip in augmenting the airloading in this portion of the rotor disk. Note that the higher oscillatory content in responses for the lower spring rates generally allow positive (leading edge down) deflection excursions and an overly negative peak at the 90 deg azimuth position. Both of these excessive response

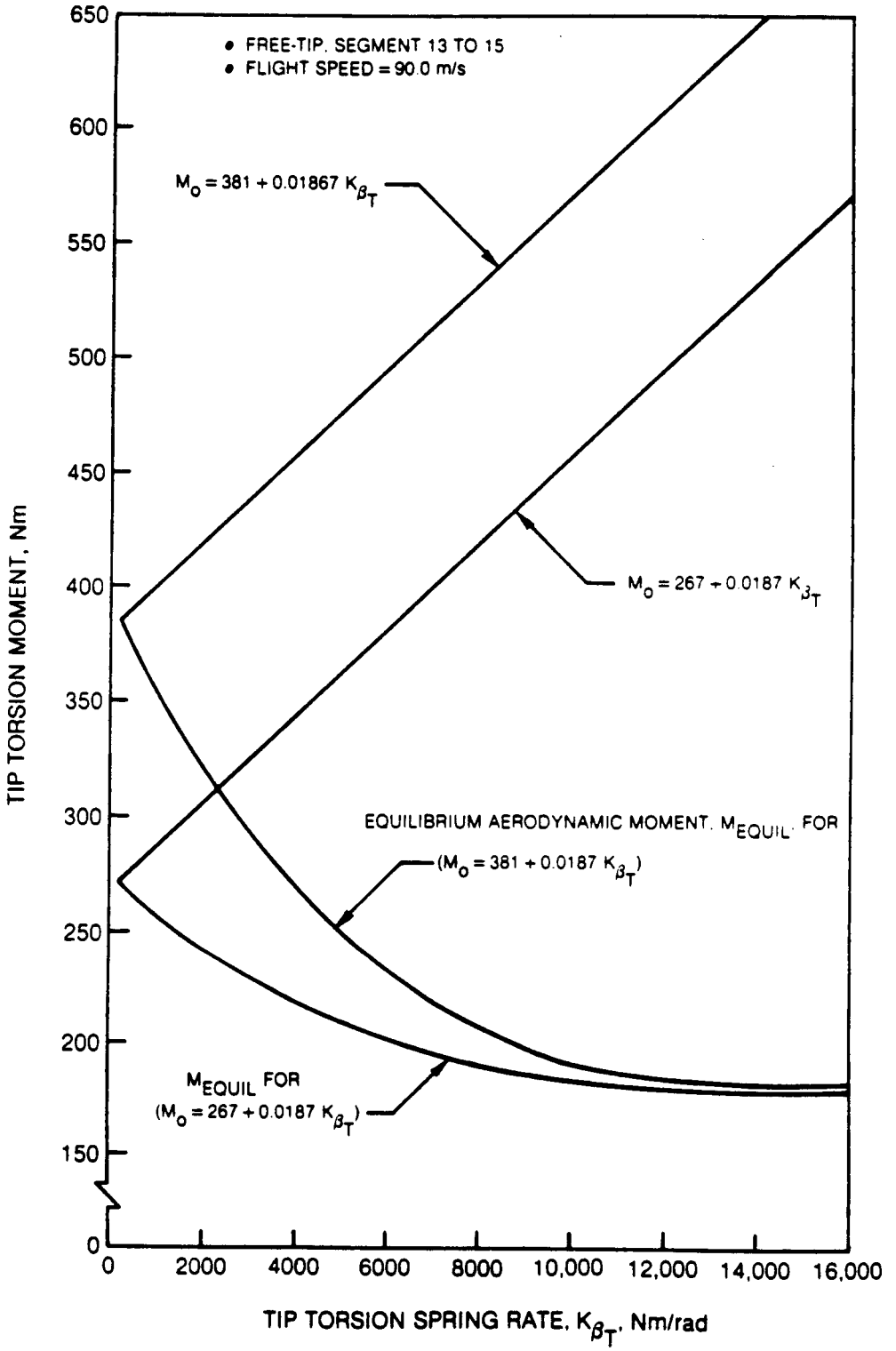

Figure 21. Comparison of Equilibrium Moment Characteristics for All-Flying Tip Using Alternate Applied Moments, 90 m/s Flight Speed ($\mu = 0.407$), 0.10R Tip Span

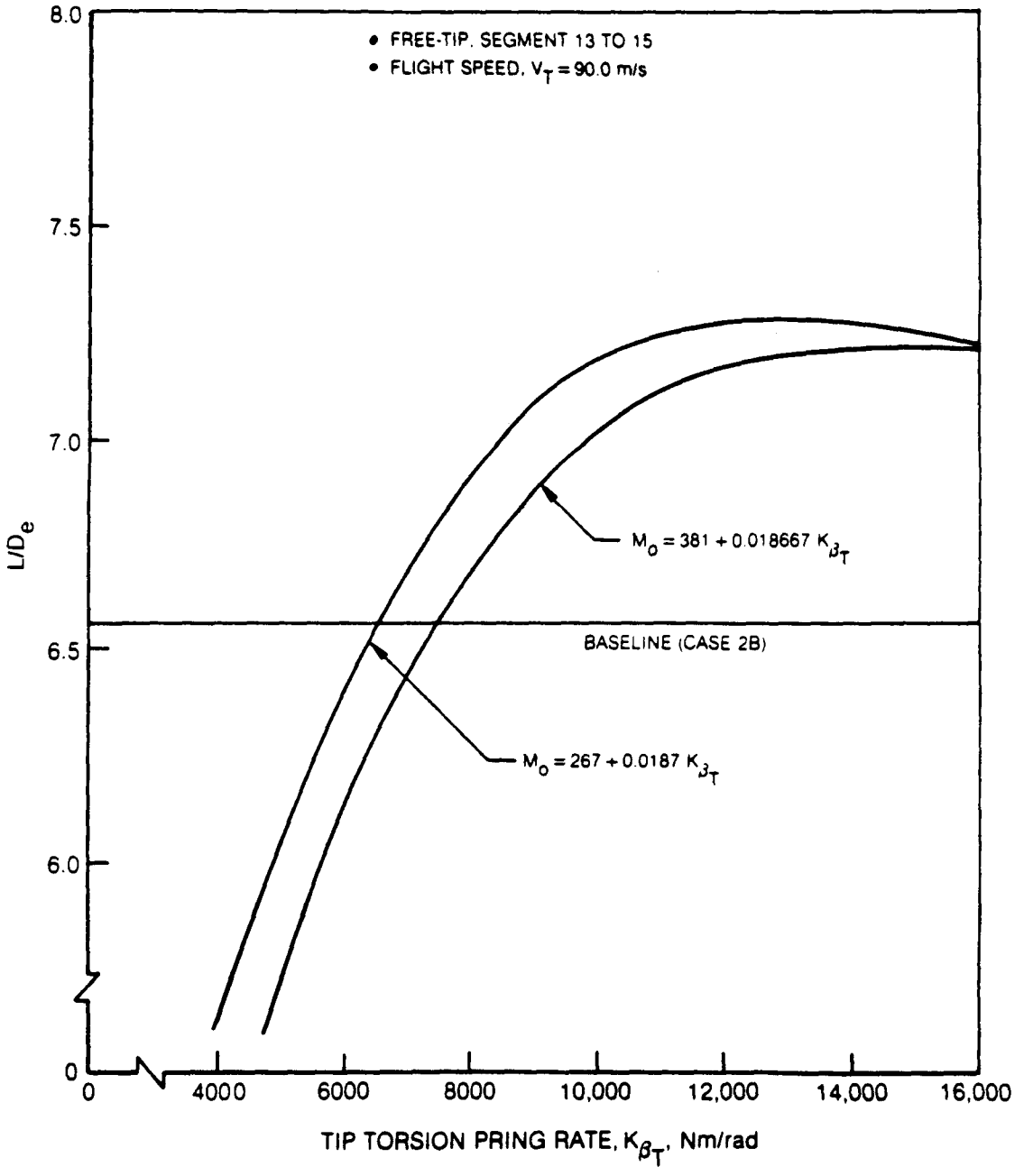

Figure 22. Comparison of L/D_e Characteristics of All-Flyig Tip Using Alternate Offset Moment Schedules, $\mu = 0.407$, 0.10R Tip Span

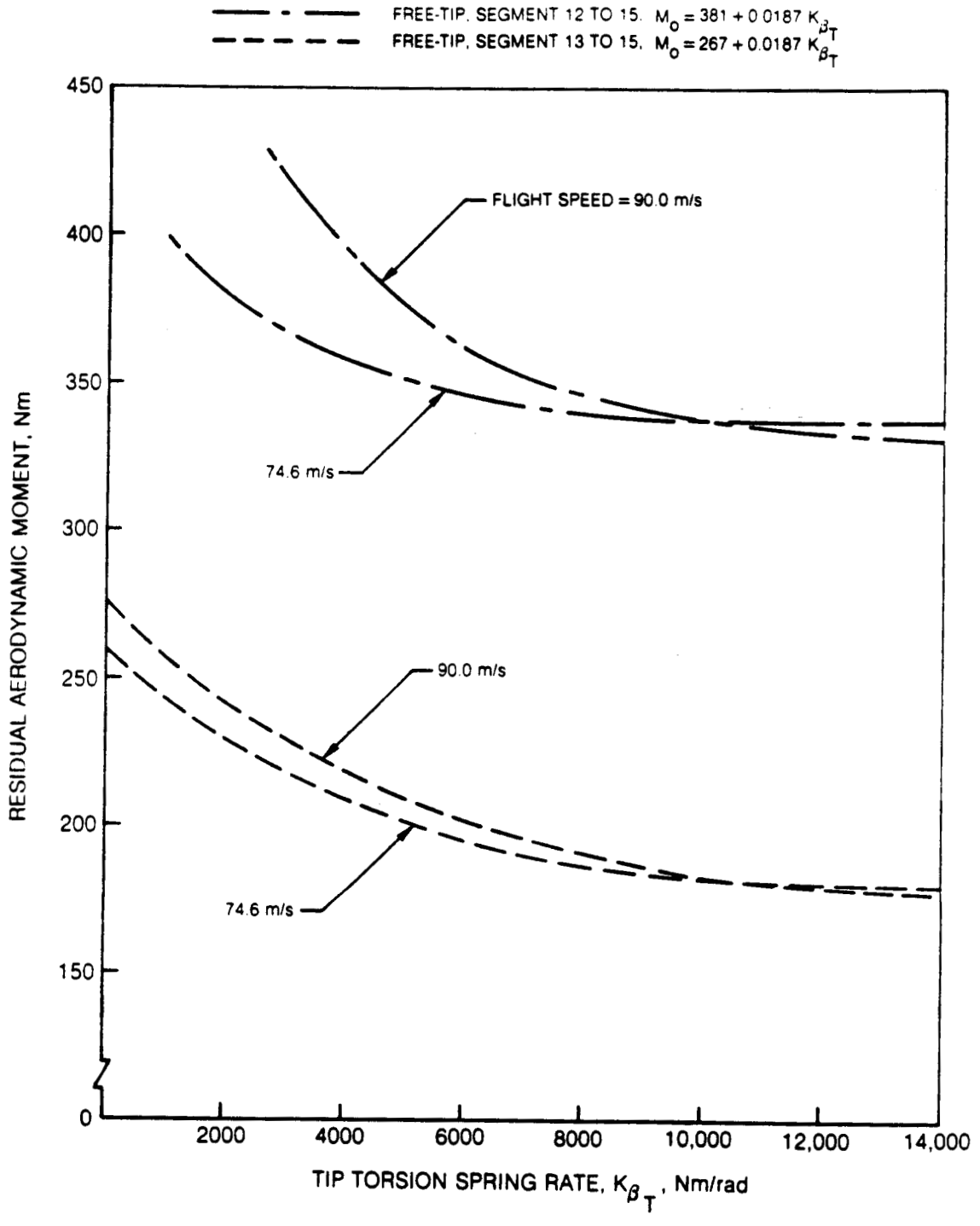

Figure 23. Comparison of Equilibrium Moment Characteristics of All-Flying Tip for Alternate Flight Speeds and Tip Spans

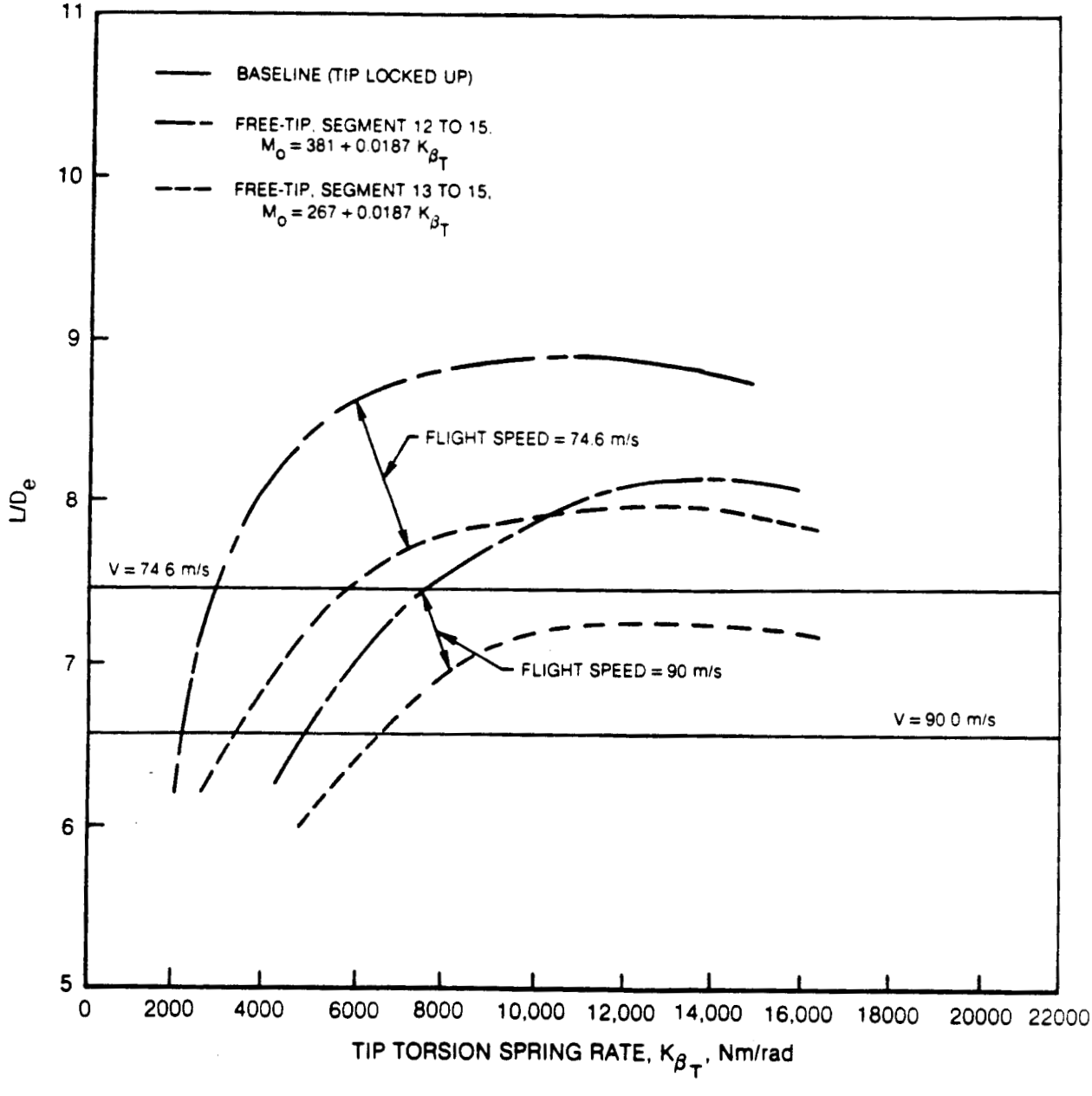

Figure 24. Comparison of L/D_e Characteristics of All-Flying Tip for Alternate Flight Speeds and Tip Spans

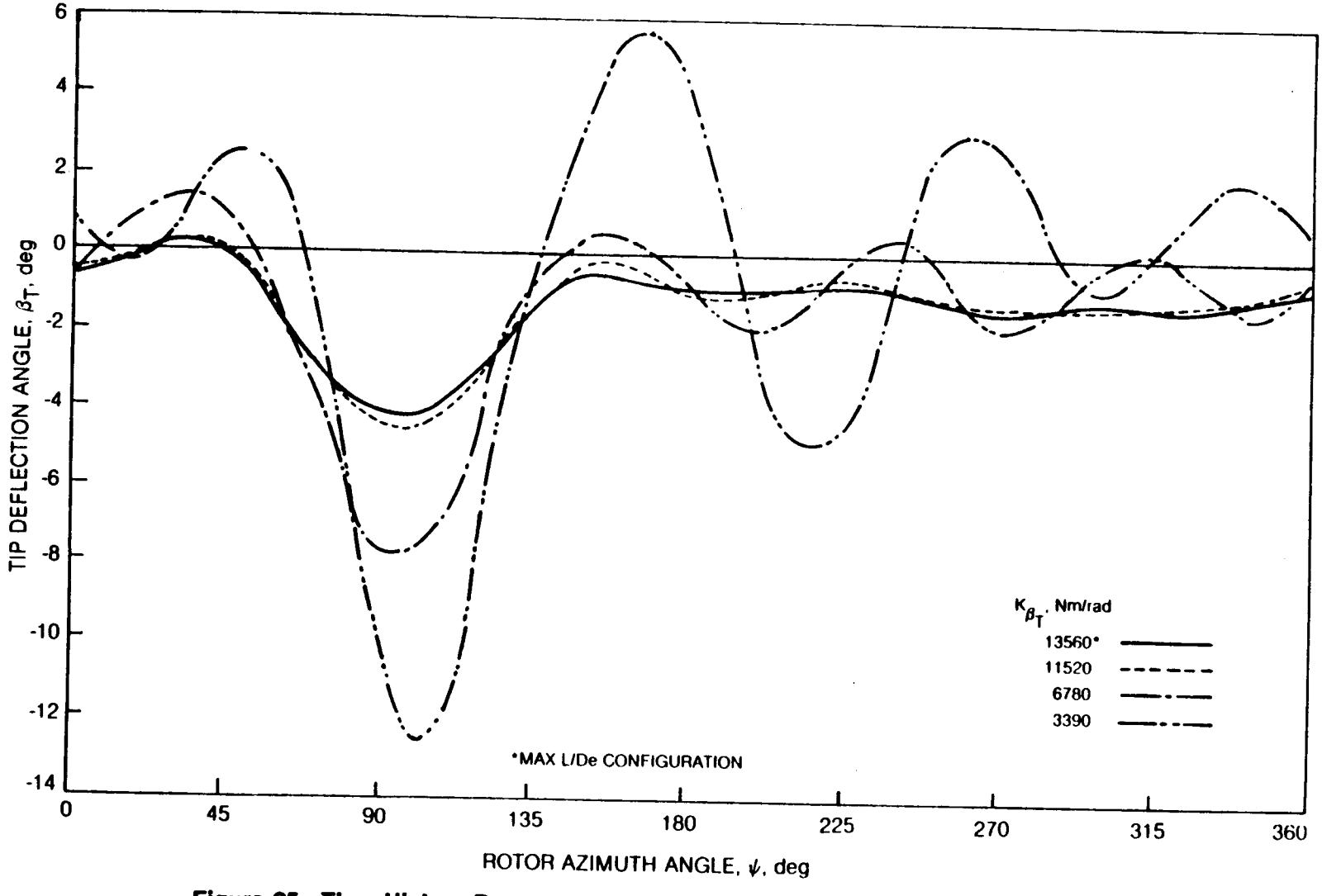

Figure 25. Time-History Responses of All-Flying Tip for Alternate Spring Rates, 0.15R Tip Span, $\mu = 0.407$

83-8-61-3

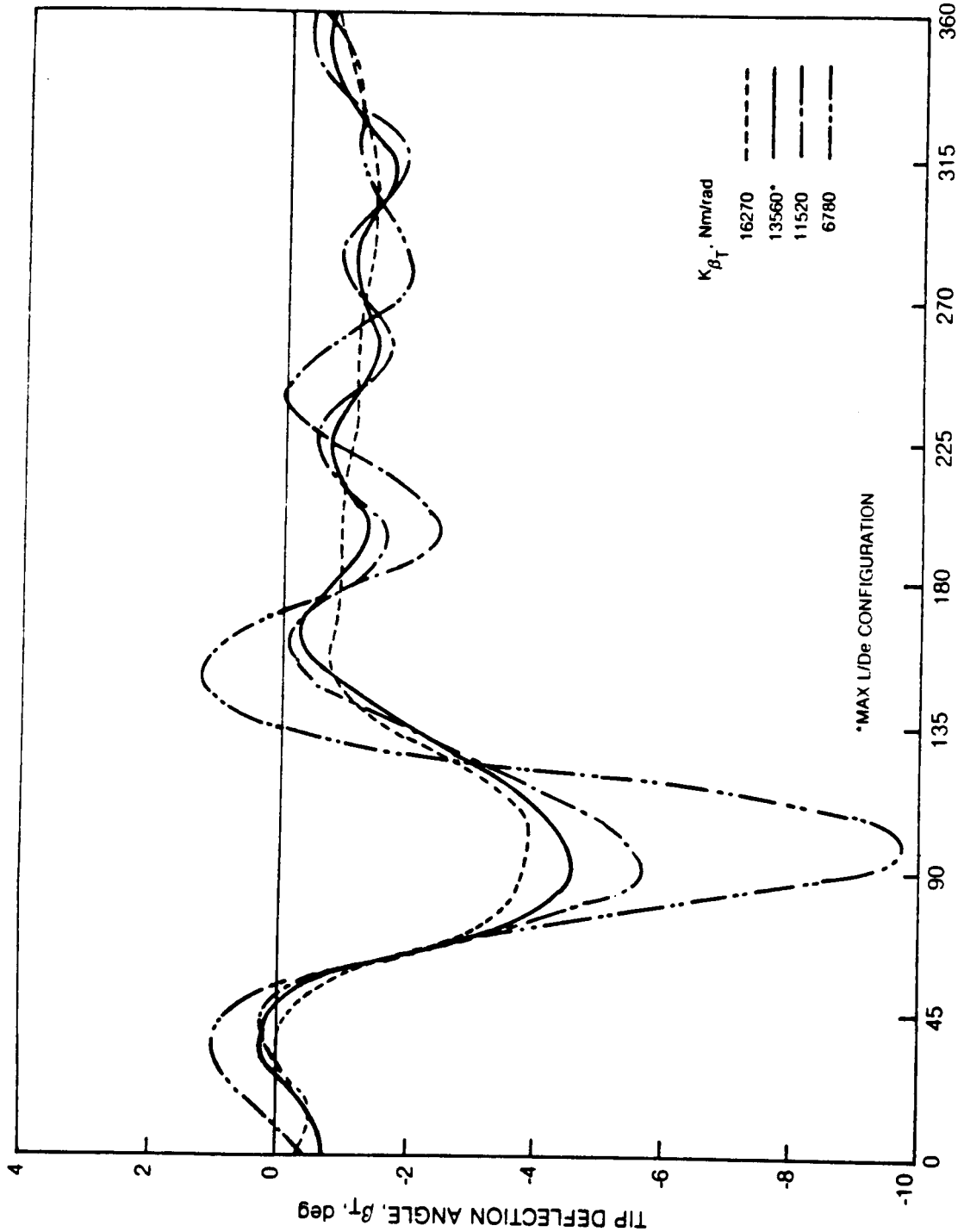

Figure 26. Time-History Responses of All-Flying Tip for Alternate Spring Rates, 0.10R Tip Span, $\mu = 0.407$

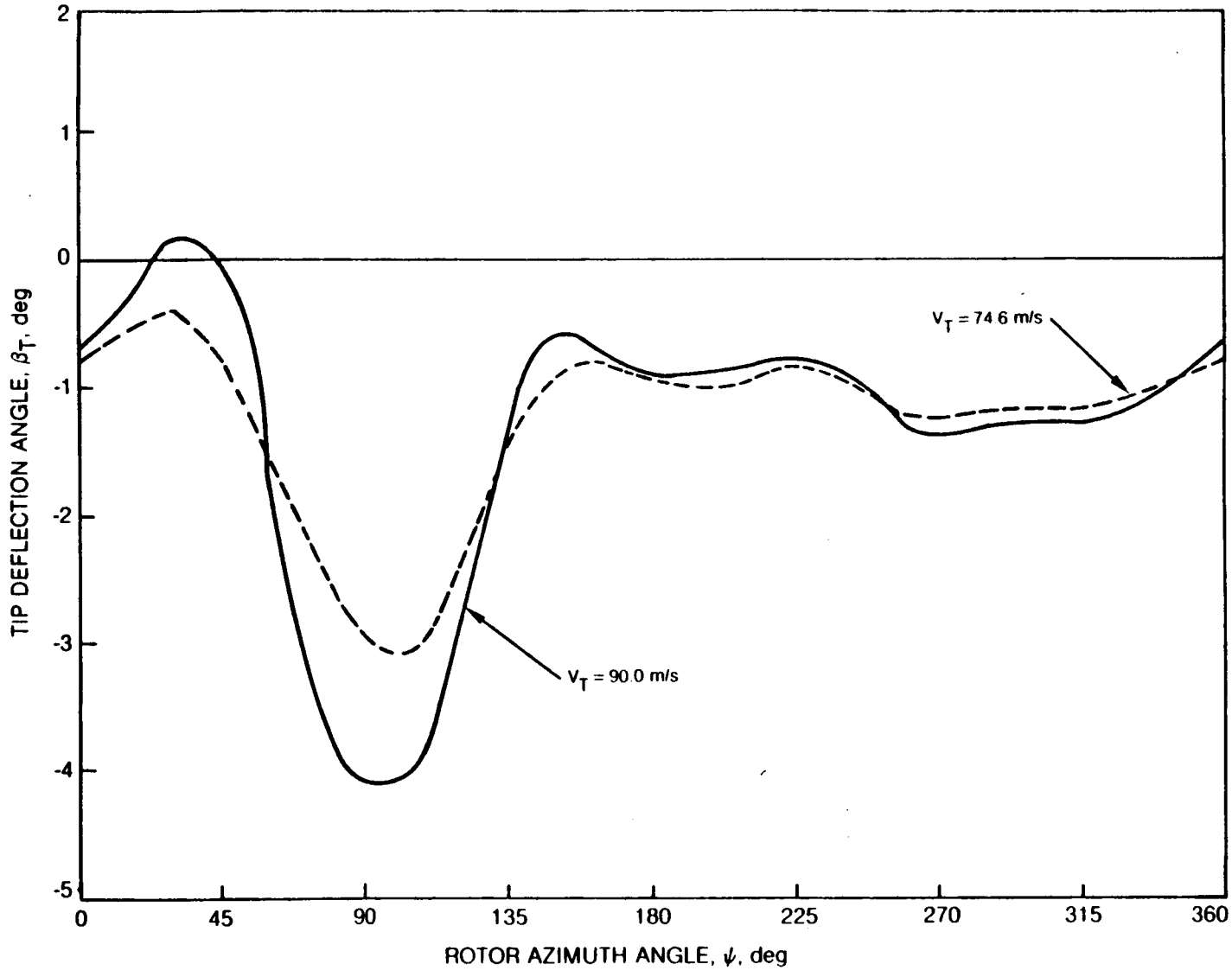

Figure 27. Variation of Time-History Responses of All-Flying Tip with Flight Speed, Maximum L/D_e Configuration, 0.15R Tip Span

83-8-61-4

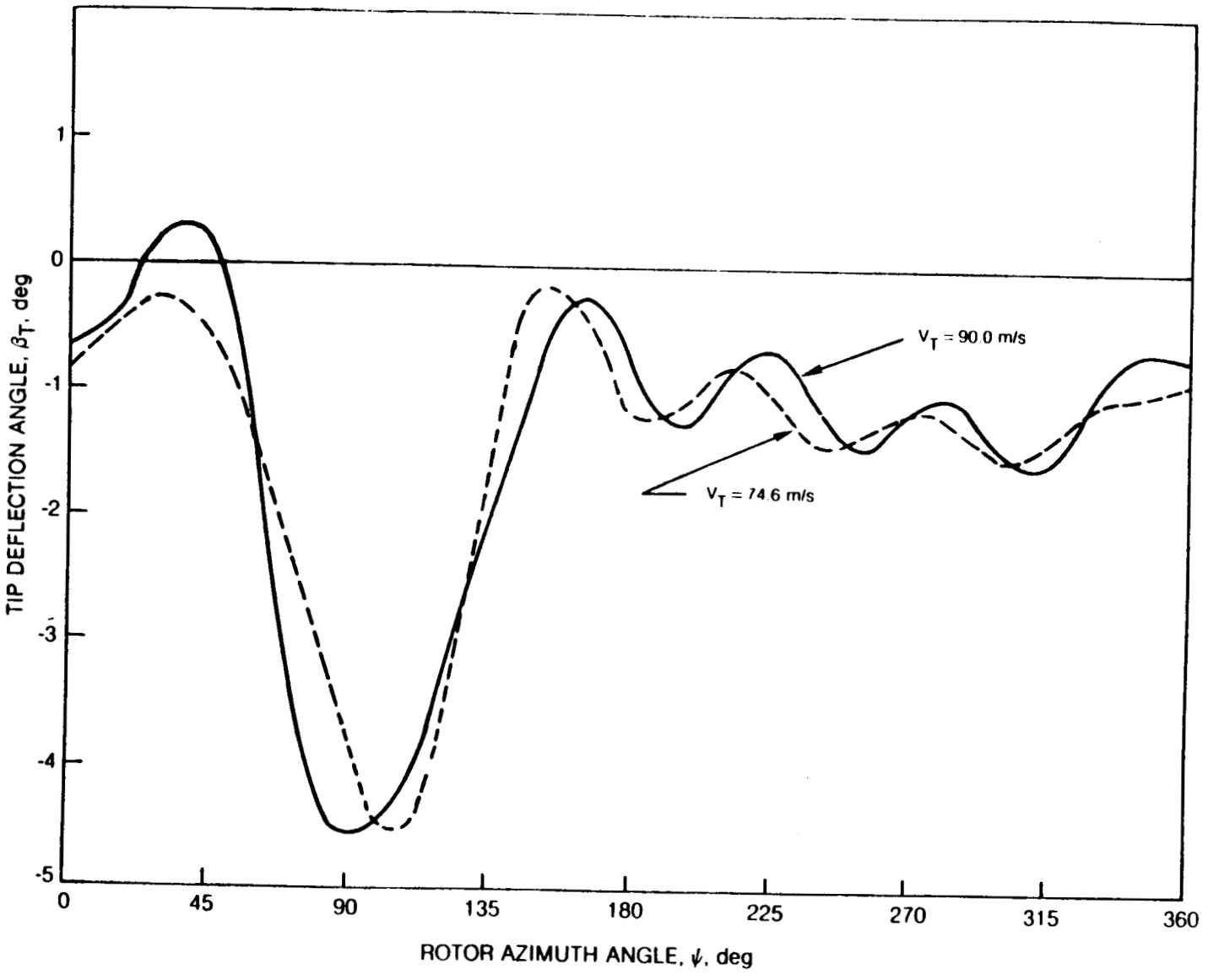

Figure 28. Variation of Time-History Responses of All-Flying Tip with Flight Speed, Maximum L/D_e Configuration, 0.10R Tip Span

83-8-61-2

features would detract from conditions favorable to optimum L/D_e: reduction of local lift due to positive tip deflection and increase in equivalent L/D_e: reduction of local lift due to positive tip deflection and increase in equivalent drag due to too high an angle-of-attack on the advancing side. Generally, the observed trends shown in Figure 25 for the 15% tip span carry over to the 10% tip span responses shown in Figure 26. Included on both of these figures are the tip responses for the maximum L/D_e configurations. Each of these optimal responses are characterized by a well-damped signature, a negative peak at the 90 degree azimuth position and a generally negative mean value of about 1 deg. for the remainder of the rotor period. Figures 27 and 28 show the variations of the tip time-history responses with flight speed for the 15% and 10% tip span optimal configurations, respectively. For both of these spanwise extent configurations, the same spring rate (K_{β_T}=13560 Nm/rad) was used. The higher oscillatory content in the 10% span responses can be attributed to (1) a higher natural frequency (resulting from a reduced torsion inertia) and (2) a reduction in aerodynamic damping (resulting from a reduced aerodynamic area and the less effective airloading of the tip sections). Generally, the response characteristics of the tip section are not strong functions of flight speed.

Tip Section Angle-of-Attack Dynamic Characteristics

Figures 29 and 30 present the time-histories of the effective angle-of-attack, α_E, characteristics of the $\bar{r}$ = 0.925 radial station (corresponding to the center section of the 15% tip span configuration), for the two flight conditions, μ= 0.338 and 0.407, respectively. In each of these figures are (1) the appropriate baseline results (no tip), (2) the results for the tip section activated but responses with the increment due to tip motion artificially subtracted out, and (3) with the tip motion included. The responses clearly show the reductions in negative angle-of-attack at the advancing blade portions of the disk provided by the device. The figures also show that the blade proper responses with the tip activated are even more negative than the baseline values in this portion of the disk. A probable reason for this response characteristic is the blade's response to the reaction moment imparted by the tip device.

Observations and Interpretations

Observations which can be made from the non-variable inflow results are as follows:

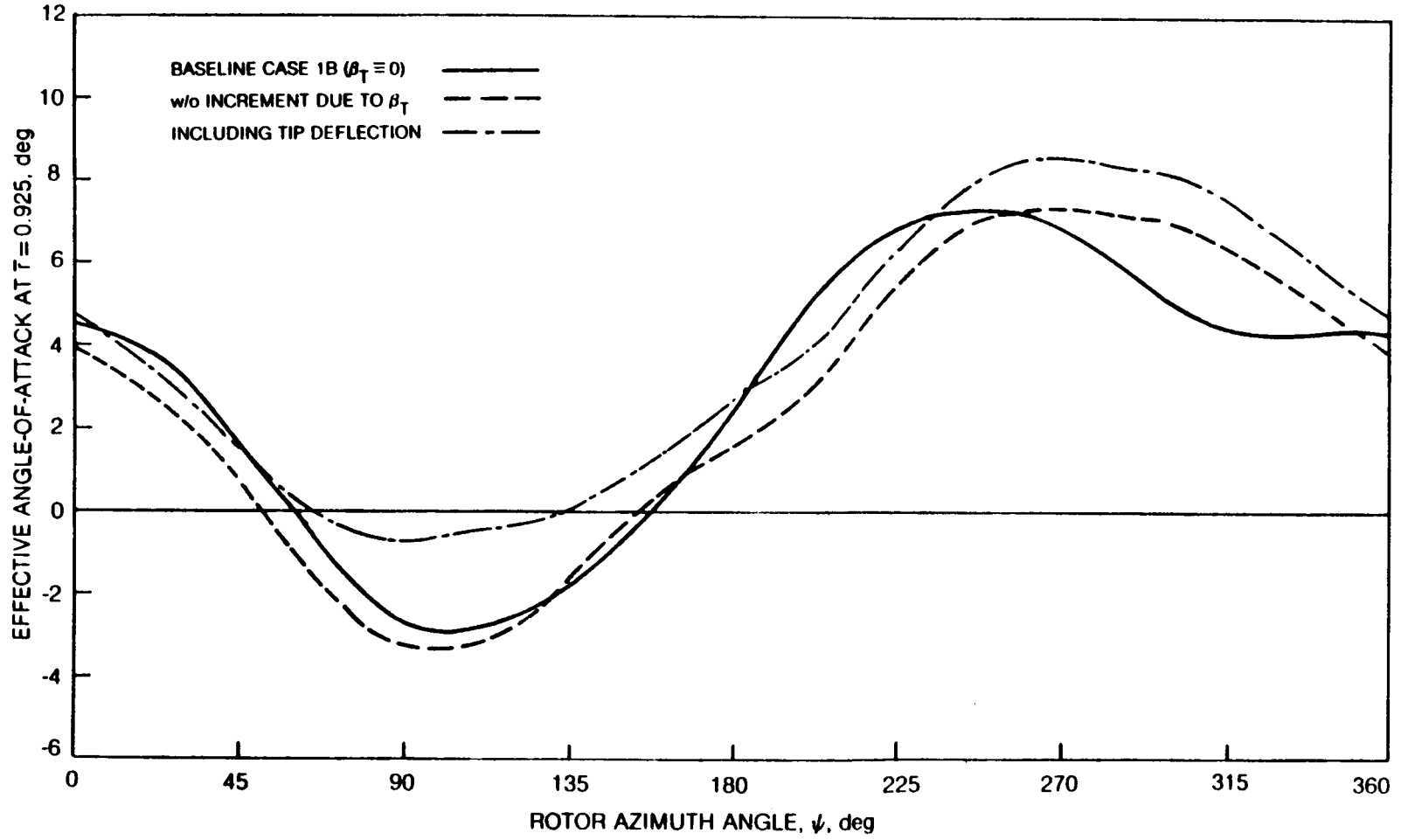

Figure 29. Angle-of-Attack Time-Histories at r = 0.925R for All-Flying Tip, Maximum L/D_e Configuration, 0.15R Tip Span, $\mu = 0.338$

83-8-61-5

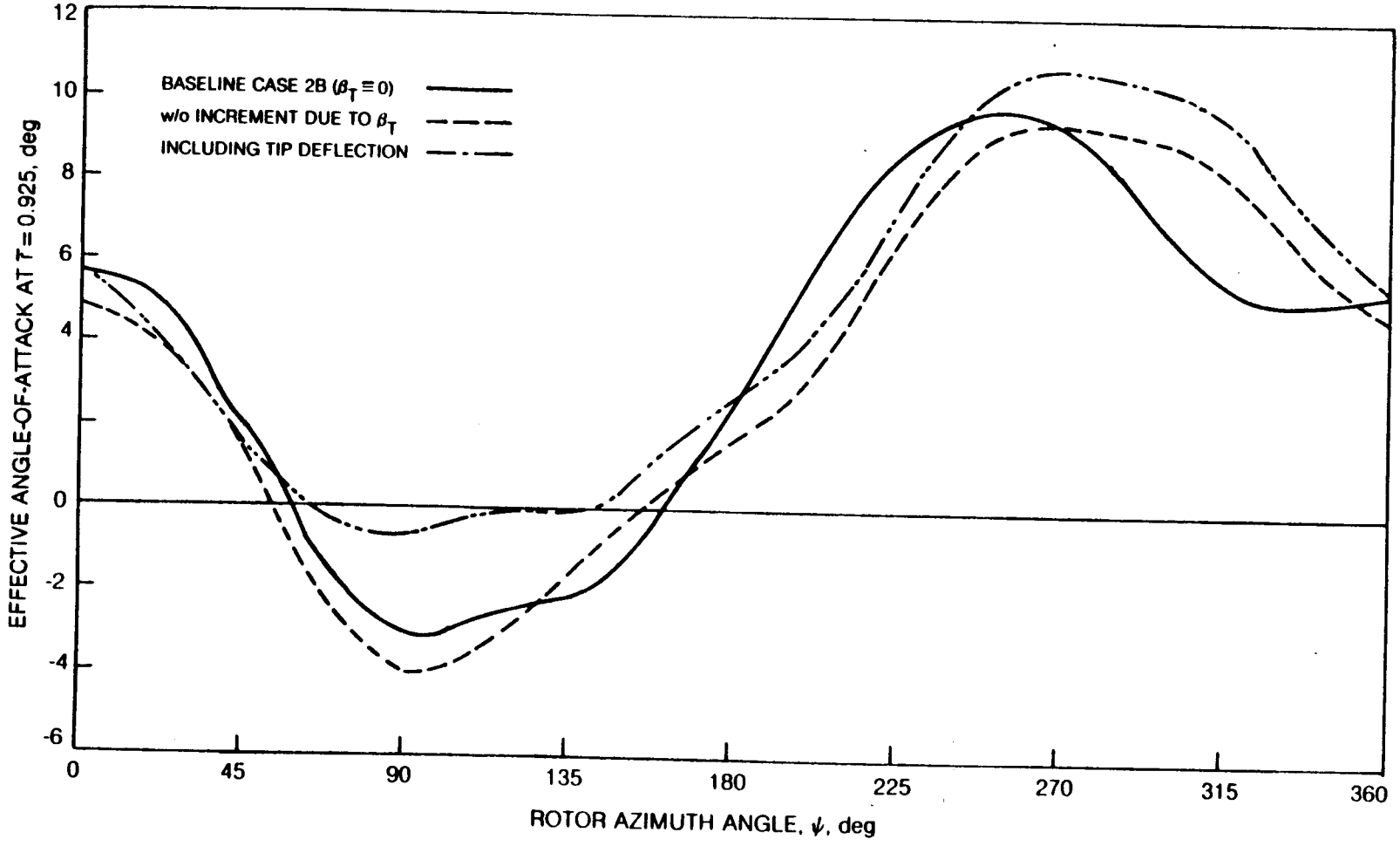

Figure 30. Angle-of-Attack Time-Histories at r = 0.925R for All-Flying Tip, Maximum L/D_e Configuration, 0.15R Tip Span, $\mu = 0.407$

1. The increase in performance obtained for the device tracks the performance variation with respect to airspeed for the unappended device.

2. The effect of increased tip span on performance is a monotonic function of the tip span.

3. The spring rate for maximum L/D_e varies with flight speed; the off-optimum penalty does not appear great, however.

4. The maximum performance gains for the device (again neglecting variable inflow for the moment) are approximately 20% for the 0.15R configuration and 10% for the 0.10R configuration.

5. The operation of the device is truly dynamic in that it not only provides a more or less steady increase in angle-of-attack over most of the rotor azimuth, but with an incremental dynamic peak where it is most needed on the advancing blade portions of the aximuthal period.

6. Off-optimal responses at the reduced spring rates are characterized by excessive oscillatory motion.

Quasi-Variable Inflow

As discussed in an above subsection, the variable inflow distributions appropriate to trimmed flight at the two flight speeds were calculated and input to G400PA, without interprogram iteration. These distributions were used to provide a preliminary estimate of the effect of variable inflow on one closely optimized configuration. Generally, the results obtained with the use of quasi-variable inflow are suspect. Comparison of trim cases 1B with 1C, and 2B with 2C shows a deterioration in the incremental performance due to variable inflow where typically the reverse is the norm. On the other hand, results for the rotor with the selected optimized all-flying tip configuration, at the two advance ratios, both showed substantial aerodynamic gains: L/D_e values well in excess of 10. The most valid observation to be drawn from these results is that the true effect of variable inflow on the performance of the all-flying tip is moot and requires a more rigorous inclusion of this methodology.

Blade Vibratory Loads

Figures 31 and 32 present comparisons of internal vibratory blade loads for a configuration selected for best L/D_e at the two flight speeds. Discernable trends from these results are as follows:

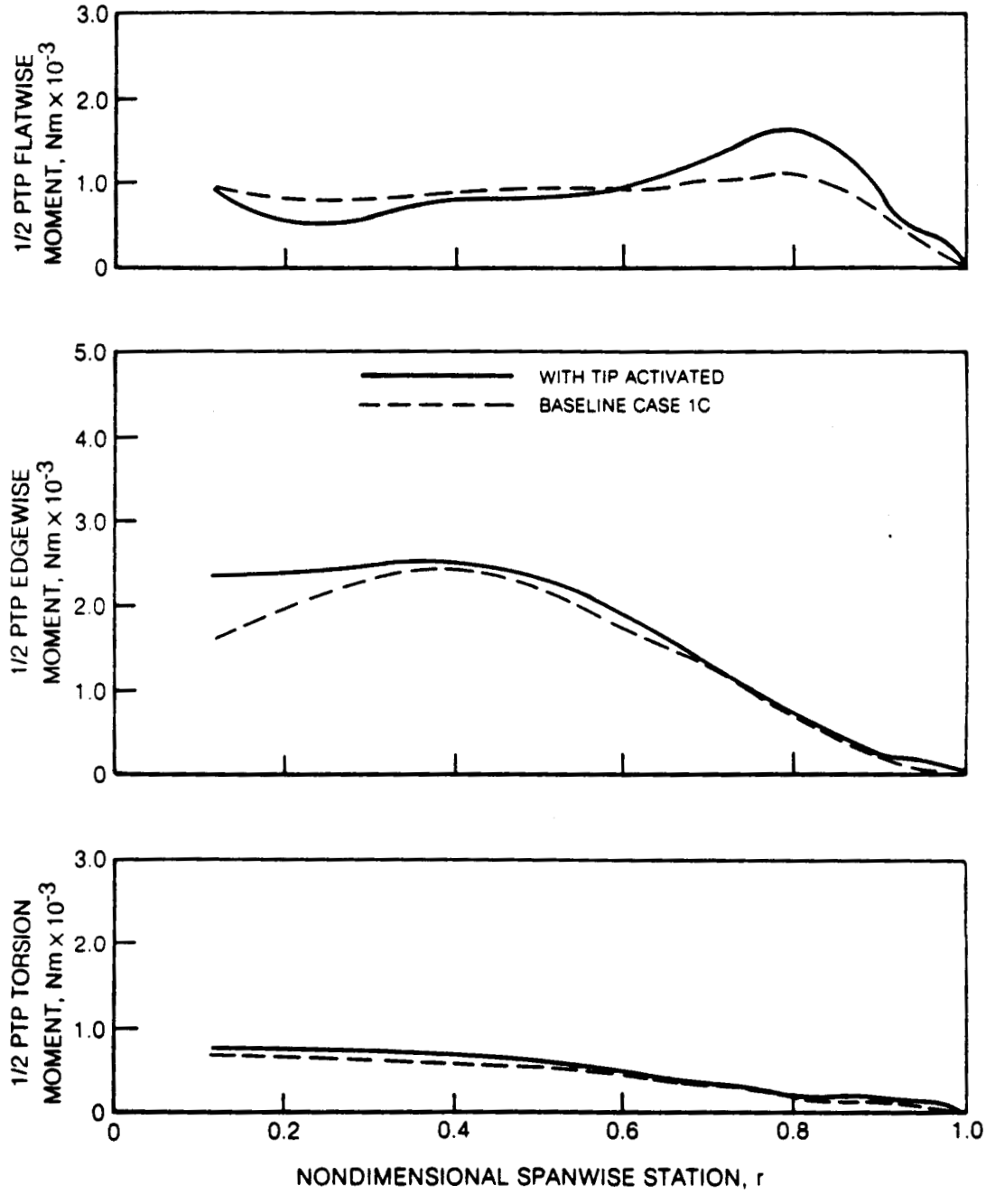

Figure 31. Vibratory Blade Bending and Torsion Moment Characteristics for All-FLying Tip, 0.15R Tip Span, $\mu = 0.338$, Maximum L/D_e Conditions

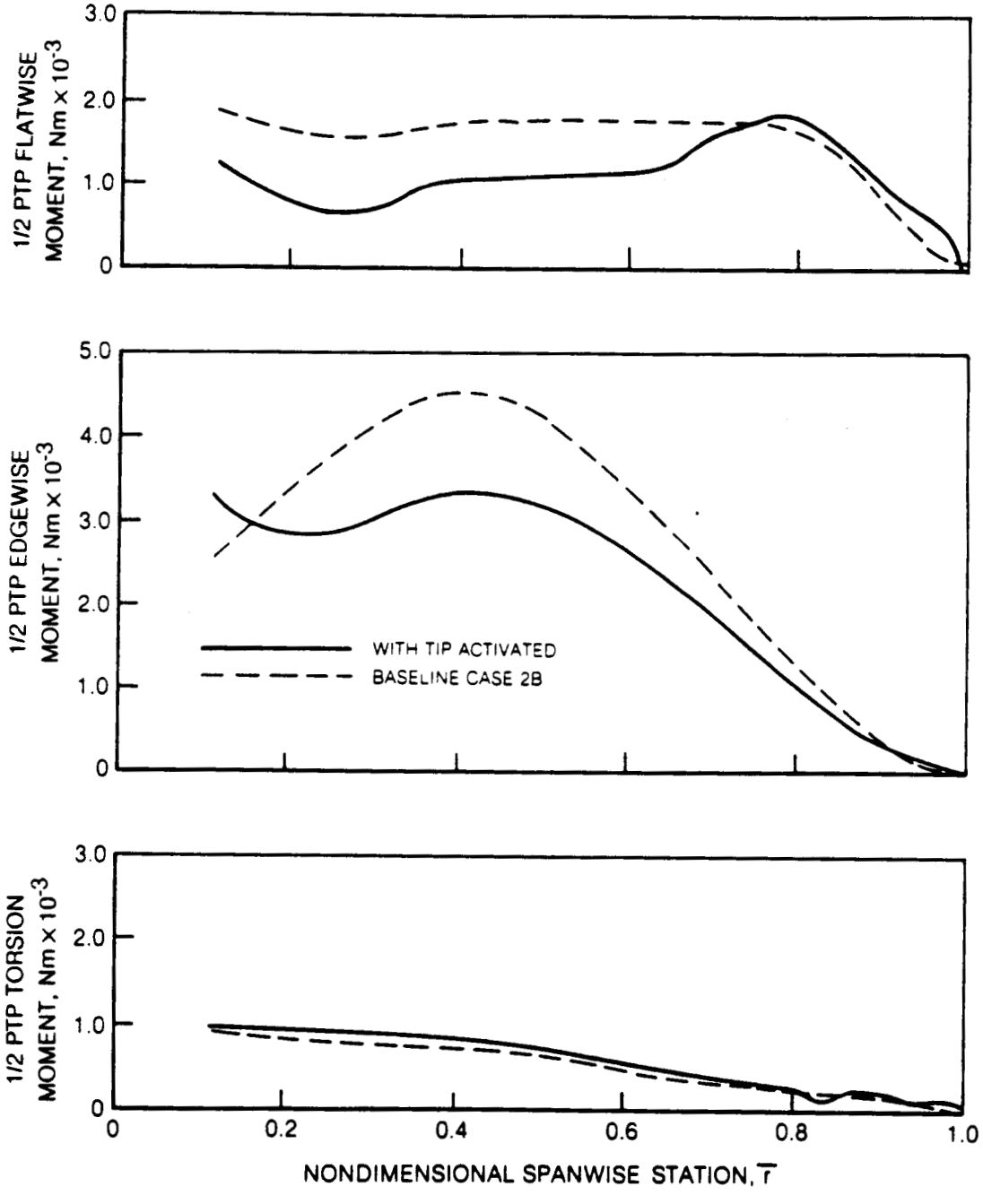

Figure 32. Vibratory Blade Bending and Torsion Moment Characteristics for All-Flying Tip, 0.15R Tip Span, $\mu = 0.407$, Maximum L/D_e Conditions

- o The principal impact of the device on the 1/2 PTP flatwise bending moment distribution is the local increase just inboard of the device attachment. This would be expected based on the increased loading of the tip sections.

- o Apart from the tip regions the device produces negligible increases, where increases are noted, in the bending moments.

- o The 1/2 PTP torsion moments are, as would be expected, relatively unaffected by the operation of the device.

Harmonically Dilational Airfoil Tip

The aeromechanical operation of the Harmonically Dilational Airfoil Tip (HDAT) is assumed to be more benign than those for the torsionally active devices, which are potentially susceptible to aeromechanical and/or aeroelastic instability. In the absence of test, no known instabilities can be linked with the HDAT at this time. Consequently, the G400PA calculations for this device pose no special considerations and are relatively routine. The device is aerodynamic performance related and, hence, all G400PA calculations generally require trim computations.

Parameter Selection for G400PA Calculations

The G400PA calculations of the HDAT utilize airfoil aerodynamic data look-ups based on thickness ratio instead of radial station. The thickness ration distribution for the baseline (UH-60A) helicopter rotor blade is given in Table II. This distribution based on the SC1095 airfoil series is generally constant and reflects a current trend to cambered, relatively thinner sections. For successful operation of the HDAT, the airfoil must contract to as thin a section as is possible on the advancing side and commensurate dilation must be implemented on the retreating blade side.

The principal parameter selection required for the G400PA HDAT calculations therefore consisted of acquiring and preparing for G400PA input aerodynamic airfoil data at a variety of thickness ratios. The following table lists the airfoil used to construct the required airfoil data table:

Thickness Ratio	Airfoil
0.080	RC-08
0.0945	SC1095
0.0955	SC1095/R8
0.120	SC1012
0.150	NACA 0015

Note that the thickness ratio range thus available indicates that more dilational range (.0945→.15) is available than contractual (.0945→.08). Thus, the total thickness ratios calculated assuming a harmonic perturbation were truncated to minimum and maximum values of .08 and .15, respectively.

The parameter variations used in the G400PA calculations are as follows:

- o amplitude of perturbational thickness ratios, $\Delta\tau/c$ . . . (0→.06)
- o rotor azimuth angle for minimum thickness ratios, $\psi_{\tau/c_{min}}$ (70, 90, 110 deg)
- o spanwise extent: . . . . . (0.10R, 0.15R)
- o flight airspeed: . . . . . (74.6, 90.0 m/s)

G400PA Calculation Results

The appropriate performance index for the DHAT as for the all-flying tip is the lift per equivalent drag ratio, L/D_e, (see Equation 19). The calculation results for the DHAT are presented in Figures 31 and 32. These figures show the comparisons of the L/D_e with variations in the parameters discussed above.

Observations and Interpretations

The results shown in Figures 33 and 34 confirm the expected result that the HDAT is capable of increasing the aerodynamic performance of helicopter rotors in forward flight. Specific observations and interpretations of these results are as follows:

1. Maximum performance gains in L/D_e of approximately 11% and 9% are indicated at the μ=0.338 and 0.407 advance ratios, respectively.

2. The maximum performance gains occur, as would be expected, for configurations with a minimum thickness aximuth angle of 90 deg. (full advancing blade condition).

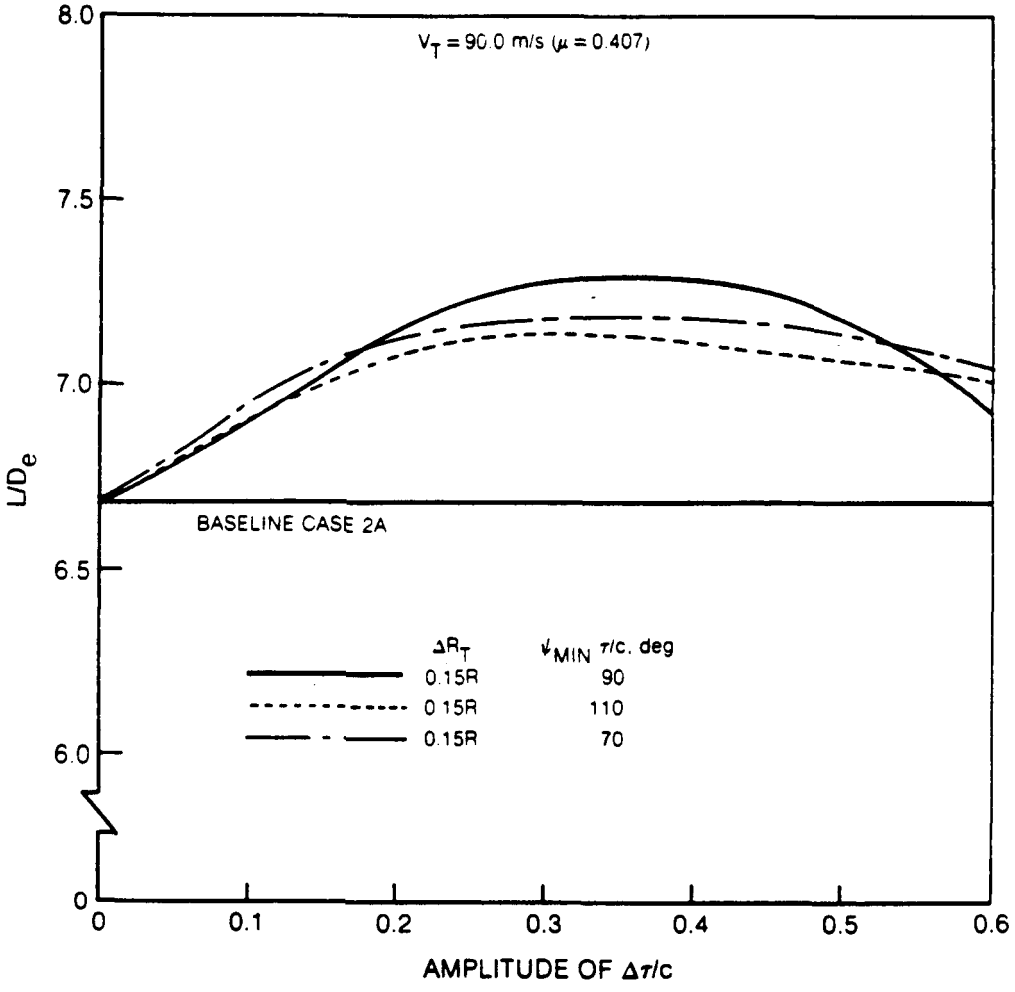

Figure 33. Variation of L/D_e Characteristics of Harmonically Dilational Tip with Amplitude of Perturbational Thickness Ratio, 0.15R Tip Span, $\mu = 0.407$

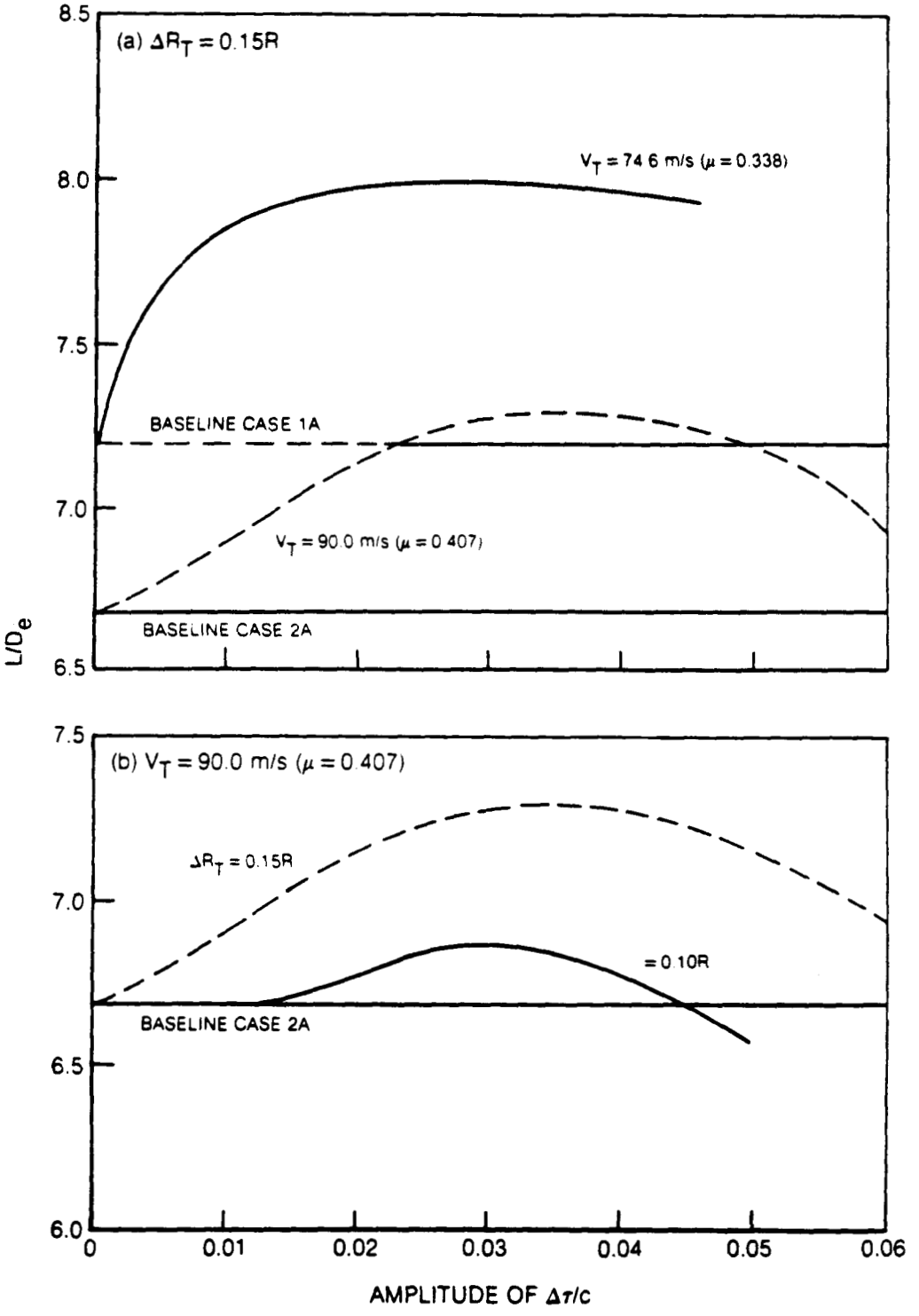

Figure 34. Comparison of L/D$_e$ Characteristics of Harmonically Dilational Tip for Variations in Flight Speed and Tip Span

3. The maximum performance gains occur at perturbational thickness ratio amplitudes of .03 to .035.

4. The gain in performance between 0.10R and 0.15R tip span configurations is in excess of what would be expected from the ratio of tip areas. One possible explanation of this result is the secondary gains obtained from the increased thickness on the retreating blade side.

CONCLUSIONS AND RECOMMENDATIONS

An analytic study has been performed of the practicality of four different passive aeroelastic devices appended to helicopter rotor blades for improving rotor aerodynamic performance, reducing control loads and/or alleviating airframe vibration. Since this study was strictly analytic, the validity of the conclusions is heavily dependent on the accuracy of the modeling assumptions employed and on the depth of the study performed herein.

Conclusions

General Assessment of Devices

1. The passive tuned tab as configured in this study is impractical. This is based on the significantly amplified 4P vertical hub shear loads and the relatively small attenuations achieved in the longitudinal and lateral loads.

2. The control coupled tab as configured in this study is impractical. This is based on the relatively excessive incremental rotor lift changes per coupling gain (and consequently tab deflection) obtained as compared with the incremental blade torsion moment changes forming the basis of this device.

3. The all-flying tip offers the potential for significant increases in aerodynamic performance. Present findings project an approximately 20% increase in L/D_e for this device with no significant increases in blade bending or torsion moments.

4. The harmonically dilational airfoil tip offers the potential for moderate increases in aerodynamic performance. Present findings project an approximately 10% increase in L/D_e for this device.

5. Favorable findings for the all-flying tip and the harmonically dilational airfoil tip should be additive to a significant degree. This is because the former device achieves performance gains by eliminating performance robbing inefficiencies in lift (notably rotor areas of negative lift, whereas the latter device achieves gain by reducing losses accruing from drag rises due to advancing blade compressibility.

Specific Conclusions Relating to Device Operation

1. For both performance related devices (all-flying tip and dilational airfoil tip) the gain in performance arising from increased tip span is in excess of the increase in tip area. A possible explanation is that the increase in area occurs at the inboard, aerodynamically more efficient end of the tip.

2. The benefits from the devices are not monotonic with flight speed and are generally more optimal at the moderate advance ratio (μ=0.3 to 0.35) flight speeds than at the high advance ratio ones.

3. The effects of unsteady airloads do not detract from the gains in aerodynamic performance predicted for the all-flying tip.

4. The results from the use of a quasi-variable inflow procedure were inconclusive.

5. The inclusion of unsteady aerodynamics is critical to a satisfactory modeling of the torsionally active devices for purposes of predicting aeroelastic instability (flutter).

6. All implementations of torsionally active devices on a blade should be configured such that the combined blade is appropriately configured with chordwise mass balancing to decouple critical flatwise and torsion modes and thereby preclude flutter.

Recommendations

1. Any future work to refine the assessment of the passive tuned tab should be directed to parameter variations on an active implementation of the harmonic tab responses to establish what amplitudes and phases of those responses, if any, actually attenuate the vibratory hub loads.

2. A rigorous interactional calculation, using the G400PA and Rotor Inflow Analysis (RIA) Programs should be made for the all-flying tip to more fully assess the impact of variable inflow on the improved L/D_e predictions for this device. This would require modification of the RIA to include the kinematics of the dynamic response of the all-flying tip.

3. Additional parameter variations, with regard to hinge location and the geometry of aerodynamic sweep should be made for the all-flying tip.

4. The detailed dynamic modeling and evaluation of an implementation for passive excitation of the dilational airfoil tip should be made. This evaluation would indicate (1) how practical and obtainable the ideal response is, and (2) what potential aeromechanical instabilities might exist for this device.

5. A study should be made to determine the extent to which the gains of the all-flying tip and the harmonic dilational airfoil tip are additive.

6. Future work on the control coupled tab should be directed to tab configurations which maximize the section moment/lift characteristics such as a nonattached tab located as far aft of the balde section proper as is practical.

REFERENCES

1. Blackwell, R. H.: Investigation of the Compliant Rotor Concept. USAAMRDL Technical Report 77-7, June 1977.

2. Ruddell, A. J.: Advancing Blade Concept (ABC)™ Development. Proceedings of the 23rd Annual National Forum of the American Helicopter Society, May 1976.

3. Wernicke, K. G.: Performance and Safety Aspects of the VX-15 Tilt Rotor Research Aircraft. Proceedings of the 33rd Annual National Forum of the American Helicopter Society, May 1977.

4. Gabel, R.: Pendulum Absorbers Reduce Transition Vibration. Proceedings of the 31st Annual National Forum of the American Helicopter Society, May 1975.

5. Stroub, R. H: Performance Improvements With the Free-Tip Rotor. Proceedings of the Specialists' Meetings on Rotor System Design of the American Helicopter Society, Philadelphia, PA., October 1980.

6. Bielawa, R. L.: Aeroelastic Analysis for Helicopter Rotor Blades With Time-Variable, Nonlinear Structural Twist and Multiple Structural Redundancy - Mathematical Derivation and Program User's Manual. NASA Contractor Report CR-2638, October 1976.

7. Houbolt, J. C. and G. W. Brooks: Differential Equations of Motions for Combined Flapwise Bending, Chordwise Bending, and Torsion of Twisted Nonuniform Rotor Blades. NACA Report 1346, 1958.

8. Bielawa, R. L.: Blade Stress Calculations - Mode Deflection vs. Force Integration. J. of the American Helicopter Society, Vol. 24, No. 3, July 1978.

9. Bielawa, R. L.: Aeroelastic Analysis for Helicopter Rotors With Blade Appended Pendulum Vibration Asorbers -- Mathematical Derivations and Program User's Manual. NASA CR-165896, June 1982.

10. Theodorsen, T. and I. E. Garrick: Nonstationary Flow About a Wing-Aileron-Tab Combination Including Aerodynamic Balance. NACA Technical Report 736, 1941.

11. Bielawa, R. L., S. A. Johnson, R. M. Chi, and S. T. Gangwani: Aeroelastic Analysis for Propellers - Mathematical Formulation and Program User's Manual. NASA CR-3729, December 1983.

12. Bisplinghoff, R. L., H. Ashley, and R. L. Halfman: Aeroelasticity. Addison-Wesley Publishing Co., Inc., Reading, MA., 1955, pp 281-286.

13. Reissner, E.: Effect of Finite Span on the Airload Distributions for Oscillating Wings, Vol. I - Aerodynamic Theory of Oscillating Wings of Finite Span. NACA TN 1194, March 1947.

14. Rowe, W. S., J. D. Sebastian, and M. C. Redman: Recent Developments in Predicting Unsteady Airloads Caused by Control Surface Motions. J. of Aircraft, Vol. 13, No. 12, December 1976, pp 955-961.

15. Egolf, T. A. and A. J. Landgrebe: A Prescribed Wake Rotor Inflow and Flow Field Prediction Analysis - User's Manual and Technical Approach. NASA CR 165894, June 1984.

16. Blackwell, R. H., et al.: Predesign Study for an Advanced Flight Research Rotor. Sikorsky Aircraft Report SER-510105, NASA CR-166405, December 1982.

17. Prouty, R. W.: A State-of-the-Art Survey of Two-Dimensional Airfoil Data, Journal of the American Helicopter Society, Vol. 20, No. 4, October 1974, pp 14-25.

18. Chopra, I.: Dynamic Analysis of Constant-Lift and Free-Tip Rotors. J. of the American Helicopter Society, Vol. 28, No. 1, January 1983.

1. Report No.	2. Government Accession No.	3. Recipient's Catalog No.
NASA CR166525		

4. Title and Subtitle	5. Report Date
Analytic Investigation of Helicopter Rotor Blade Appended Aeroelastic Devices	February 1984
	6. Performing Organization Code
7. Author(s)	8. Performing Organization Report No.
Richard L. Bielawa	R84-915774-24
9. Performing Organization Name and Address	10. Work Unit No.
United Technologies Research Center East Hartford, CT 06108	T5476A
	11. Contract or Grant No.
	NAS2-11008
12. Sponsoring Agency Name and Address	13. Type of Report and Period Covered
NASA-Ames Research Center Moffett Field, CA 94035	Contractor Report
	14. Sponsoring Agency Code
	505 42 11

15. Supplementary Notes

Point of Contact: Robert H. Stroub
NASA-Ames Research Center
Moffett Field, CA 94035 (415) 965-6653

16. Abstract

Analytic evaluations of four different passive aeroelastic devices appended to helicopter rotor blades is presented. The devices consist of a passive tuned tab, a control coupled tab, and all-flying tip and a harmonic dilational airfoil tip; each device was conceived for improving either aerodynamic performance, or reducing vibratory control loads or hub shears. The evaluation was performed using a comprehensive rotor aeroelastic analysis (the G400PA code with appropriate modifications), together with data for a realistic helicopter rotor blade (the UH-60A Blackhawk), in high speed flight (90 m/s, 175 kts). The results of this study show that significant performance (L/D_e) gains can be achieved with the all-flying free tip. Results for the harmonic dilational airfoil tip show the potential for moderate improvements in L/D_e. Finally, the results for the passive tuned tab and the control coupled tab, as configured for this study, show these devices to be impractical.

Sections are included which describe the operation of each device, the required G400PA modifications, and the detailed results obtained for each device.

17. Key Words (Suggested by Author(s))	18. Distribution Statement
Tip Configurations Tuned Tab Control Coupled Tab All-Flying Tip Harmonic Dilational Tip Helicopter Rotor	Unlimited Star Category 05

19. Security Classif. (of this report)	20. Security Classif. (of this page)	21. No. of Pages	22. Price*
None	None	100	

*For sale by the National Technical Information Service, Springfield, Virginia 22161